UNIVERSITÉ DU QUÉBEC À TROIS-RIVIÈRES

# EXPERIMENTAL AND SIMULATION ANALYSIS OF THICKNESS, WIDTH, AND POROSITY EFFECTS ON THE TEMPERATURE COEFFICIENT OF RESISTANCE (TCR) OF SCREEN-PRINTED COPPER STRIPS

THESIS PRESENTED

AS A PARTIAL REQUIREMENT FOR THE MASTER'S DEGREE IN MECHANICAL ENGINEERING

BY
MOHAMAD ALI TAHERIAN

Oct 2025

Université du Québec à Trois-Rivières

Service de la bibliothèque

Avertissement

L'auteur de ce mémoire, de cette thèse ou de cet essai a autorisé l'Université du Québec à Trois-Rivières à diffuser, à des fins non lucratives, une copie de son mémoire, de sa thèse ou de son essai.

Cette diffusion n'entraîne pas une renonciation de la part de l'auteur à ses droits de propriété intellectuelle, incluant le droit d'auteur, sur ce mémoire, cette thèse ou cet essai. Notamment, la reproduction ou la publication de la totalité ou d'une partie importante de ce mémoire, de cette thèse et de son essai requiert son autorisation.

UNIVERSITÉ DU QUÉBEC À TROIS-RIVIÈRES

MAÎTRISE EN INGÉNIERIE – CONCENTRATION GÉNIE MÉCANIQUE (1542)

**Direction de recherche** :

Martin Bolduc

Prénom Nom — Directeur de recherche

**Jury d'évaluation**

Marie Hébert

Prénom Nom, Nom établissement — Présidente

Sylvain G. Cloutier

Prénom Nom, Nom établissement — Évaluateur externe

Martin Bolduc

Prénom Nom, Nom établissement — Directeur de recherche

ACKNOWLEDGEMENTS

Above all, I offer my deepest and most sincere gratitude to my esteemed advisor, **Prof. Martin Bolduc**. His role in shaping, guiding, and completing this project has been truly invaluable. His precise academic insights, unwavering support, and belief in my abilities served as a constant source of inspiration. I also deeply appreciate his timely rigor and constructive criticism, which consistently pushed me to think more critically and strive for excellence. I consider myself incredibly fortunate to have had the privilege of working under his supervision.

I am also profoundly thankful to my brother, **Mohamad Taherian**. He supported me not only with his knowledge and guidance, but also with his quiet strength and emotional support during moments of doubt and pressure. His presence has been a true pillar throughout this journey, and I will always carry deep appreciation for his kindness.

I would also like to express my heartfelt gratitude to **my parents**, whose endless love, encouragement, and sacrifices have been the foundation of all my achievements. Their kindness and unwavering support gave me strength and peace throughout this journey.

I would also like to express my heartfelt gratitude to **Dr. Marcel Veilleux** and **Christiane Dion**. Beyond their professional kindness, they have been like family to me, my wife, and my child — offering warmth, care, and genuine support in our everyday lives. Their generosity and guidance extended far beyond the academic sphere, providing us with a true sense of home and belonging here in this city.

I also thank the administrative and technical staff at **UQTR**, as well as any organization or funding agency that contributed to the realization of this project.

Finally, I owe my utmost gratitude to my beloved and patient wife**, Fariba**. Without her unconditional love, support, and countless sacrifices, this journey would not have been possible. In the most difficult times, she was my source of calm and motivation. This achievement is as much hers as it is mine — a result of our shared commitment and resilience.

# Abstract

This study focuses on the Temperature Coefficient of Resistance (TCR) in screen-printed copper busbars made with Copprint LF-360 ink. TCR is a key property that shows how stable and reliable a conductor is when its temperature changes, and measuring it correctly is important for designing printed circuits and electrothermal devices. While most earlier research looked mainly at continuous metallic layers and did not pay much attention to the internal porosity of printed tracks, this work is among the first to measure TCR in printed copper together with a direct and quantitative evaluation of porosity using Scanning Electron Microscopy (SEM) and Ion Milling.

Three groups of samples with different numbers of layers, thicknesses, and widths were prepared under controlled laboratory conditions. Thermal tests were carried out by passing a constant current through the busbars while their temperature was increased step by step from 30 °C to 100 °C. Resistance was recorded at each temperature, and TCR values were calculated from these measurements.

To study the internal structure, cross-section images were analyzed to measure porosity directly. These data were then used as inputs for COMSOL Multiphysics simulations that combined electrical and thermal effects. In addition to modeling the actual measured porosity, two more reference levels were tested to see how sensitive TCR is to porosity changes. The comparison between experiments and simulations showed good agreement, confirming that the combined approach is reliable.

Overall, the results show that measuring TCR together with porosity analysis gives useful insight into the link between structure and performance in printed conductors. This method can support future efforts to improve printing quality and help in the design of flexible printed circuits and electrothermal systems.

Keywords: Temperature Coefficient of Resistance (TCR); Screen-Printed Copper Busbars; Porosity; Electro-Thermal Simulation; COMSOL Multiphysics; Scanning Electron Microscopy (SEM); Printed Electronics

# Résumé

Cette étude porte sur le coefficient de température de la résistance (TCR) dans des barres omnibus en cuivre déposées par sérigraphie à l'aide de l'encre Copprint LF-360. Le TCR est une propriété clé qui indique la stabilité et la fiabilité d'un conducteur lorsque sa température varie ; sa mesure précise est essentielle pour la conception de circuits imprimés et de dispositifs électrothermiques. Alors que la plupart des recherches antérieures portaient principalement sur des couches métalliques continues et accordaient peu d'attention à la porosité interne des pistes imprimées, le présent travail fait partie des premières études à mesurer le TCR dans le cuivre imprimé tout en procédant à une évaluation directe et quantitative de la porosité à l'aide de la microscopie électronique à balayage (MEB) et du fraisage ionique.

Trois groupes d'échantillons présentant différents nombres de couches, épaisseurs et largeurs ont été préparés dans des conditions de laboratoire contrôlées. Les essais thermiques ont consisté à faire circuler un courant constant dans les barres omnibus, tandis que leur température était augmentée par paliers de 30 °C à 100 °C. La résistance a été enregistrée à chaque température et les valeurs de TCR ont été calculées à partir de ces mesures.

Pour étudier la structure interne, les images de coupe transversale ont été analysées afin de mesurer directement la porosité. Ces données ont ensuite servi d'entrées pour les simulations multiphysiques réalisées sous COMSOL Multiphysics, combinant les effets électriques et thermiques. En plus de modéliser la porosité mesurée, deux niveaux de référence supplémentaires ont été testés afin d'évaluer la sensibilité du TCR aux variations de porosité. La comparaison entre les résultats expérimentaux et les simulations a montré une bonne concordance, confirmant la fiabilité de l'approche combinée.

Dans l'ensemble, les résultats démontrent que la mesure du TCR associée à l'analyse de la porosité fournit une compréhension approfondie du lien entre la structure et les performances des conducteurs imprimés. Cette méthode peut contribuer à l'amélioration de la qualité d'impression et à la conception de circuits imprimés flexibles et de systèmes électrothermiques plus stables.

Mots-clés : Coefficient de température de la résistance (TCR) ; barres omnibus en cuivre sérigraphiées ; porosité ; simulation électrothermique ; COMSOL Multiphysics ; microscopie électronique à balayage (MEB) ; électronique imprimée

# Table of Contents

**ABSTRACT .......... II**

**RÉSUMÉ .......... III**

**CHAPTER-1 - INTRODUCTION .......... 14**

**1.1 INTRODUCTION TO SCREEN PRINTING TECHNOLOGY AND ITS IMPORTANCE .......... 14**
**1.2 TEMPERATURE COEFFICIENT OF RESISTANCE (TCR) AND ITS IMPORTANCE .......... 16**
**1.3 BACKGROUND ON PRINTED COPPER STRUCTURES AND THEIR THERMAL–ELECTRICAL BEHAVIOR .......... 16**
**1.4 RESEARCH PROBLEM AND MOTIVATION .......... 19**
**1.5 RESEARCH OBJECTIVES AND QUESTIONS .......... 19**
1.5.1 SPECIFIC OBJECTIVES .......... 19
1.5.2 RESEARCH QUESTIONS .......... 20
1.5.3 HYPOTHESES .......... 20
**1.6 INNOVATION AND SIGNIFICANCE OF THE STUDY .......... 21**
1.6.1 SCIENTIFIC INNOVATIONS .......... 21
1.6.2 PRACTICAL SIGNIFICANCE .......... 21
**1.7 STRUCTURE OF THE THESIS .......... 22**

**CHAPTER-2 LITERATURE REVIEW .......... 24**

**2.1 OVERVIEW OF PRINTED ELECTRONICS AND TEMPERATURE COEFFICIENT OF RESISTANCE (TCR) .......... 24**
2.1.1 INTRODUCTION TO SCREEN PRINTING TECHNOLOGY AND ITS CHALLENGES .......... 24
2.1.2 LITERATURE REVIEW ON TEMPERATURE COEFFICIENT OF RESISTANCE (TCR) .......... 25
2.1.3 MATHEMATICAL RELATIONS FOR TCR .......... 25
2.1.4 EXPERIMENTAL THERMAL ANALYSIS OF COPPER-BASED PRINTED STRUCTURES .......... 26
**2.2 ROLE OF GEOMETRICAL PARAMETERS (WIDTH & THICKNESS) .......... 27**
**2.3 INFLUENCE OF MICROSTRUCTURAL POROSITY .......... 28**
**2.4 NUMERICAL AND MULTIPHYSICS SIMULATION APPROACHES .......... 29**
**2.5 GAPS AND LIMITATIONS IN EXISTING LITERATURE .......... 30**
**2.6 SAMPLE PREPARATION TECHNIQUES FOR PRINTED COPPER STRUCTURES .......... 31**
2.6.1 CHALLENGES IN FRACTURING PRINTED COPPER SAMPLES FOR MICROSTRUCTURAL ANALYSIS .......... 31
2.6.2. APPLICATION OF ION MILLING TO PRESERVE THE MICROSTRUCTURE OF PRINTED LAYERS .......... 31
**2.7 SUMMARY AND JUSTIFICATION FOR THE CURRENT STUDY .......... 32**

**CHAPTER-3 METHODOLOGY .......... 33**

**3.1 OVERALL RESEARCH DESIGN .......... 33**
**3.2 MATERIALS AND INK .......... 34**
**3.3 PRINTING AND CURING PROCESS .......... 35**
**3.4 SAMPLE SERIES .......... 35**
**3.5 MEASUREMENT OF RESISTANCE AND CALCULATION OF TCR .......... 36**
**3.6 NUMERICAL SIMULATION .......... 37**

3.6.1 ELECTRICAL CONDUCTIVITY CALCULATIONS FOR NUMERICAL SIMULATION INPUT ..... 38
**3.7 NUMERICAL SIMULATION SETUP AND EXECUTION ..... 40**
3.7.1 NUMERICAL DESIGN, DATA, AND ANALYSIS PROCEDURE ..... 42
**3.8 SAMPLE PREPARATION WITH ION MILLING ..... 43**
**3.9 SEM IMAGING AND ANALYSIS ..... 44**
**3.10 SEM IMAGING AND IMAGEJ ANALYSIS PROTOCOL ..... 44**
**3.11 INSTRUMENTS, CALIBRATION, AND MEASUREMENT UNCERTAINTY ..... 45**
3.11.1 SOURCE MEASURE UNIT (SMU): KEITHLEY 2400 ..... 45
3.11.2 THERMOMETER: B&K PRECISION 390A WITH TYPE-K THERMOCOUPLE ..... 45
3.11.3 FOUR-POINT PROBE SYSTEM ..... 46
3.11.4 SCANNING ELECTRON MICROSCOPE (SEM): HITACHI SU8230 ..... 46

**CHAPTER-4 RESULTS AND DISCUSSION ..... 47**

**4.1 CHAPTER INTRODUCTION ..... 47**
**4.2 SEM AND IMAGEJ RESULTS ..... 47**
**4.3 EXPERIMENTAL R–T AND TCR RESULTS ..... 52**
4.3.1 EXPERIMENTAL R–T DATA MEASURED BY THE TWO-PROBE METHOD ..... 53
4.3.2 EXPERIMENTAL R–T DATA MEASURED BY THE FOUR-PROBE METHOD ..... 55
4.3.3 EXPERIMENTAL TCR CALCULATION METHOD ..... 57
4.3.4 EXPERIMENTAL TCR RESULTS (COMPARISON OF TWO-PROBE AND FOUR-PROBE METHODS) ..... 58
4.3.5 FINAL TCR RESULTS BASED ON FOUR-PROBE DATA ..... 60
**4.4 NUMERICAL RESULTS ..... 61**
4.4.1 NUMERICAL R–T DATA (POROSITY-FREE MODEL) ..... 61
4.4.2 NUMERICAL MODEL FOR SENSITIVITY EVALUATION USING TAGUCHI L9 ..... 66
**4.5 DISCUSSION AND INTERPRETATION OF RESULTS ..... 71**
4.5.1 CONNECTION BETWEEN MICROSTRUCTURE AND ELECTRO-THERMAL BEHAVIOR ..... 72
4.5.2 TWO-PROBE AND FOUR-PROBE COMPARISON AND THEIR ROLE IN TCR ANALYSIS ..... 72
4.5.3 EFFECT OF THICKNESS AND WIDTH ON TCR IN THE EXPERIMENTAL RESULTS ..... 72
4.5.4 COMPARISON BETWEEN EXPERIMENTAL AND NUMERICAL RESULTS ..... 73
4.5.5 TAGUCHI AND ANOVA RESULTS: CONCISE INTERPRETATION ..... 73
4.5.6 SUMMARY OF INTERPRETATION FOR CHAPTER 4 ..... 73
**4.6 SUMMARY OF CHAPTER 4 ..... 74**

**CHAPTER-5 CONCLUSION AND RECOMMENDATIONS ..... 76**

**5.1 SUMMARY OF MAIN FINDINGS ..... 76**
**5.2 DISCUSSION OF RESULTS IN THE SCIENTIFIC CONTEXT ..... 77**
**5.3 SCIENTIFIC CONTRIBUTIONS AND INNOVATIONS ..... 80**
**5.4 LIMITATIONS OF THE STUDY ..... 81**
**5.5 FUTURE WORK AND RECOMMENDATIONS ..... 82**

**CHAPTER-6 REFERENCES ..... 85**

**CHAPTER-7 APPENDICES ..... 90**

**7.1 APPENDIX A – ADDITIONAL WIDTH MEASUREMENTS (2.5 AND 1 MM) ..... 90**
**7.2 APPENDIX B – FOUR-PROBE RESISTANCE–TEMPERATURE MEASUREMENTS ..... 91**

**7.3 APPENDIX C – NUMERICAL R–T DATA USED IN THE SIMULATIONS ........................................92**
**7.4 APPENDIX D – GRAPHICAL INTERFACE OF THE COMSOL MODEL ........................................93**

## Table of Figures

Figure 1-1 Schematic representation of the screen printing process, including mesh, conductive paste, and squeegee applying ink to the substrate [2]. 15
Figure 1-2 Schematic view of key innovations in TCR analysis of screen-printed copper strips. 22
Figure 3-1 Workflow of the research methodology, illustrating the sequence from sample fabrication to measurement, simulation, and validation. 34
Figure 3-2 Schematic of the printed copper strips with a fixed length (3 in) and varying widths from 1 to 20 mm (B1–B8). 41
Figure 4-1 A. Raw SEM cross-sectional image of the printed copper strip (magnification ×5000). B. Segmented SEM image processed with ImageJ: yellow = copper, red = pores with high certainty, blue = uncertain transition regions. Estimated porosity: 8.6%.] 48
Figure 4-2 a) Binary (black/white) ImageJ output. White areas correspond to pores. Estimated porosity: 8.6%. b) Processed high-contrast image showing pore boundaries more clearly. 49
Figure 4-3 Additional SEM micrographs and ImageJ segmentation outputs illustrating other analyzed regions used for porosity estimation. The calculated porosity values from these images fall within the reported range (7.8%–10.7%) and contribute to the overall average of approximately 8.9%. 51
Figure 4-4 Experimental R–T curves for single-layer printed copper strips (≈17 µm), measured using the two-probe method. 53
Figure 4-5 Experimental R–T curves for double-layer printed copper strips (≈34 µm), measured using the two-probe method. 54
Figure 4-6 Experimental R–T curves for triple-layer printed copper strips (≈51 µm), measured using the two-probe method. 54
Figure 4-7 Experimental R–T curves for single-layer printed copper strips (≈17 µm), measured using the four-probe method. 55
Figure 4-8 Experimental R–T curves for double-layer printed copper strips (≈34 µm), measured using the four-probe method. 56
Figure 4-9Experimental R–T curves for Triple-layer printed copper strips (≈34 µm), measured using the four-probe method. 56
Figure 4-10Comparison of TCR by width using two-probe and four-probe measurements 59
Figure 4-11 Comparison of TCR by thickness using two-probe and four-probe measurements 60
Figure 4-12summary by thikness (experimental) 60
Figure 4-13summary by width (experimental) 61
Figure 4-14 Numerical R–T curves for single-layer printed copper strips (≈17 µm), simulated using the porosity-free model. 62
Figure 4-15 Numerical R–T curves for double-layer printed copper strips (≈34 µm), simulated using the porosity-free model. 63
Figure 4-16 Numerical R–T curves for triple-layer printed copper strips (≈51 µm), simulated using the porosity-free model. 63
Figure 4-17 Numerical TCR comparison by thickness using Average-Interval and Linear-Fit methods 65
Figure 4-18 Numerical TCR comparison by width using Average-Interval and Linear-Fit methods 65
Figure 4-19 Main effects plot for TCR (Taguchi L9) 71
Figure 7-1 94

Figure 7-2 Graphical user interface of the COMSOL Multiphysics model used for parameter input and resistance calculation. ........................................................................................ 94

**Table of Tables**

Table 3-1 Input parameters used in the COMSOL model for porosity levels of 0% and 9%. The calibration resistivity for 0% porosity was set to $1.50\times10^{-7}$ Ω·m, and the corresponding value obtained for 9% porosity was $1.3061\times10^{-7}$ Ω·m. ... 39
Table 3-2 Input parameters used in the COMSOL model. The symbols A, B, C, and D represent interface-defined input values within the software, included here to illustrate the overall structure of parameters required for the simulation workflow. The numerical values associated with these parameters are reported in the Results section. ... 41
Table 4-7. Experimental TCR Values by Thickness measured by two-probe method ... 57
Table 4-8. Experimental TCR Values by width measured by two-probe method ... 57
Table 4-9Experimental TCR Values by Thickness measured by four-probe method ... 57
Table 4-10Experimental TCR Values by width measured by four-probe method ... 58
Table 4-11Comparison of TCR values measured by the two-probe and four-probe methods (by thickness) ... 58
Table 4-12Comparison of TCR values measured by the two-probe and four-probe methods (by width) ... 58
Table 4-16 Summary of numerical TCR values by thickness, calculated using the Average-Interval and Linear-Fit methods. ... 64
Table 4-17 Summary of numerical TCR values by width, calculated using the Average-Interval and Linear-Fit methods. ... 64
Tables 4-18 and 4-197 summarize the computed TCR values by **thickness** and **width**, respectively. Figures 4-20 and 4-217 illustrate the corresponding bar charts, comparing the two TCR estimation methods. ... 64
Table 4-22 Taguchi L9 ($3^3$) orthogonal array ... 67
Table 4-23 Taguchi L9 R–T Results (Porosity 0 %, Thickness ≈17 µm, Width = 5 mm) ... 67
Table 4-24 Taguchi L9 R–T Results (Porosity 0 %, Thickness ≈ 34 µm, Width = 12.5 mm) ... 67
Table 4-25 Taguchi L9 R–T Results (Porosity 0 %, Thickness ≈ 51 µm, Width = 20 mm) ... 68
Table 4-26 Taguchi L9 R–T Results (Porosity 9 %, Thickness ≈ 17 µm, Width = 12.5 mm) ... 68
Table 4-27Taguchi L9 R–T Results (Porosity 9 %, Thickness ≈ 34 µm, Width = 20 mm) ... 68
Table 4-28 Taguchi L9 R–T Results (Porosity 9 %, Thickness ≈ 51 µm, Width = 5 mm) ... 68
Table 4-29 Taguchi L9 R–T Results (Porosity 18 %, Thickness ≈ 17 µm, Width = 20 mm) ... 68
Table 4-30 Taguchi L9 R–T Results (Porosity 18 %, Thickness ≈ 34 µm, Width = 5 mm) ... 68
Table 4-31 Taguchi L9 R–T Results (Porosity 18 %, Thickness ≈ 51 µm, Width = 12.5 mm) ... 69
Table 4-32 Temperature Coefficient of Resistance (TCR) values for the nine Taguchi runs. Obtained from simulation results. ... 69
Table 4-33 ANOVA results for TCR values obtained from the Taguchi L9 simulations ... 70
Table 7-1 Experimental resistance–temperature (R–T) data for single-layer printed copper strips (≈17 µm), measured using the two-probe method. ... 90
Table 7-2Experimental resistance–temperature (R–T) data for double-layer printed copper strips (≈34 µm), measured using the two-probe method. ... 90
Table 7-3Experimental resistance–temperature (R–T) data for triple-layer printed copper strips (≈51 µm), measured using the two-probe method. ... 91
Table 7-4 Experimental resistance–temperature (R–T) data for single-layer printed copper strips (≈17 µm), measured using the four-probe method. ... 91
Table 7-5 Experimental resistance–temperature (R–T) data for Double-Layer printed copper strips (≈34 µm), measured using the four-probe method. ... 92

Table 7-6 Experimental resistance–temperature (R–T) data for Triple-Layer printed copper strips (≈51 µm), measured using the four-probe method. ........................................................... 92
Table 7-7 Numerical resistance–temperature (R–T) data for single-layer printed copper strips (≈17 µm), obtained from the numerical model. ........................................................... 92
Table 7-8 Numerical resistance–temperature (R–T) data for double-layer printed copper strips (≈34 µm), obtained from the numerical model ........................................................... 93
Table 7-9 Numerical resistance–temperature (R–T) data for triple-layer printed copper strips (≈51 µm), obtained from the numerical model. ........................................................... 93

## LIST OF ABBREVIATIONS

| | |
|---|---|
| TCR | Temperature Coefficient of Resistance |
| SEM | Scanning Electron Microscope |
| COMSOL | COMSOL Multiphysics Software |
| FEM | Finite Element Method |
| RT | Resistance–Temperature |
| SMU | Source Measure Unit |
| TDS | Technical Data Sheet |
| SDS | Safety Data Sheet |
| LF-360 | Copprint Copper Ink Model LF-360 |
| DoE | Design of Experiments |
| FCC | Face-Centered Cubic |
| R–T | Resistance–Temperature Relationship |
| ΔR/ΔT | Incremental Resistance-to-Temperature Ratio |
| L9 | Taguchi Orthogonal Array ($3^3$) |
| ANOVA | Analysis of Variance |
| FLIR | Forward-Looking Infrared (Thermal Camera) |
| MEB | Microscopie Électronique à Balayage |
| EC | Electric Current |
| HT | Heat Transfer |
| PI | Polyimide (Kapton) |

## LIST OF SYMBOLS

| Symbol | Description |
|---|---|
| $R$ | Electrical resistance (Ω) |
| $R_0$ | Resistance at reference temperature (Ω) |
| $T$ | Temperature (°C or K) |
| $\Delta R$ | Change in resistance (Ω) |
| $\Delta T$ | Change in temperature (°C) |
| $\alpha$ | Temperature coefficient of resistance ($°C^{-1}$) |
| $\rho$ | Electrical resistivity (Ω·m) |
| $\sigma$ | Electrical conductivity ($S \cdot m^{-1}$) |
| $t$ | Thickness (μm or m) |
| $w$ | Width (mm) |
| $L$ | Length (m) |
| $\Phi$ | Electric potential (V) |
| $\varepsilon$ | Porosity (%) |
| $P$ | Electrical power (W) |
| $Q$ | Heat (J) |
| $J$ | Current density ($A \cdot m^{-2}$) |
| $k$ | Thermal conductivity ($W \cdot m^{-1} \cdot K^{-1}$) |
| $\rho_m$ | Material density ($kg \cdot m^{-3}$) |

# Chapter-1 - Introduction

## 1.1 Introduction to Screen Printing Technology and Its Importance

Printed electronics has emerged as a rapidly expanding field due to its ability to fabricate low-cost, lightweight, and flexible electronic components using scalable manufacturing techniques. Among the various printing methods, screen printing remains one of the most widely adopted because it can deposit functional materials in controlled thicknesses over large areas, making it suitable for applications such as sensors, solar cells, antennas, and power-distribution circuits. The electrical and thermal performance of printed conductors plays a central role in determining the reliability of these systems, especially when devices operate under varying temperatures or mechanical constraints.

Screen printing is one of the most widely used techniques for fabricating conductive structures in printed electronics. In this method, ink is transferred through a patterned mesh onto a substrate, using a mesh—commonly made of polyester or stainless steel—a squeegee to apply uniform pressure, and a stencil to define the desired pattern. The quality of the printed structure depends on several factors, including the mesh count, thread diameter, ink viscosity, and the snap-off distance. For example, high mesh counts allow for finer details but reduce the amount of deposited ink, while the ink formulation must be optimized to flow smoothly through the mesh and retain its shape after deposition [1]. A schematic representation of the screen printing process is shown in Fig. 1-1.

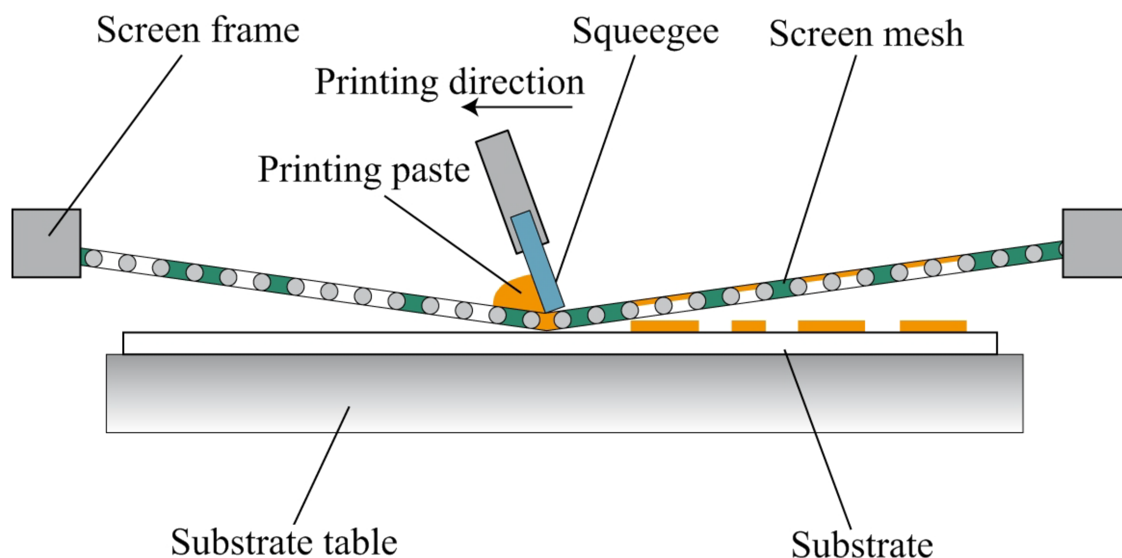

Figure 1-1 Schematic representation of the screen printing process, including mesh, conductive paste, and squeegee applying ink to the substrate [2].

In this thesis, the Temperature Coefficient of Resistance (TCR) of screen-printed copper busbars is investigated with a particular focus on the influence of thickness, width, and internal porosity. Although printed copper conductors offer advantages such as low cost and compatibility with flexible substrates, their electrical and thermal stability still differs significantly from bulk copper. In particular, the combined effects of structural porosity and multilayer geometry on the temperature-dependent resistance remain insufficiently characterized. This motivates the present study, which aims to provide a systematic evaluation of these factors under controlled experimental and numerical conditions.

Among conductive materials, copper is considered a valuable alternative to silver because of its high electrical conductivity, mechanical stability, and low cost. Copper-based inks generally consist of nanoparticles or copper complexes stabilized by protective agents to prevent oxidation. Li et al. developed copper–nickel complex inks that showed excellent oxidation resistance and high electrical conductivity, making them suitable for flexible electronic applications [3]. Similarly, Sarwar et al. reported citrate-capped copper nanoparticles that could be sintered at low temperatures, resulting in conductive and oxidation-resistant films [4].

Recent advances have focused on improving conductivity and reducing electrical resistance in printed copper structures. Zhang et al. fabricated dense and flexible copper films with low resistivity by carefully controlling the decomposition of copper complex inks [5]. Jang et al. applied multiple intense pulsed light sintering to copper oxide pastes, which not only lowered the sintering temperature but also improved the thermal stability and electrical conductivity of solar cell electrodes [6]. Rosen et al. introduced self-reducing copper precursor inks processed under intense pulsed light, reducing the sintering energy by up to 25% while achieving high-quality conductive patterns [7].

Porosity remains one of the main challenges in printed copper structures. Small voids within the printed layers increase electrical resistance and can alter the temperature-dependent resistance behavior (TCR). Recent studies have shown that optimizing ink rheology and sintering conditions can effectively reduce porosity, thereby improving conductivity and stabilizing resistance behavior [1]. The use of stabilizing additives and uniform particle distribution has also been found essential for reducing cracking and enhancing thermal durability.

Despite these advances, the electrical conductivity of printed copper structures is still lower than that of bulk copper. Fast oxidation, limited thermal stability, and the difficulty of controlling porosity—especially in thicker layers exceeding 25 µm—remain significant challenges. Future research is expected to focus on developing environmentally stable inks, employing photothermal additives to lower the sintering temperature below 120 °C, and designing optimized multilayer architectures to achieve electrical and thermal performances closer to industrial standards [1].

## 1.2 Temperature Coefficient of Resistance (TCR) and Its Importance

The Temperature Coefficient of Resistance (TCR) is one of the key parameters for evaluating the thermal stability and electrical performance of conductive structures. Temperature fluctuations can cause undesirable changes in resistance, which negatively affect the accuracy and reliability of electronic systems. In precision circuits, analog-to-digital converters, and calibration instruments, the use of components with low TCR is essential to ensure stable operation and minimize measurement errors [8], [9], [10].

TCR is defined as the relative change in resistance per degree Celsius (ppm/°C), and its control is crucial in thin-film and alloy-based resistors. Alloys such as NiCr, TaN, and SiCr are widely used due to their low TCR. One reason for this low TCR is the limited electron mean free path; according to the Drude model, further reduction of the mean free path at high temperatures is impossible due to strong scattering, which leads to very small changes in resistance [11], [12].

However, pure metals such as copper have a much higher TCR. For example, the TCR of copper exceeds 3900 ppm/°C, whereas alloys such as CuNi and CrNi show TCR values lower than 100 ppm/°C [12], [13].

## 1.3 Background on Printed Copper Structures and Their Thermal–Electrical Behavior

Despite significant advancements in printed electronics technologies, accurately analyzing the temperature-dependent resistance (TCR) of screen-printed conductive tracks remains a scientific and industrial challenge. Most past studies in this field have focused on optimizing electrical conductivity [14], improving layer adhesion to substrates, or reducing surface resistance. In contrast, thermal performance and temperature effect on electrical resistance has often been treated as a secondary concern.

While studies such as [15] concentrate solely on analytical models for design optimization—without integrating experimental validation of thermal behavior—our work adopts a data-driven approach, using real experimental measurements to calibrate and validate the simulations. This integration allows for a more realistic prediction of TCR values under actual operating conditions.
In one study, Szulborski et al. (2021) [16] conducted a thermal analysis of current-carrying paths in miniature circuit breakers using the finite element method. A key strength of this research was its focus on transient thermal behavior, while most similar studies were limited to steady-state analysis. This time-dependent approach allowed for a more accurate evaluation of thermal response during real operating conditions. However, structural irregularities and porosity were still not considered.

In another study, Im and Roh (2024) [17] investigated the electrical performance of silver-ink screen-printed tracks on textile substrates. While they examined parameters like substrate type, mesh density, and number of printing passes, they did not address the direct impact of track width, thickness, or temperature-dependent resistance behavior (TCR).

Similarly, Mohan et al. (2025) [18] explored the electrothermal behavior of copper ink lines printed without particles on flexible substrates. Their work focused mainly on the laser sintering process, showing that precise control of laser profiles significantly affects the conductivity and microstructure of the final print. However, thermal modeling and temperature effect on electrical resistance were not directly studied and remain open research gaps.

Among the limited number of studies that focus specifically on porous metallic structures, Zhou et al. (2012) [19] conducted a comprehensive analysis of copper fiber sintered sheets (PMFSS) using a four-point probe method. Their research clearly demonstrated that increased porosity significantly reduces electrical conductivity, and that sintering conditions (temperature and time) strongly influence the internal structure and resultant conductivity. Although their study focused on sintered copper fibers rather than screen-printed films, the findings emphasize the critical role of porosity and microstructure in determining electrical—and by extension, thermal—behavior in conductive media.

In most of these studies, the printed structures were modeled as homogeneous bulk materials, while in reality, the screen printing process often leads to microscopic porosity, layer non-uniformity, and local thickness variations. These inhomogeneities can seriously impact resistance–temperature behavior, altering the TCR and stability of conductive paths.

Therefore, it is essential to carry out a more comprehensive, multi-dimensional study that considers geometric parameters (such as width and thickness), microstructural features (like porosity), and and temperature influence on electrical resistance of printed conductive tracks. The present research aims to address this need through a combination of experimental measurements, SEM image analysis, and numerical thermal simulations—to provide a clearer scientific understanding of thermal behavior in screen-printed copper conductors.

Initially, an attempt was made to estimate the porosity of the printed copper structures using the method presented by Jeong et al. (2023). In their study, porosity was calculated based on the ratio of the measured density to the bulk copper density (8960 kg/m³), using the equation $\varepsilon = 1 - (\rho_{measured} / \rho_{bulk})$ [20]. However, upon further examination, it became clear that the experimental conditions in their work were significantly different from those used in the present study. For example, their sintering process involved 100 nm copper nanoparticles, applied without pressure and conducted in an argon environment at temperatures up to 400°C. In contrast, in this work, the curing process was carried out strictly in accordance with the technical guidelines provided by Copprint for the LF360 ink [21]

According to the Technical Data Sheet (TDS) issued by Copprint, one of the recommended sintering methods for LF360 is the S2S (sheet-to-sheet) process, involving hot pressing at 160°C for 120 seconds, which explicitly includes the application of pressure [22]. This mechanical pressure is expected to significantly influence particle packing and reduce porosity, making it unsuitable to adopt Jeong's estimation model directly. Furthermore, as described in the MSDS of Copprint, the copper ink used in this study contains a mixture of submicron (~0.15 µm) and micron-sized particles (0.8 to 10 µm) [21] which differs significantly from the monodisperse 100 nm nanoparticles used in Jeong's work. Due to these differences in material properties and processing conditions, the porosity estimation approach from Jeong et al. did not yield realistic or reliable results for our samples. Therefore, it was ultimately decided to experimentally determine the porosity using SEM-based image analysis, providing more accurate input data for simulation and temperature effect evaluation. The porosity in this study is reported solely based on SEM cross-section analysis and ImageJ image processing, and no density-based conversion is applied.

## 1.4 Research Problem and Motivation

Screen-printed copper busbars are increasingly used in flexible electronics, solar panels, and energy-storage systems because they are low-cost and easy to manufacture. However, their thermo-electrical reliability is still not well understood. In particular, the Temperature Coefficient of Resistance (TCR) — an important measure of stability under temperature changes — has not been clearly characterized for printed copper conductors.

Unlike bulk copper or vacuum-processed thin films, screen-printed structures show natural microstructural variations, such as internal porosity, local thickness changes, and irregular cross-sections. These factors can strongly influence resistance as temperature changes, but their combined effect on TCR has not been well quantified. To the best of our knowledge, no previous study has examined the simultaneous influence of thickness, width, and internal porosity on the TCR of screen-printed copper busbars. As a result, an important gap remains in the scientific understanding of these materials.

The goal of this research is to address this gap by providing clear experimental data and simulation results that show how thickness, width, and porosity affect TCR. A better understanding of these relationships can support improved design strategies, reduce thermal instability, and increase the long-term reliability of printed conductors in temperature-sensitive and high-precision electronic systems.

## 1.5 Research Objectives and Questions

The primary aim of this study is to systematically investigate the effects of geometric features (specifically thickness and width) and internal structural characteristics (namely porosity) on the Temperature Coefficient of Resistance (TCR) in screen-printed copper strips. This objective is achieved through a combination of laboratory experiments, image-based analysis using Scanning Electron Microscopy (SEM), and numerical simulations performed in COMSOL Multiphysics.

### 1.5.1 Specific Objectives

- To evaluate how variations in copper strip thickness and width influence TCR within a defined temperature range
- To accurately measure internal porosity using SEM images and quantitative image analysis

- To explore the relationship between porosity and the variation of electrical resistance with temperature
- To derive an empirical TCR equation based on experimental resistance measurements from 30°C to 100°C
- To simulate resistance–temperature behavior in printed copper structures using porosity-integrated finite element models in COMSOL
- To compare experimental and simulated results in order to assess the validity and accuracy of the thermal model
- To provide practical design recommendations aimed at reducing TCR and enhancing thermal stability in printed copper traces on flexible substrates

### 1.5.2 Research Questions

To address the above objectives, the following research questions are formulated:

1. How do strip thickness and width affect the TCR within an operational temperature range?
2. How does internal porosity contribute to increased electrical resistance, and what is its quantitative relationship with TCR?
3. Is there a critical porosity threshold that significantly affects TCR, and can this threshold be defined experimentally?
4. Can the proposed numerical model accurately reproduce resistance–temperature behavior (TCR) in printed copper conductors?
5. How can the findings of this study be used to optimize the design of printed conductors for improved thermal performance and long-term reliability in sensitive electronic systems?

### 1.5.3 Hypotheses

Based on the literature and the known microstructural behavior of printed conductors, the following hypotheses are defined for this study:

Hypothesis 1 — Effect of Thickness

H0: The thickness of the printed copper strip has no significant effect on TCR.

H1: An increase in thickness causes a significant change in TCR.

Hypothesis 2 — Effect of Width

H0: The width of the printed copper strip has no significant effect on TCR.

H1: The width of the printed copper strip may lead to a measurable change in TCR.

(The initial assumption is that this effect will be very small or negligible.)

Hypothesis 3 — Effect of Porosity

H0: Internal porosity has no significant effect on TCR.

H1: An increase in porosity causes a measurable change in TCR.

(The initial assumption is that porosity will not have a major impact within the studied range.)

## 1.6 Innovation and Significance of the Study

### 1.6.1 Scientific Innovations

This research provides a detailed investigation of the Temperature Coefficient of Resistance (TCR) in screen-printed copper strips. It introduces several innovative contributions that have not been widely explored in previous studies. First, TCR is measured directly on real printed copper structures under controlled temperature conditions, which is rarely reported in the literature. Second, the numerical models in COMSOL are built using actual measurements of thickness, width, and porosity, allowing the simulations to closely represent the real printed geometry. Third, this study examines the combined influence of three key factors—thickness, width, and internal porosity—which have not previously been analyzed together in the context of TCR.

### 1.6.2 Practical Significance

The findings of this work have practical relevance for the development of more reliable printed conductors, especially in flexible electronics. By using industrially relevant printing and curing conditions, the results better reflect real manufacturing processes. In addition, experimental resistance–temperature measurements are used to validate the simulations, increasing confidence in the modeling approach. This research also contributes to addressing the lack of thermal evaluation criteria in printed electronics. By improving the understanding of temperature-dependent resistance in porous printed structures, it supports better design strategies for long-term stability and performance in sensitive electronic applications.

Figure 1-2 Schematic view of key innovations in TCR analysis of screen-printed copper strips.

## 1.7 Structure of the Thesis

This thesis is organized into six chapters, each addressing a specific aspect of the research:

- **Chapter 1 – Introduction:**
  Introduces the research topic, highlights the importance of screen printing, reviews initial scientific context, defines the research problem, and states the objectives, questions, and hypotheses.
- **Chapter 2 – Literature Review:**
  Provides a detailed analysis of previous studies related to printed electronics, electrothermal behavior, and the role of geometric and microstructural factors. Special

attention is given to porosity, temperature effect on electrical resistance, and simulation techniques used in prior work.

- **Chapter 3 – Methodology:**
  Describes the experimental procedures and numerical modeling strategies used in the study. This includes sample fabrication, resistance and temperature measurements, SEM analysis, and temperature effect on electrical resistance simulations in COMSOL Multiphysics.
- **Chapter 4 – Results and Discussion:**
  Presents and interprets the experimental and simulation results. It compares different scenarios based on track geometry and porosity, and evaluates the consistency of findings with the proposed hypotheses.
- **Chapter 5 – Conclusion and Recommendations:**
  Summarizes the key findings, discusses the limitations of the study, and proposes directions for future research and practical design improvements.
- **References and Appendices:**
  Lists all cited literature and provides additional data, images, or raw outputs that support the main content.

# Chapter-2 LITERATURE REVIEW

## 2.1 Overview of Printed Electronics and Temperature Coefficient of Resistance (TCR)

### 2.1.1 Introduction to Screen Printing Technology and Its Challenges

Screen printing is one of the oldest and most commonly used techniques for forming functional patterns on different substrates. Its simplicity, repeatability, and low production cost make it highly attractive for flexible electronics, sensors, heaters, and copper-based conductive tracks [23], [7]. In this process, a patterned mesh is placed on the substrate, and ink is pressed through the mesh openings using controlled pressure. This straightforward setup allows fast and repeatable fabrication of identical patterns, especially in large-scale production [24].

One major advantage of screen printing is its ability to deposit material on uneven surfaces while providing reasonable control over layer thickness. Parameters such as mesh size, ink viscosity, and printing speed can be adjusted to tune the printed layer [23]. However, several challenges still limit printing resolution. Edge spreading, stencil deformation, and ink overflow can reduce pattern accuracy, especially in fine features [23].

Another challenge arises from the internal porosity of printed metallic layers. In conductive inks such as copper, microscopic pores increase electrical resistance and may promote local current crowding [7]. Post-processing steps, including thermal drying or intense pulsed light (IPL) sintering, also influence the final conductivity, adhesion, and microstructure of the printed paths [23], [7]. In addition, copper is highly prone to oxidation, which makes it difficult to maintain long-term electrical stability [25].

To address these limitations, recent studies have focused on improving ink formulations, adding light-absorbing additives such as carbon nanotubes, and optimizing curing parameters [7]. Despite these challenges, screen printing remains one of the most promising fabrication routes for flexible conductive components due to its low cost, compatibility with various inks, and scalability.

A relevant example is the work of Mohan et al. (2025) [18], who investigated laser sintering of particle-free copper inks based on copper(II) formate and amino-2-propanol (CuF-A2P) on polyimide and PET substrates. They optimized the laser energy window and evaluated the resulting electrical, morphological, and adhesion properties. Their reported resistivity of 3.24 $\mu\Omega \cdot cm$ was only 1.87 times higher than bulk copper, demonstrating the effectiveness of proper

sintering conditions. This study is a useful reference for the present work, particularly in understanding how process parameters influence the conductivity and uniformity of printed copper structures.

## 2.1.2 Literature Review on Temperature Coefficient of Resistance (TCR)

The electrical and thermal behavior of screen-printed copper conductors is strongly influenced by their Temperature Coefficient of Resistance (TCR). Parameters such as thickness, grain size, and porosity directly affect electron scattering mechanisms, which determine both TCR and long-term stability [26].

## 2.1.3 Mathematical Relations for TCR

### 2.1.3.1 Differential definition at a reference temperature $\boldsymbol{T_0}$

$$\alpha(T_0) = \frac{1}{R(T_0)} \cdot \frac{dR}{dT}\Big|_{T_0} \, [K^{-1}]$$

This definition is widely applied in thin-film studies [27].

### 2.1.3.2 Finite-difference definition (experimental form)

$$\text{TCR} = \frac{R(T) - R_0}{R_0(T - T_0)} \times 10^6 \ [\text{ppm}/^\circ\text{C}]$$

with $R_0 = R(T_0)$. This is the most common form used in experimental measurements [26].

### 2.1.3.3 Polynomial approximation around 300 K

$$R(T) = R'\left[1 + \alpha(T - 300) + \beta(T - 300)^2\right]$$

where $\alpha$ is the first-order TCR term and $\beta$ represents a second-order correction for weak nonlinearities [26].

### 2.1.3.4 Resistivity form

$$\alpha_\rho(T_0) = \frac{1}{\rho(T_0)} \cdot \frac{d\rho}{dT}\Big|_{T_0}, \quad \alpha_{\rho,\,\text{ppm}} = 10^6 \alpha_\rho$$

or in finite-difference form:

$$\alpha_\rho \approx \frac{\rho(T) - \rho_0}{\rho_0(T - T_0)}$$

This definition is commonly used in resistivity-based analyses [27].

Liu et al. [26] reported that TCR is governed by electron–phonon, surface, and grain-boundary scattering. In bulk copper, electron–phonon scattering dominates; however, when thickness or grain size decreases, surface and boundary scattering become significant and reduce TCR. This behavior is consistent with the Mayadas–Shatzkes grain-boundary model [28] and the Fuchs–Sondheimer surface scattering model [29]. As a result, screen-printed copper—where grains are small and porosity is present—typically exhibits lower TCR than bulk copper ($\approx 3.9\times10^{-3}$ $K^{-1}$).

Siniscalchi et al. [27] showed that copper films thinner than 10 nm exhibit reduced TCR and nonlinear temperature dependence due to strong surface scattering. These findings confirm earlier results by Steinhögl et al. [30]and Ke et al. [31]. In printed copper conductors, similar effects may occur, with additional resistance caused by porosity and incomplete sintering.

Dukarov et al. [32] observed that nanocrystalline copper films can exhibit TCR values as low as $1.2\times10^{-3}$ $K^{-1}$, mainly due to grain-boundary scattering, which shortens the electron mean free path. This behavior also aligns with the Mayadas–Shatzkes model [28]. Since printed copper structures include numerous grain boundaries from the curing process, similar TCR reduction is expected.

Timalsina et al. [33]found that increased surface roughness and reduced correlation length raise resistivity and lower TCR in ultrathin copper films. Their explanation was based on Soffer's statistical model [34] and Prange–Nee quantum size-effect theory [35]. Printed copper, which inherits rough surfaces from particle-based inks, is therefore subject to the same mechanisms.

Yang et al. [36] emphasized that microstructural defects, such as grain boundaries and second-phase particles, degrade conductivity and influence TCR in copper alloys. Rubio and Bolduc [37] highlighted that in screen printing, parameters such as viscosity, mesh size, squeegee pressure, and curing conditions determine porosity and structural uniformity, and therefore affect TCR.

### 2.1.4 Experimental Thermal Analysis of Copper-Based Printed Structures

The experimental investigation of the Temperature Coefficient of Resistance (TCR) in copper-based printed conductors has been widely explored, and several studies provide a strong foundation for the present research. These works highlight reliable measurement techniques, validation approaches, and complementary thermal analysis methods that are directly relevant to this study.

Liu et al. [38] performed systematic experiments on thin-film resistors to minimize TCR and improve long-term resistance stability. By conducting measurements under controlled thermal conditions, they demonstrated that accurate TCR characterization is essential for evaluating material reliability over a wide temperature range. Their findings support the need for precise temperature-controlled measurements in the present work, where the thermal stability of screen-printed copper busbars is a key objective.

Allassem et al. [39] used both the four-point probe and Van der Pauw configurations to measure the resistivity of copper thin films with different thicknesses. Their results confirmed that these methods produce stable and repeatable measurements, which justifies the use of the same four-point probe method in the current project. By employing a well-established technique, the resistance measurements of the printed copper strips in this study remain consistent with accepted experimental practices.

In addition, Payette et al. [40] utilized a FLIR One thermal camera to monitor the temperature distribution of conductive structures. Their observations showed that thermal imaging can effectively validate resistance–temperature behavior and reveal localized variations in heating. This approach is conceptually valuable for the present research, as it supports the use of thermal imaging to cross-check electrical measurements and assess uniformity along printed conductors.

Together, these studies directly contribute to the experimental methodology adopted in this work. They provide a clear framework for reliable TCR measurement, verification using thermal imaging, and interpretation of thermal-electrical behavior in printed copper structures.

## 2.2 Role of Geometrical Parameters (Width & Thickness)

The geometry of metallic conductors plays an important role in their electrical and thermal behavior, especially when dimensions become small enough to influence electron transport. In printed conductive films, thickness and width are two key parameters that can affect the overall resistance and, to a lesser extent, the temperature coefficient of resistance (TCR). Literature shows that these geometrical effects become increasingly noticeable as the conductor size approaches micro- and nanoscale ranges, where additional scattering mechanisms alter current flow and heat distribution.

Film thickness has a stronger influence on resistance and thermal behavior than width. When the thickness is reduced, electrons experience more frequent scattering at surfaces and grain

boundaries, which increases resistivity and can modify the slope of the R–T curve at very small scales [41], [42]. These effects are especially significant in ultrathin or nanometric films, where the thickness becomes comparable to the electron mean free path and deviations from bulk behavior are frequently reported [43]. However, studies on screen-printed conductors with micrometer-scale thicknesses show that the R–T relationship remains linear and stable, and the TCR stays close to bulk values as long as the printed layer is continuous and well-sintered . Lacy's theoretical model further supports this behavior by showing that reduced thickness mainly increases resistivity through enhanced surface scattering, without drastically changing the temperature dependence unless the film becomes extremely thin [44]. Overall, in typical printed films with tens of micrometers of thickness, changes in thickness influence the initial resistance ($R_0$) more than the TCR itself.

The width of a conductor can also alter its electrical behavior, though its influence on TCR is generally weaker than that of thickness. Narrow conductive paths may exhibit higher resistance due to current crowding and localized variations in current density, particularly near edges or contact regions [45], [46]. Experimental observations on printed structures confirm that width-dependent spreading resistance can increase the effective resistivity, but this effect remains small unless the geometry approaches micro- or nanoscale dimensions [47]. Numerical studies by Yang et al. demonstrated that irregular or sharp current paths intensify current crowding and localized heating, emphasizing that geometrical non-uniformities become more critical as the line width decreases [48]. Nevertheless, for conventional printed conductors, the width mainly affects the total resistance and has only a minor role in shaping the thermal response or modifying the TCR. In summary, literature indicates that thickness is the dominant geometrical factor affecting electrical behavior, particularly at very small dimensions where surface and grain-boundary scattering are significant. Width-related effects exist but are typically secondary and become relevant only for very narrow lines. For printed metallic films with micrometer-scale geometries, both parameters influence resistance, while their impact on TCR remains limited, and the R–T behavior generally follows a stable, bulk-like trend [41]– [47].

## 2.3 Influence of Microstructural Porosity

The microstructural porosity of printed copper conductors plays a key role in determining their electrical and thermal behavior. In this project, SEM imaging combined with ImageJ analysis was

used to quantify porosity-related parameters, including average pore size, pore size distribution, and surface porosity. The choice of ImageJ is supported by previous studies, which demonstrated its reliability in extracting quantitative metrics from porous structures. For example, Lifton et al. [49] highlighted that accurate magnification, proper thresholding, and high-quality imaging are essential to obtain meaningful porosity data. These observations further justify the use of ImageJ in the present work.

Similarly, Matej Vesenjak et al. [50] showed that ImageJ can effectively measure pore size and distribution in porous copper structures. Their findings confirm that image-based analysis provides a consistent and repeatable way to evaluate porosity, which aligns with the objectives of this project.

In addition, Zhou et al. [51] demonstrated that an increase in porosity leads to a reduction in electrical conductivity in porous copper sheets. Using the four-point probe technique, they reported that higher porosity weakens the conductive network, while improved sintering conditions enhance conductivity through better particle bonding. Since the current work also investigates the influence of porosity on the electrical response of printed structures, this study provides a useful reference for interpreting experimental results.

## 2.4 Numerical and Multiphysics Simulation Approaches

Szulborski et al. [52] modeled low-voltage busbars under rated current using a coupled ANSYS workflow (Maxwell 3D + transient thermal + CFD). Their results show that geometry and arrangement strongly shape temperature distribution, ohmic losses, and current crowding—leading to local hot spots. These insights are directly relevant here, even though the present work uses COMSOL, because the underlying electro-thermal coupling and design sensitivities are the same [52].

Ramírez and Castillo [53] used COMSOL to study how contact resistances affect Joule heating in thermoelectric modules. They reported that thermal contact resistance can increase the temperature difference (improving apparent performance), while electrical contact resistance has a smaller effect. Their simulations agreed with experiments at low currents, with deviations at higher currents attributed to Joule heating and property assumptions. This supports our choice to include contact effects and to validate electro-thermal models against measurements [53].

Wang et al. [49] analyzed the diffusion and separation of transient electromagnetic and thermal fields. Although their focus is eddy-current thermography physics rather than printed conductors, the takeaway is directly useful: early-time heating is governed by electromagnetic energy deposition, while later-time patterns are dominated by thermal diffusion. Practically, this means initial transients best capture localized effects (e.g., porosity/thickness contrasts) before diffusion blurs them—an insight we use when interpreting simulations and thermal maps [54].

Across busbars, thermoelectric modules, and pulsed thermography, prior work agrees on one point: accurate predictions require **coupled** electrical–thermal modeling with realistic geometry and interfaces. Building on that, our COMSOL models for screen-printed copper strips focus on thickness and porosity, evaluate early-time vs. diffusive regimes, and include contact effects where relevant [52], [53], [54].

## 2.5 Gaps and Limitations in Existing Literature

A review of the current literature reveals several recurring gaps related to the thermal behavior of printed copper structures. First, most studies focus on either experimental investigation or analytical and numerical modeling, while only a limited number combine both approaches in a unified framework. However, due to differences in materials, operating conditions, and geometries, their findings are often not directly applicable to printed copper conductors.

Second, previous research typically analyzes only one or two geometric parameters—usually thickness or porosity—without examining their combined influence. In screen-printed structures, the interaction between width, thickness, and porosity plays a critical role in electrical resistance, current crowding, and heat distribution. Evaluating these parameters separately can therefore overlook important multiphysics interactions.

Third, only a few studies integrate experimental measurements, microstructural characterization, and numerical simulations. Yet, such a combined approach is essential for understanding how porous conductive structures behave under real operating conditions. In addition, most reported work remains limited to laboratory-scale configurations, with insufficient attention given to industrially relevant processes such as multilayer screen printing or high-conductivity ink systems.

In summary, the literature shows a need for studies that simultaneously combine numerical modeling, experimental validation, and microstructural analysis while considering multiple geometric parameters together. The present work addresses this gap by examining the coupled

electro-thermal behavior of screen-printed copper strips as a function of width, thickness, and porosity, supported by SEM-based image analysis and COMSOL simulations.

## 2.6 Sample Preparation Techniques for Printed Copper Structures

### 2.6.1 Challenges in Fracturing Printed Copper Samples for Microstructural Analysis

Mechanical cutting was initially considered for cross-section preparation, but this method can deform porous printed layers and alter their internal structure. As an alternative, we explored the idea of cooling the samples to induce brittle fracture at a ductile-to-brittle transition temperature (DBTT). This approach is commonly effective for ceramics and BCC metals, which exhibit a clear DBTT and can be fractured cleanly at low temperatures. However, copper has an FCC crystal structure and remains ductile even under cryogenic conditions, meaning no sharp DBTT is observed [55]. Because FCC metals maintain multiple active slip systems, plastic deformation continues over a wide temperature range. As a result, copper cannot be embrittled sufficiently to produce clean fracture surfaces for microstructural observation.

This behavior is also supported by results from W–Cu composites. When the copper content is relatively low (below ~40%), a DBTT can still be detected; however, when the copper fraction exceeds ~48%, ductility becomes dominant and the transition disappears [56]. These findings confirm that copper—either in pure form or as the main phase in composites—suppresses brittle fracture and prevents the formation of sharp cross-sections.

### 2.6.2. Application of Ion Milling to Preserve the Microstructure of Printed Layers

To avoid the deformation issues associated with cutting or failed fracture attempts, ion milling was selected for preparing cross-sections of the printed copper strips. In this technique, a focused argon ion beam removes material gradually and without applying mechanical stress. This makes ion milling especially suitable for fragile or porous metal layers, where structural damage or cracking must be avoided. Compared to Ga-FIB, which may introduce artifacts such as phase changes or surface modification, ion milling produces cleaner surfaces that are better suited for SEM imaging and microstructural evaluation [57].

By preserving the delicate porous network, ion milling provided accurate cross-sections for porosity measurement and ensured that the resulting SEM images could be directly used for quantitative analysis and subsequent thermal–electrical simulations.

## 2.7 Summary and Justification for the Current Study

A detailed review of the literature highlights several important gaps that limit our understanding of the thermal and electrical behavior of screen-printed copper conductors. Although many studies have examined resistivity, heat generation, or current transport in metallic structures, only a small number have focused specifically on the Temperature Coefficient of Resistance (TCR) as a key indicator of reliability. Even among those studies, the combined influence of porosity, thickness, and width has rarely been explored, despite the fact that these three parameters act simultaneously on electron scattering, Joule heating, and current distribution in printed conductors.

Another limitation in previous work is the lack of an integrated methodology. Most studies rely on experimental measurements, microstructural imaging, or numerical simulations, but seldom attempt to link all three approaches together. For porous printed structures, however, these domains are directly interconnected. The microstructure governs electrical conductivity, conductivity affects heat generation, and the resulting thermal field influences long-term structural stability. Without combining these perspectives, the actual behavior of printed copper under operating temperatures cannot be fully understood.

In addition, many existing investigations are based on idealized laboratory conditions, thin-film assumptions, or fabrication methods that differ from industrial screen-printing processes. As a result, their findings cannot be easily applied to printed copper busbars on flexible substrates, where porosity, surface roughness, and cross-sectional non-uniformity are inherent features of the process.

To address these gaps, the present study adopts a comprehensive approach that incorporates experimental TCR measurements, SEM-based porosity analysis using ImageJ, and coupled electro-thermal simulations in COMSOL. By directly linking geometrical parameters and microstructural features to the thermal and electrical response, this research provides a more realistic understanding of TCR behavior in printed copper conductors. The outcome of this integrated method is expected to support improved reliability, stability, and performance in future printed electronic structures.

# Chapter-3 METHODOLOGY

## 3.1 Overall Research Design

This research was structured in three sequential phases to maintain consistency between fabrication, experimental measurements, and numerical modeling. The objective was to extract the Temperature Coefficient of Resistance (TCR) of printed copper conductors and to evaluate the influence of geometry and porosity on their thermo-electrical behavior. The hypotheses of the study were already presented in Chapter 1 and are not repeated here; in summary, previous studies suggest that thickness may influence TCR, while width and porosity are expected to have only minor or limited effects.

**Phase 1: Fabrication and sample preparation**

Copper strips were screen-printed on polyimide substrates following the industrial LF-360 protocol provided by Copprint. After drying and curing, the geometric parameters of each sample (including width and thickness, based on the number of printed layers) were measured and recorded for traceability, characterization, and later use in simulations.

**Phase 2: Resistance measurement and TCR calculation**

The electrical resistance of the samples was measured between 30 °C and 100 °C in order to compute TCR. The two-probe method was used as the primary measurement technique so that natural contact effects and surface irregularities in the printed conductors would not be removed. Since TCR is based on relative changes in resistance with temperature, these small contact effects do not significantly influence the final TCR value and instead provide a more realistic representation of the actual performance of printed copper tracks in real conditions. To validate the reliability of the data, four-probe measurements were also performed on selected samples. This method eliminates contact resistance and was used as a cross-validation reference to confirm the accuracy of the baseline resistance.

**Phase 3: Numerical modeling and comparison with experiments**

Electro-thermal simulations were carried out in COMSOL Multiphysics using the actual sample geometry and the porosity values obtained from SEM/ImageJ analysis. The simulated resistance–temperature curves were then compared with the experimental results to evaluate the accuracy of the model and to analyze the sensitivity of TCR to the studied parameters.

This three-phase workflow creates a clear and coherent methodology in which fabrication, measurement, and modeling support each other, enabling a realistic and reliable evaluation of the thermo-electrical behavior of screen-printed copper conductors.

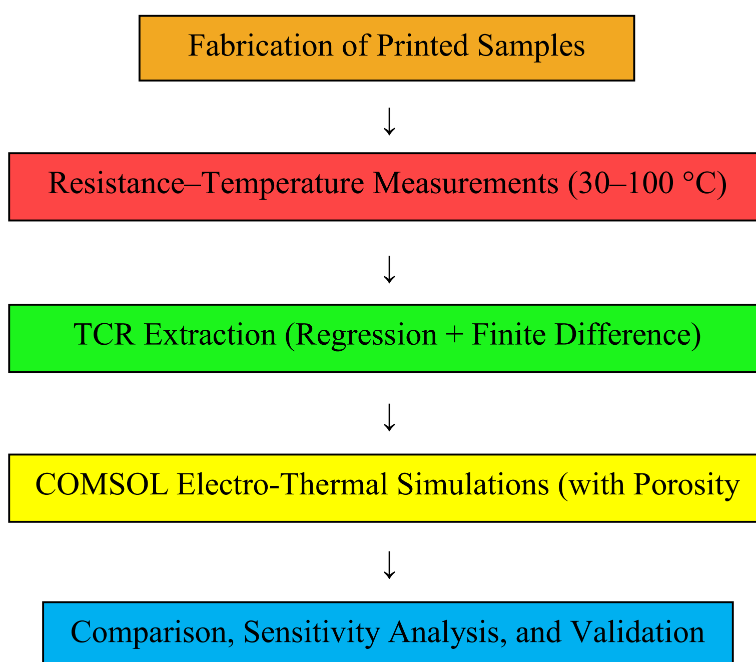


Figure 3-1 Workflow of the research methodology, illustrating the sequence from sample fabrication to measurement, simulation, and validation.

## 3.2 Materials and Ink

The conductive paste used in this study was Copprint LF-360, a copper-based ink developed for screen-printed electronic applications. According to the Technical Data Sheet, this material is a sinter-ready formulation that provides high metal loading, good adhesion, and reliable transfer through industrial screen-printing meshes. The uncured ink exhibits a viscosity of 13,000 to 17,000 mPa·s at 25 °C, a solids content of approximately 90 percent after a short drying step at 150 °C, and a density of about 4 g/mL. The copper particles follow a controlled size distribution (D50 < 1.0 µm and D90 < 7.0 µm), which helps improve packing during the curing process and contributes to the final electrical performance. Under sheet-to-sheet curing conditions, consisting of hot

pressing at 160 °C for 120 seconds, a dry film thickness of 25 µm can reach a sheet resistivity of less than 0.006 ohm per square. Recommended screen parameters for printing include polyester or stainless-steel meshes between 100 and 300, with emulsion thicknesses in the range of 10 to 40 µm, and squeegees with a hardness of 70 to 90 Shore[22].

Safety and handling information was taken from the product Safety Data Sheet. The LF-360 paste belongs to the LF3XX product family and contains a high proportion of copper particles, consistent with its target use in printed electronics. The material is supplied as a paste, with a reported density between 2 and 4.5 g/mL in the uncured state. The SDS identifies the intended use of the ink for screen-printed conductive structures, and it specifies storage below minus 10 degrees Celsius to maintain material stability. Only the essential handling notes relevant to the printing process were considered in this work, and detailed safety instructions are provided in another section of this thesis [21].

## 3.3 Printing and Curing Process

The samples in this study were produced through a screen-printing process using the LF-360 paste. The ink was mixed before printing and applied using meshes between 100 and 300, with an emulsion thickness of 10 to 40 µm and a squeegee hardness of 70 to 90 Shore. These settings provided a uniform printed layer and ensured stable ink transfer across the substrate surface [22]. After printing, the samples were dried at 90 °C for 120 seconds, using either a hot-air system or a reflow oven. They were then sintered according to the sheet-to-sheet curing protocol, consisting of hot pressing at 160 °C for 120 seconds. This curing method increases film density by improving particle contact and reducing voids, which directly supports the sheet resistivity and conductivity values noted in Section 3.2. Additional relaxation cycles are recommended by the manufacturer for certain polymer substrates, although they were not required for this work. The study also followed the storage and handling recommendations in the Safety Data Sheet to ensure reproducibility of the material properties across all fabricated samples [21].

## 3.4 Sample Series

To study the influence of geometry on the electrical and thermal behavior of the printed copper strips, samples with different widths and layer-based thicknesses were prepared. The main analysis focused on six widths: 20, 15, 12.5, 10, 7.5, and 5 millimeters. These samples provided complete

resistance–temperature data and were therefore used for calculating the Temperature Coefficient of Resistance (TCR).

Each width was printed in one, two, or three layers, resulting in approximate cured thicknesses of 17, 34, and 51 micrometers, respectively. These thickness values were later used to examine whether the current distribution and thermal response depend on the printed layer count.

Two narrower strips, with widths of 2.5 millimeters and 1 millimeter, were also fabricated. However, due to limited repetitions and incomplete temperature coverage, these samples were excluded from the main analysis. They are included only in the Appendix for transparency and completeness, but they do not contribute to the core results presented in this chapter.

## 3.5 Measurement of Resistance and Calculation of TCR

For each printed strip, the electrical resistance was measured from 30 °C to 100 °C in increments of 10 °C. At each step, the sample was allowed to reach thermal equilibrium before recording the resistance using a digital multimeter. Thermal equilibrium was confirmed when the measured temperature drifted by less than 0.2 °C over a period of at least 60 seconds, with the reference temperature defined as $T_0$ = 30 °C. The two-probe method was selected as the primary measurement technique because it preserves realistic contact conditions and natural surface irregularities in printed conductors. To verify the baseline resistance and confirm the validity of the results, selected measurements were repeated using the four-probe method on representative samples. The instrument accuracies and specifications are summarized in Section 3.10.

The Temperature Coefficient of Resistance (TCR) was determined using two complementary approaches. In the first approach, referred to as the Linear Regression Method, TCR was obtained from the slope of a best-fit line applied to the R–T measurement curve. This method captures the overall trend of resistance change with temperature and reduces the influence of random fluctuations in individual data points. In the second approach, called the Finite-Difference Method, TCR was calculated using the incremental change in resistance relative to the incremental change in temperature ($\Delta R/\Delta T$) between each pair of consecutive measurement steps. These finite-difference values were then combined using the arithmetic mean across the full range. Only data points with a clear and identifiable technical cause, such as unstable contact or incomplete thermal stabilization, were excluded as outliers.

Using two calculation methods provided a consistency check. The Linear Regression Method served as the primary reference for TCR, while the Finite-Difference Method was used to verify

that the resistance–temperature behavior remained approximately linear throughout the measurement range. The close agreement between the two methods increased confidence in the final reported TCR values and ensured that the results were not dependent on a single calculation approach.

## 3.6 Numerical Simulation

To better understand the electrical behavior of the printed copper strips under increasing temperature, numerical simulations were carried out using COMSOL Multiphysics. This software provides a powerful environment based on the Finite Element Method (FEM), allowing the physical conditions of the experiment to be reproduced numerically.

In these simulations, the temperature was increased from 30 °C to 100 °C in steps of 10 °C, exactly as in the experimental tests. At each temperature step, the total electrical resistance of the printed strip was calculated. This made it possible to establish the resistance–temperature (R–T) relationship and, in turn, determine the Temperature Coefficient of Resistance (TCR) numerically. Each sample was modeled according to its real geometry, defined by its measured width and number of printed layers. This ensured the highest possible consistency between the experimental setup and the numerical model.

The simulation process was carried out in two main stages:

Stage 1 — Direct Simulation of Experimental Tests (Without Porosity Variation) In the first stage, the same experimental conditions were reproduced without introducing any porosity changes. The electrical conductivity of each sample was set equal to the experimentally determined value. The temperature was increased step by step, and the resistance was recorded at each step. The obtained data were then compared directly with the experimental measurements to verify the accuracy and validity of the numerical model.

Stage 2 — Design of Experiments for Porosity Effect (DoE for Porosity Study) Since including all possible porosity and geometry combinations would result in an extremely large number of simulations, a Design of Experiments (DoE) approach was used to minimize the required runs while maintaining meaningful results. Three porosity levels — 0%, 9%, and 18% — were defined as factor levels to evaluate how internal voids affect electrical resistance and the resulting TCR.

This approach made it possible to analyze the main effect of porosity in a systematic and efficient way, without the need for excessive simulations. For each porosity level, resistance values were

calculated at different temperatures, and the corresponding TCR values were extracted separately for comparison.

### 3.6.1 Electrical Conductivity Calculations for Numerical Simulation Input

In this study, the electrical parameters of the printed copper tracks were derived directly from the Copprint LF-360

**Calculations:**

Electrical resistivity was calculated from the sheet resistance and reference thickness using:

$$\rho = R_sheet \times t_ref \quad (3\text{-}1)$$

where

$\rho$ is the bulk resistivity ($\Omega \cdot m$),

R_sheet is the sheet resistance ($\Omega/\square$),

t_reft is the reference cured thickness.

Substituting the reported values:

$$\rho = 0.006 \times 25\times10^{-6} = 1.5\times10^{-7}\ \Omega\cdot m$$

The electrical conductivity used in the COMSOL model was then computed as:

$$\sigma = 1 / \rho \quad (3\text{-}2)$$

which yields:

$$\sigma = 1 / (1.5\times10^{-7}) = 6.67\times10^{6}\ S/m$$

datasheet. According to the manufacturer's specifications, the sheet resistance of cured samples under standard S2S conditions (hot press at 160 °C, reference thickness 25 µm) is reported to be less than **0.**006 $\Omega/\square$ [22].

To use these data in COMSOL, the sheet resistance was converted into bulk resistivity and then into electrical conductivity, as shown below:

Since the datasheet specifies *less than* 0.006 $\Omega/\square$, the actual conductivity of the printed copper is expected to be slightly higher than $6.67\times10^{6}$ S/m. However, in this work a conservative value of $\sigma = 6.67\times10^{6}$ S/m was used as the input parameter in the numerical simulations. This ensured that the numerical model remained fully consistent with the experimental data and avoided introducing artificial parameters that could otherwise distort the physical behavior of the printed copper tracks.

In the Copprint documentation, the company reports only the sheet resistance of the cured copper layer, without providing any information about its internal porosity. Since printed copper films naturally contain voids after sintering, the value reported by Copprint represents the effective resistivity of a porous layer, not the intrinsic resistivity of fully dense copper.

However, in numerical simulation, the effect of porosity must be controlled and studied independently. For this reason, an equivalent porosity-free resistivity was calculated in this work. This intrinsic value was then used in the COMSOL model, while porosity was applied separately as a material-level parameter. In this way, the influence of porosity on electrical behavior could be isolated and scientifically analyzed.

To verify this approach, two different input configurations were tested in COMSOL:

Using the intrinsic resistivity (no-porosity) and then applying porosity inside the material model,

Using the effective resistivity reported by Copprint, without applying porosity in the model.

$$\rho_{\text{Copprint}} \Leftrightarrow \rho_{\textbf{intrinsic}} + \text{porosity effect}$$

$$1.50\times10^{-7}\ \Omega\cdot\text{m [porosity 0\%]} \Leftrightarrow 1.3061\times10^{-7}\ \Omega\cdot\text{m [porosity 9\%]}$$

Both configurations produced identical results, which confirms that Copprint’s reported data is equivalent to the intrinsic resistivity combined with a certain level of porosity. This validates our method for separating porosity effects in the simulations.

Table 3-1 Input parameters used in the COMSOL model for porosity levels of 0% and 9%. The calibration resistivity for 0% porosity was set to $1.50\times10^{-7}\ \Omega\cdot\text{m}$, and the corresponding value obtained for 9% porosity was $1.3061\times10^{-7}\ \Omega\cdot\text{m}$.

| **Parameter** | **Value** | **Value** | **Unit** | **Notes** |
|---|---|---|---|---|
| Porosity | 0 | 9 | % | input parameter |
| Resistivity | 1.5e-7 | 1.3061e-7 | Ω·m | used for initial calibration |

| Parameter | Value | Value | Unit | Notes |
|---|---|---|---|---|
| Environment Temp | 25 | 25 | °C | — |
| Busbar Temp | 30 | 30 | °C | input parameter |
| Busbar Width | 5 | 5 | mm | printed |
| Busbar Thickness | 0.017 | 0.017 | mm | measured |
| Busbar Length | 3 | 3 | in | printed |
| Resulting Resistance | 0.1371 | 0.1371 | Ω | COMSOL output |

## 3.7 Numerical Simulation Setup and Execution

Each printed copper strip was modeled in COMSOL Multiphysics based on its actual geometry, including the measured width and the number of printed layers. The models were designed to closely reproduce the real experimental setup so that the simulated and measured data could be directly compared.

The electrical resistivity and conductivity values used in the model were taken from the calculations presented in Section 3.6.1. Porosity values were obtained from the SEM image analysis using ImageJ and applied as material-level parameters in the model. This approach made it possible to consider how the internal structure and voids in the printed copper affect its electrical conductivity.

The simulations were performed at temperature points between 30 °C and 100 °C, with steps of 10 °C, matching the experimental procedure. At each temperature step, COMSOL automatically calculated the total electrical resistance of the copper strip. This method allowed for a direct, point-by-point comparison between numerical and experimental resistance–temperature (R–T) data, and the Temperature Coefficient of Resistance (TCR) was then extracted from the simulated results.

Figure 5 shows the COMSOL user interface used for this study. All important parameters such as porosity, reference resistivity, busbar dimensions, and temperature inputs were defined in this interface. The model automatically recalculated resistance values whenever any parameter was changed, making it a flexible tool for sensitivity analysis.

Table 3-2 Input parameters used in the COMSOL model. The symbols A, B, C, and D represent interface-defined input values within the software, included here to illustrate the overall structure of parameters required for the simulation workflow. The numerical values associated with these parameters are reported in the Results section.

| Parameter | Value | Unit |
|---|---|---|
| Porosity | A | % |
| Resistivity | 1.3061e-7 | Ω·m |
| Environment Temp | 25 | °C |
| Busbar Temp | B | °C |
| Busbar Width | C | mm |
| Busbar Thickness | D | mm |
| Busbar Length | 3 | in |
| Resulting Resistance | Result | Ω |

In the geometry setup, the strip length was fixed at 3 inches, while the widths were varied from 5 to 20 mm (5, 7.5, 10, 12.5, 15, and 20 mm). These dimensions were the same as those used in the actual printing process, ensuring full consistency between the experimental and numerical results.

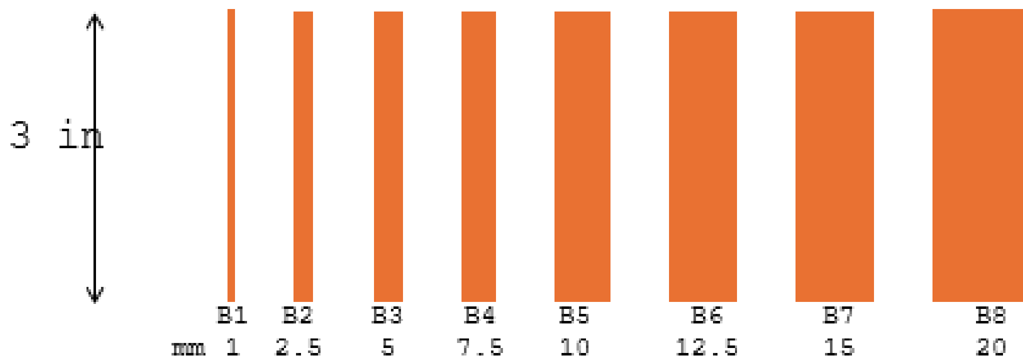


Figure 3-2 Schematic of the printed copper strips with a fixed length (3 in) and varying widths from 1 to 20 mm (B1–B8).

### 3.7.1 Numerical Design, Data, and Analysis Procedure

The numerical analysis in this study was conducted to better understand how porosity, thickness, and width influence the electrical resistance and temperature behavior of printed copper strips. The goal was to keep the simulations consistent with the experimental setup while minimizing the number of simulation runs through a systematic and efficient design.

The same procedure used in the experimental resistance–temperature (R–T) measurements was applied in the simulations. The temperature range was set between 30 °C and 100 °C, increasing in 10 °C steps, and the total electrical resistance of each printed strip was calculated at each point. The samples included three nominal thicknesses (approximately 17, 34, and 51 μm) and six widths ranging from 5 to 20 mm (5, 7.5, 10, 12.5, 15, and 20 mm).

The very narrow strips (1 and 2.5 mm) were not included in this part of the work because their experimental data were unstable and could not be validated. Since these samples already showed poor and unreliable data during the experimental phase, they were excluded from the numerical modeling as well. Only the consistent and validated datasets were used for the simulations and further analysis.

Before importing the data into COMSOL, each R–T curve was reviewed for smoothness and consistency. All measurements showed a clear and nearly linear increase in resistance with temperature, confirming that the results were accurate and suitable for numerical use.

The Temperature Coefficient of Resistance (TCR) was calculated using two complementary approaches: a finite-difference method, which determined TCR from the change in resistance between consecutive temperature steps, and a linear-fit method based on the slope of the R–T curve. Both methods gave consistent and comparable results, confirming that the printed copper strips followed a stable and predictable thermal–electrical response.

This combined experimental–numerical approach provided reliable data for comparison, ensuring that the simulations accurately represented the physical behavior of the real samples.

#### 3.7.1.1 Numerical Model and Comparison with Experimental Data

The numerical model was created in COMSOL Multiphysics using the Electric Currents module. The simulated geometry was identical to the printed samples, with a fixed length of 3 inches, and the same measured widths and thicknesses used in the experiments. The electrical parameters, including resistivity and conductivity, were taken directly from the calculations in Section 3.6.1,

while porosity values were obtained from SEM image analysis using ImageJ and applied as material properties in the model.

No calibration or parameter adjustment was performed in this part. The simulations were executed exactly as designed, using the same conditions and parameters defined by the experimental data. The results were then compared directly with the experimental measurements. Although small differences were observed between the two datasets, they were completely explainable based on realistic factors such as porosity and small variations in current distribution. Because these differences were physically consistent and scientifically reasonable, the simulated and experimental results were considered to be in good agreement.

#### 3.7.1.2 *Sensitivity Analysis Using Taguchi Design*

To study the influence of all main parameters while minimizing the number of simulations, a Taguchi L9 orthogonal design was applied. This design made it possible to evaluate three factors—porosity, thickness, and width—each at three levels, resulting in nine well-structured simulation runs.

The factor levels were as follows:

Porosity: 0%, 9%, and 18%

Thickness: 17 μm, 34 μm, and 51 μm

Width: 5 mm, 12.5 mm, and 20 mm

For each combination, the resistance–temperature (R–T) relationship was simulated, and the TCR values were extracted using both methods described earlier. The Taguchi analysis identified which parameter had the most significant effect on TCR and how the factors interacted.

This structured approach allowed the influence of porosity and geometry to be studied in a systematic and efficient way, without requiring a large number of simulations. The results provided a clear understanding of how structural and geometrical features affect the electrical performance of printed copper strips, forming the basis for further discussion in Chapter 5.

## 3.8 Sample Preparation with Ion Milling

To prepare accurate cross-sections of the printed copper strips, several approaches were considered. Although brittle-fracture methods are sometimes used for ceramics and BCC metals due to the presence of a Ductile-to-Brittle Transition Temperature (DBTT), this approach is not suitable for copper. As an FCC metal, copper remains ductile even at very low temperatures because of its multiple active slip systems, and therefore does not exhibit a clear brittle transition.

Previous studies also indicate that in W–Cu composites, when copper is present above approximately 48%, no brittle transition is observed. As a result, the brittle-fracture technique could not be applied to our samples.

To avoid mechanically induced artifacts such as cracks, deformation, or delamination, ion milling was selected as the sample-preparation method. In ion milling, a controlled beam of argon ions gradually removes material from the surface without applying mechanical force. This ensures that the internal porous structure formed during printing and sintering remains unchanged, providing a true representation of the microstructure.

Ion milling offered several advantages for this work, including preservation of the real pore network, prevention of stress-induced defects, suitability for soft and porous printed layers, and the ability to produce smooth, high-quality cross-sections. These clean surfaces were essential for reliable SEM imaging and for generating accurate porosity data to be used later in the simulations.

## 3.9 SEM Imaging and Analysis

After ion milling, the samples were examined using a Scanning Electron Microscope (SEM). SEM was selected because it provides sufficient resolution and magnification to observe microstructural details such as pore distribution, particle bonding, and layer uniformity, which cannot be captured by standard optical microscopy.

SEM images were used not only for qualitative observation, but also to extract quantitative information about the internal structure of the printed copper. Image analysis made it possible to calculate porosity, observe pore connectivity, and gain a clearer understanding of how the microstructure relates to electrical behavior. The numerical results obtained from the images were later used as input for the COMSOL simulations, ensuring that the numerical model reflected the real printed structure. In this way, SEM imaging served as an essential link between the experimental measurements and the numerical modeling.

## 3.10 SEM Imaging and ImageJ Analysis Protocol

To obtain porosity values in a repeatable and measurable way, SEM images of the ion-milled cross-sections were analyzed using ImageJ. The procedure consisted of the following steps:

1. Importing and scaling each image using the provided scale bar to ensure accurate dimensional calibration.
2. Applying minimal brightness and contrast adjustments, without altering structural details.
3. Using a thresholding process to separate copper regions, voids, and uncertain boundary areas. To avoid underestimating porosity, the uncertain regions were conservatively classified as voids.
4. Counting the total pixels and void pixels to calculate porosity, and extracting additional information such as pore size and distribution.
5. Repeating the analysis over multiple fields of view and averaging the results to obtain a representative porosity value for each sample.

The goal of this section is to document a clear and repeatable method for extracting porosity data from SEM images. All calculated porosity values, along with related graphs, are presented in Chapter 4.

## 3.11 Instruments, Calibration, and Measurement Uncertainty

All instruments used in this research were operated under factory calibration conditions. The measurement accuracies and tolerances were taken directly from the official manufacturer specifications, as summarized below.

### 3.11.1 Source Measure Unit (SMU): Keithley 2400

The Keithley 2400 SourceMeter was used to supply current and measure voltage in all electrical tests. According to the manufacturer's datasheet, the DC voltage accuracy (1-year, at 23 ± 5 °C) is ±(0.012% of reading + 300 μV) for the 200 mV and 2 V ranges, and ±(0.015% of reading + 1.5 mV) for the 20 V range. The DC current accuracy (1-year) ranges from ±(0.029% + 300 pA) at the 1 μA range to ±(0.22% + 570 μA) at the 1 A range. These specifications ensure reliable resistance–temperature measurements in this study.

### 3.11.2 Thermometer: B&K Precision 390A with Type-K Thermocouple

Temperature measurements were recorded using a B&K Precision 390A digital thermometer with a Type-K thermocouple. The accuracy specified by the manufacturer is ±(0.8% of reading + 2 °C)

from −50 to 400 °C and ±(1.0% of reading + 2 °C) from 0 to 1300 °C, which is adequate for the target range of 30–100 °C in this study.

### 3.11.3 Four-Point Probe System

A standard four-point probe with tungsten tips and 1.587 mm (62.5 mil) tip spacing was used to measure the electrical resistance of printed copper strips. This setup helps ensure stable contact and minimizes measurement error on surfaces with moderate roughness.

### 3.11.4 Scanning Electron Microscope (SEM): Hitachi SU8230

Surface and cross-sectional microstructures were examined using a Hitachi SU8230 field-emission SEM, which provides approximately 0.8 nm resolution at 15 kV. Since SEM imaging in this study was used qualitatively to observe morphology and porosity, no dimensional calibration was required.

The remaining uncertainty in TCR is mainly associated with temperature measurement accuracy and contact variations during two-probe tests; however, these effects were minimized through equilibrium waiting times, four-probe validation, and repeated measurements.

A summary of the measurement equipment and their specifications is provided to ensure transparency and traceability of the experimental data.

# Chapter-4 RESULTS AND DISCUSSION

## 4.1 Chapter Introduction

In this chapter, the experimental and numerical results related to the printed copper strips are presented. First, cross-sectional SEM images are shown, and the internal porosity is quantified using ImageJ software. These microstructural results are used as input parameters for the subsequent electrical measurements and simulations.

Next, the resistance–temperature data and the calculated Temperature Coefficient of Resistance (TCR) are presented for different strip geometries. The results are summarized in tables and graphs to allow a clear comparison of the measured resistance values over the temperature range.

Finally, the numerical simulation results obtained from COMSOL are presented and placed alongside the experimental measurements for reference. The results are organized in a consistent format to facilitate comparison between the different data sets.

The purpose of this chapter is to present the obtained results in a clear and structured manner, including the microstructural observations, experimental measurements, and numerical simulations of the printed copper strips.

## 4.2 SEM and ImageJ Results

To investigate the microstructure of the printed copper strips, cross-sectional samples were prepared using Ion Milling and imaged with a Scanning Electron Microscope (SEM). The images were then processed with ImageJ to quantify the internal porosity.

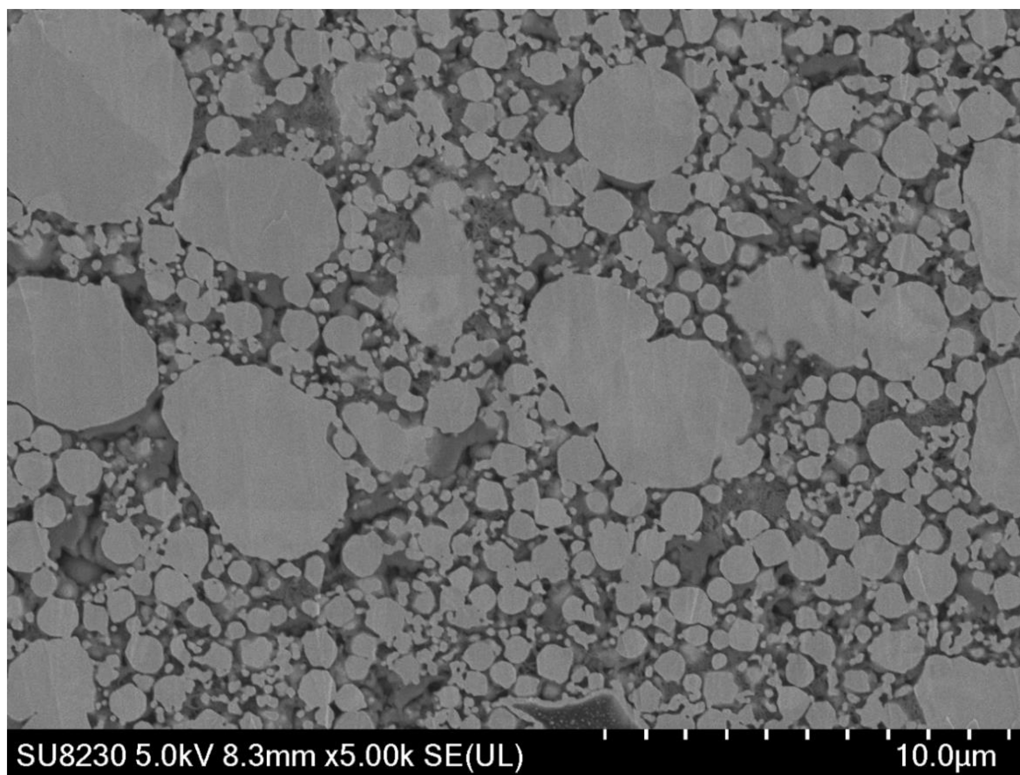


a

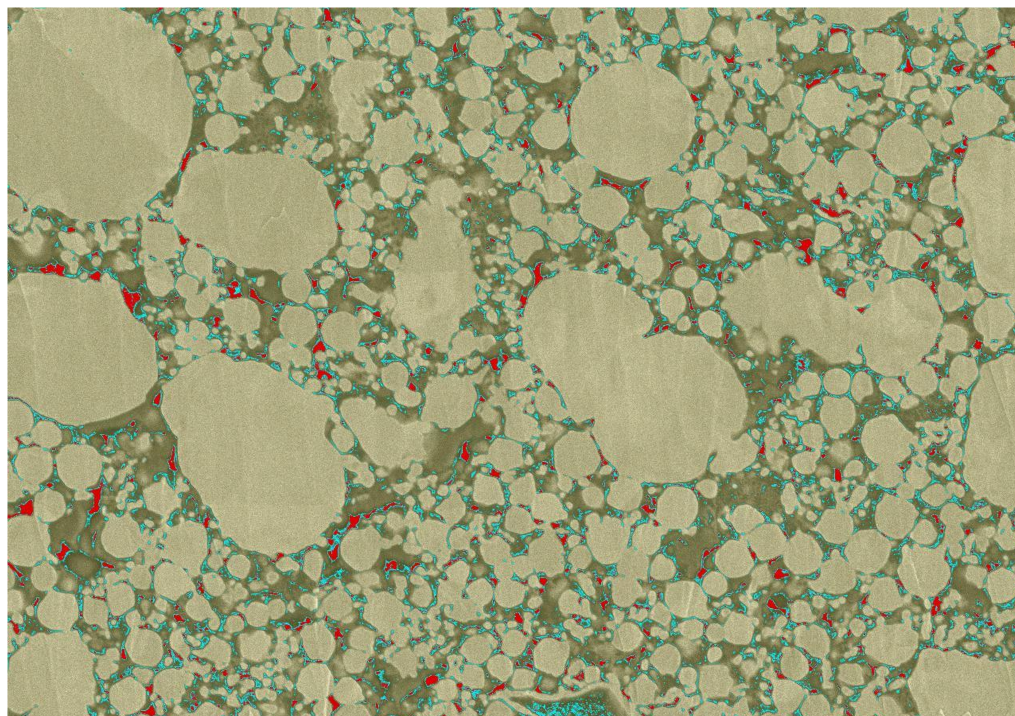

b

Figure 4-1 A. Raw SEM cross-sectional image of the printed copper strip (magnification ×5000). B. Segmented SEM image processed with ImageJ: yellow = copper, red = pores with high certainty, blue = uncertain transition regions. Estimated porosity: 8.6%.]

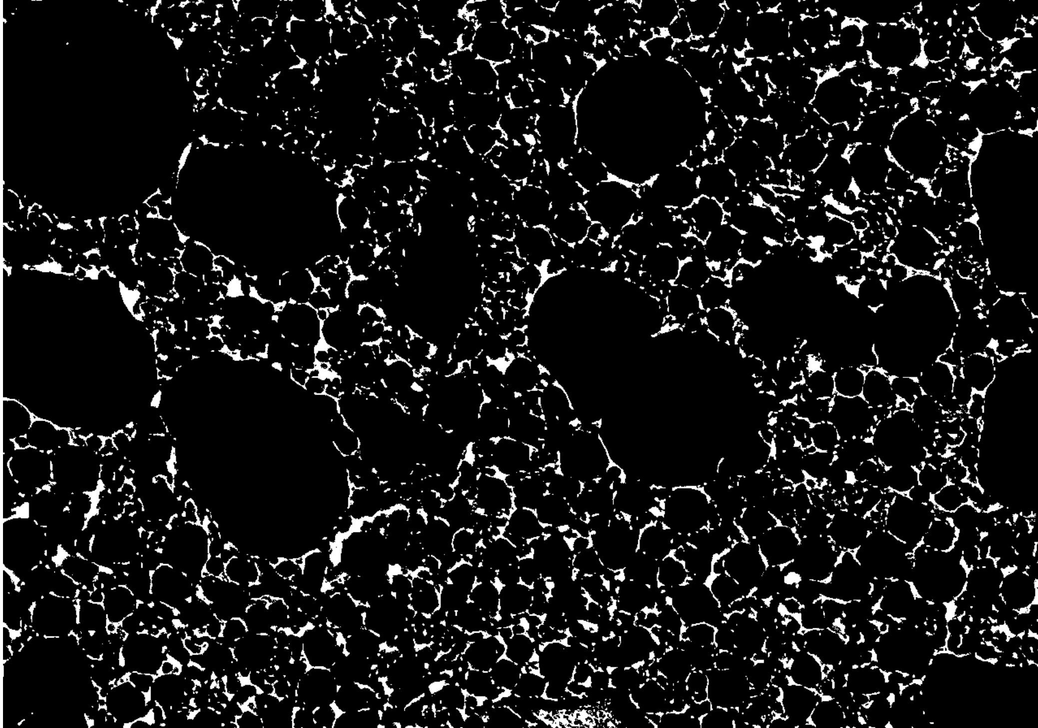

a

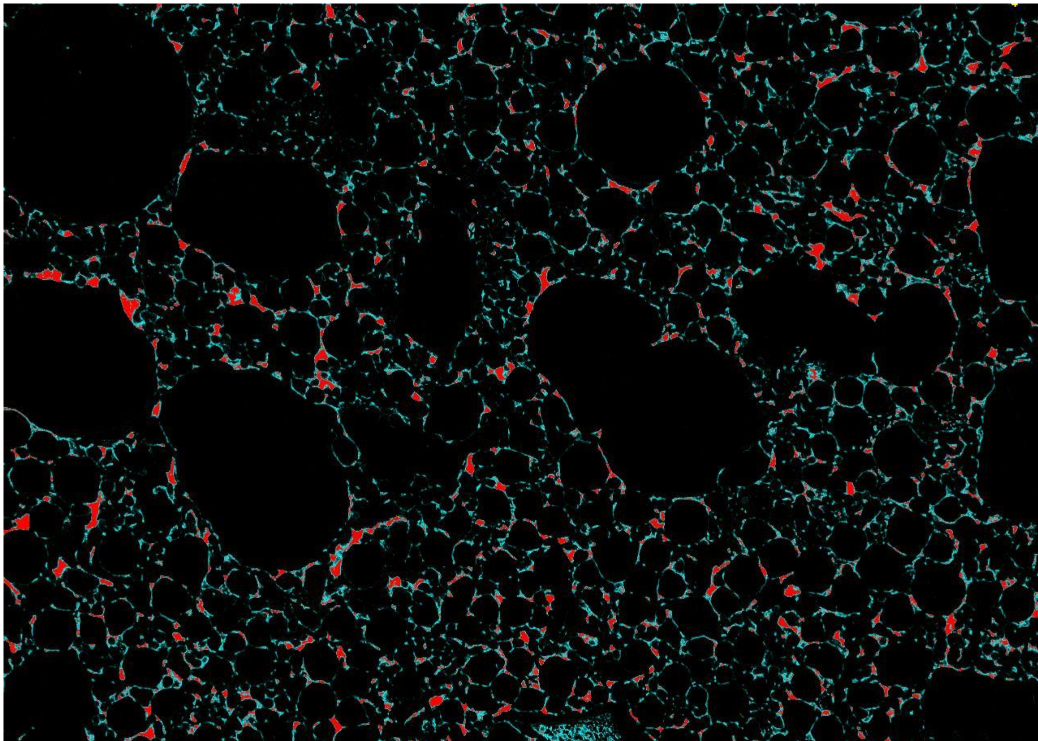

b

Figure 4-2 a) Binary (black/white) ImageJ output. White areas correspond to pores. Estimated

porosity: 8.6%. b) Processed high-contrast image showing pore boundaries more clearly.

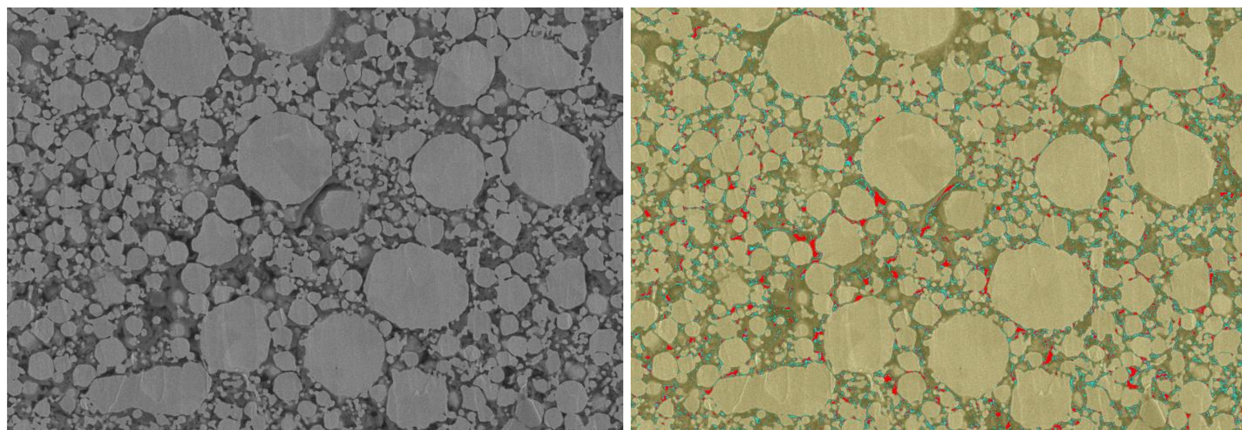

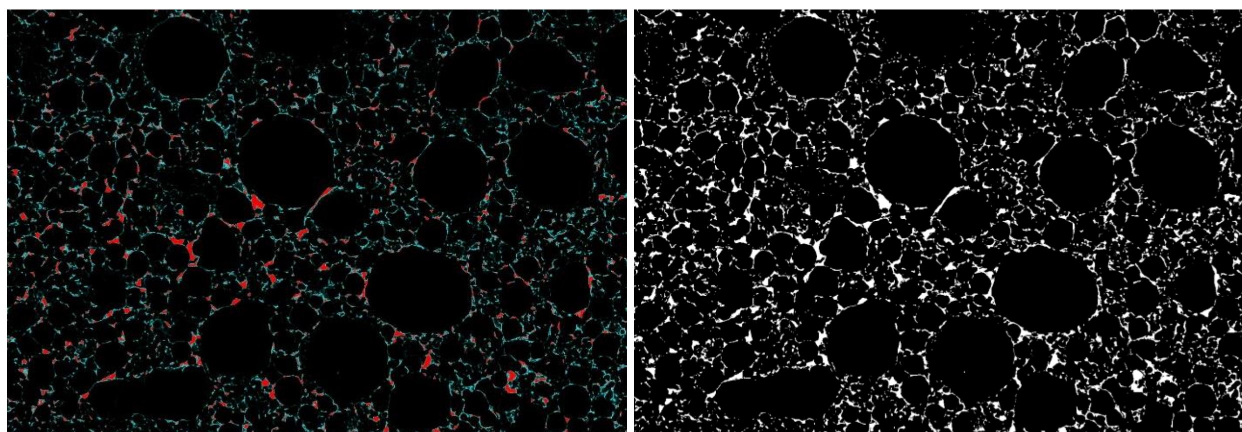

2nd series

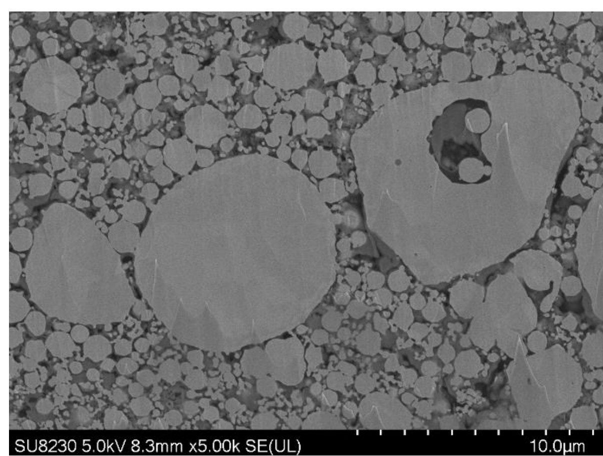


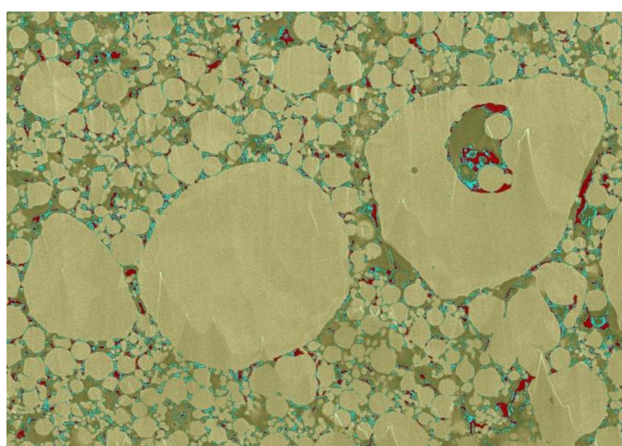

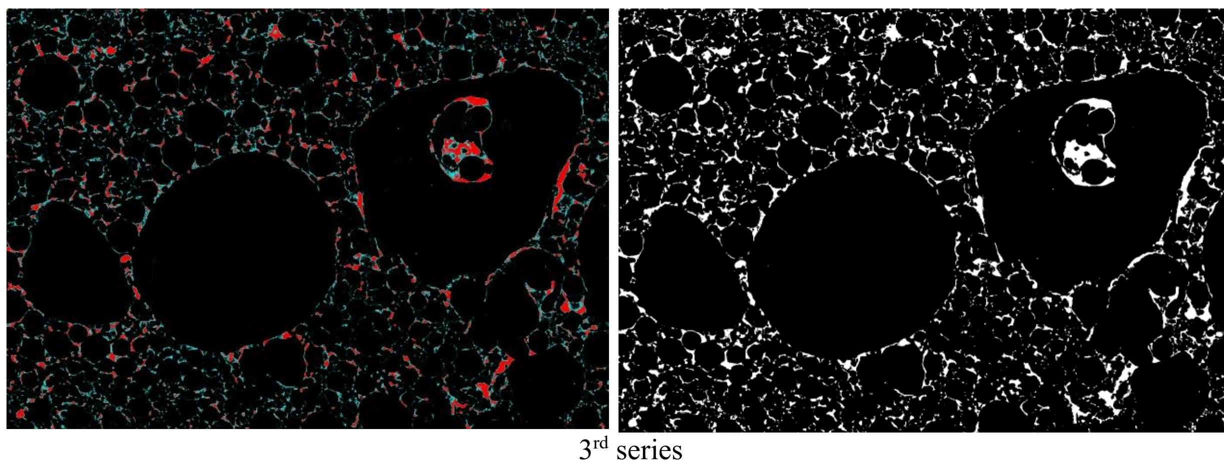

3rd series

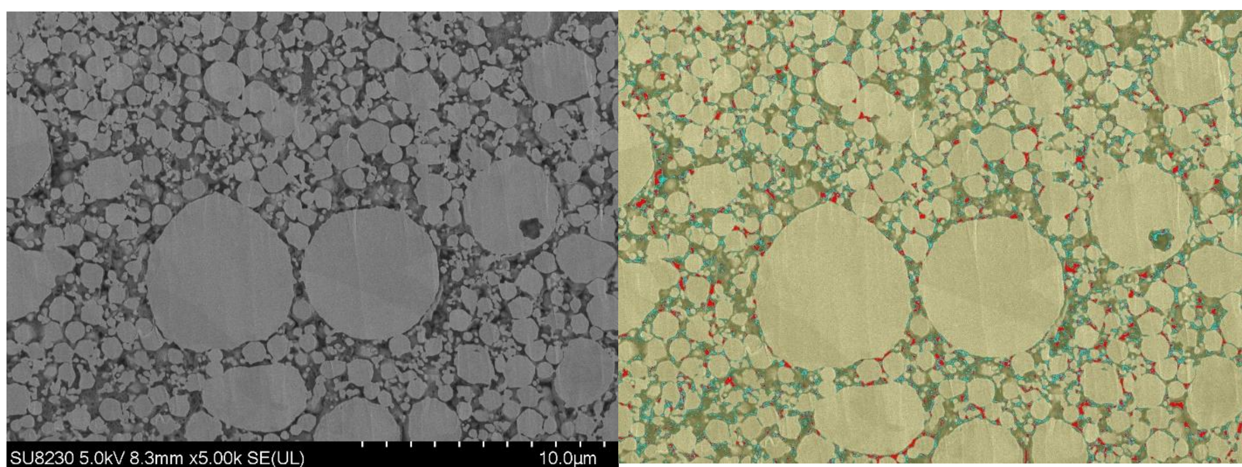


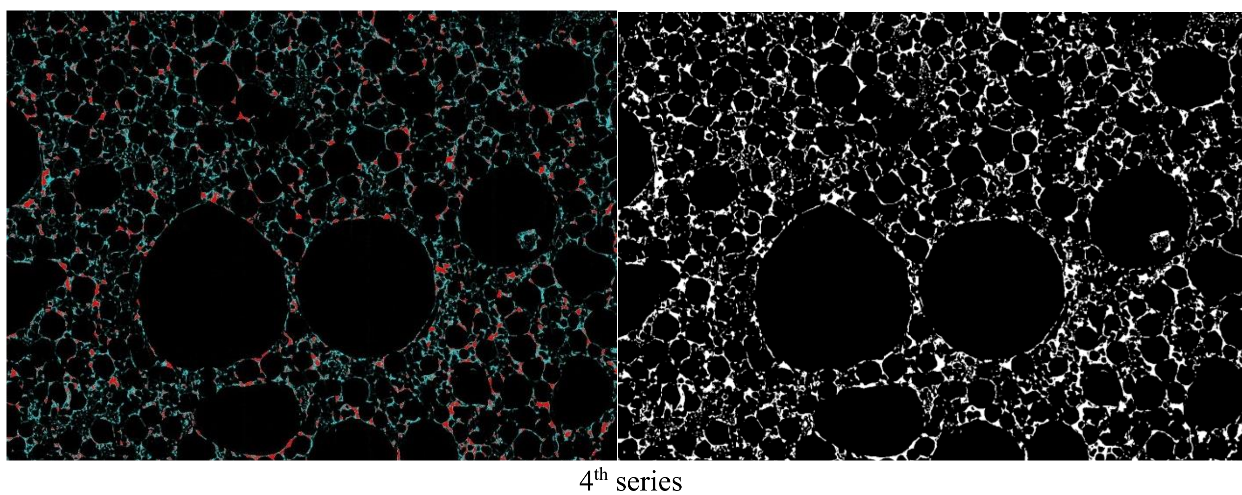

4th series

Figure 4-3 Additional SEM micrographs and ImageJ segmentation outputs illustrating other analyzed regions used for porosity estimation. The calculated porosity values from these images fall

within the reported range (7.8%–10.7%) and contribute to the overall average of approximately 8.9%.

Figure 4-1(a) shows the raw SEM image, while part (b) shows the segmented version. In the segmentation analysis, the yellow regions correspond to copper, the red regions represent pores with high certainty, and the blue regions indicate uncertain areas that were difficult to classify due to their intermediate grey contrast. Considering the three-dimensional nature of the printed structure, these uncertain regions can also be treated as voids, since they most likely represent copper located deeper than the most exposed surface of the film. Therefore, in the porosity estimation, both the certain pores (red) and the uncertain regions (blue) were included in the calculation.

In Figure 4-2 (a) presents the binary output from ImageJ, which provides a clear separation between copper (black) and voids (white). Part (b) shows the high-contrast processed image that highlights pore boundaries more distinctly. Together, these images confirm the porosity results obtained from the segmentation analysis.

In total, four different fields of view were analyzed using the same procedure. The estimated porosity values for the individual images were 7.8%, 8.6%, and 10.7%, with the fourth field yielding a similar result. The average porosity across all four images was approximately 8.9%. These porosity values show a consistent level of internal voids within the printed copper structures. The averaged porosity value was later used as an input parameter for the resistance–temperature measurements and the numerical simulations in COMSOL. Additional segmented images and detailed outputs for all analyzed fields are provided in the Appendices at the end of this thesis.

Additional SEM micrographs and their corresponding ImageJ segmentation outputs are presented in Figure 4-3 to illustrate other analyzed regions used for porosity estimation. These complementary views confirm the consistency of the measured porosity values within the reported range and support the reliability of the overall average.

## 4.3 Experimental R–T and TCR Results

In this section, the experimental resistance–temperature (R–T) measurements and the calculated Temperature Coefficient of Resistance (TCR) values for the printed copper strips are presented.

First, the R–T results obtained from the two-probe and four-probe methods are reported. Then, a comparison between the two measurement approaches is provided.

### 4.3.1 Experimental R–T Data Measured by the Two-Probe Method

The resistance of the printed copper strips was measured in the range of 30 °C to 100 °C, in 10 °C increments, for three thickness groups (≈17 µm, ≈34 µm, and ≈51 µm). To maintain consistency, only strip widths from 5 mm to 20 mm are included in the main results. The complete raw data for all widths are provided in the Appendix.

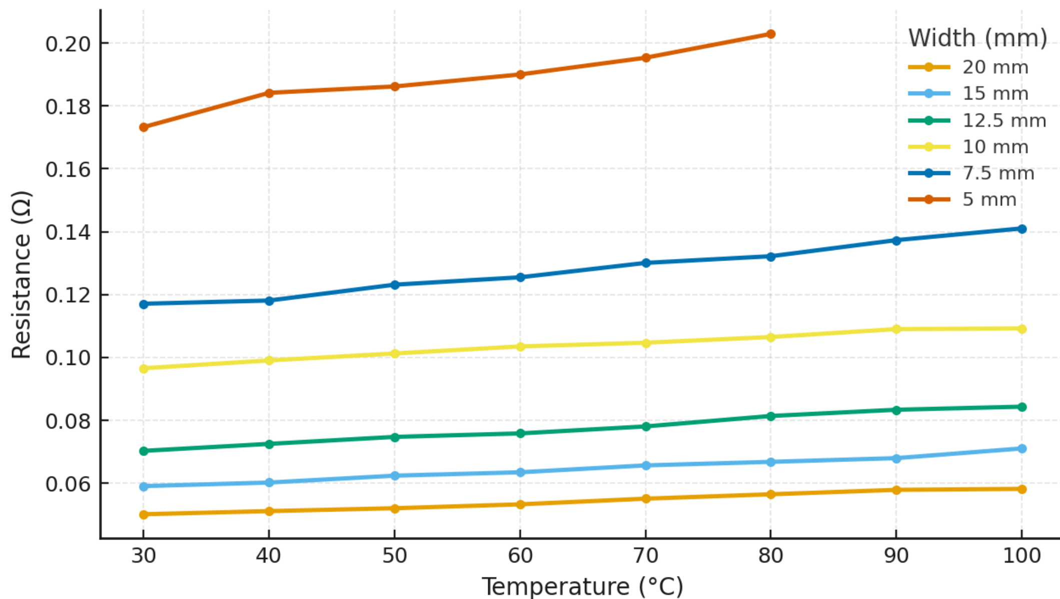


Figure 4-4 Experimental R–T curves for single-layer printed copper strips (≈17 µm), measured using the two-probe method.

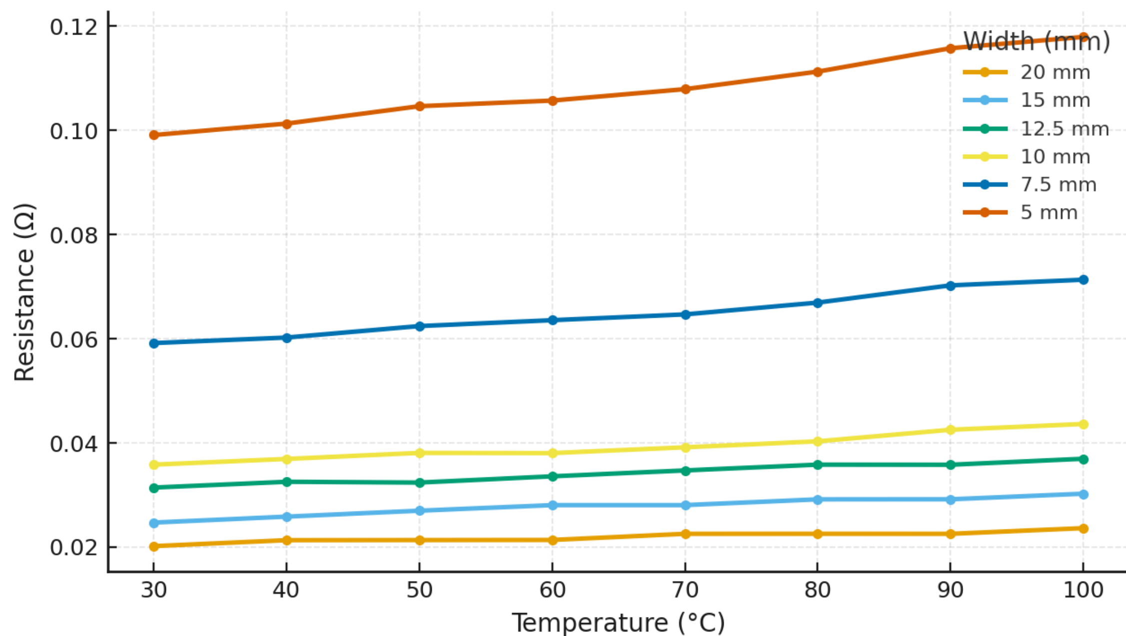


Figure 4-5 Experimental R–T curves for double-layer printed copper strips (≈34 μm), measured using the two-probe method.

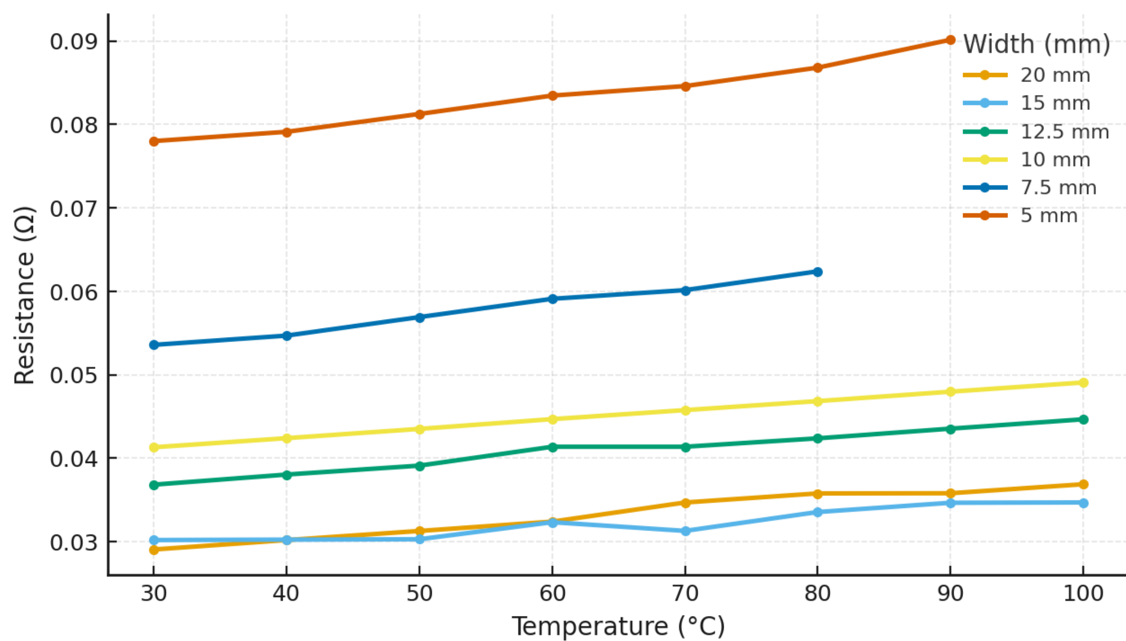


Figure 4-6 Experimental R–T curves for triple-layer printed copper strips (≈51 μm), measured using the two-probe method.

### 4.3.2 Experimental R–T Data Measured by the Four-Probe Method

The same R–T measurements were repeated using the four-probe method to eliminate the effects of contact resistance and verify the accuracy of the results. The temperature range, sample geometry, and test conditions were identical to the two-probe measurements. To avoid redundancy, only the R–T curves are presented in the main text. The complete numerical datasets used to generate these figures are provided in Appendix.

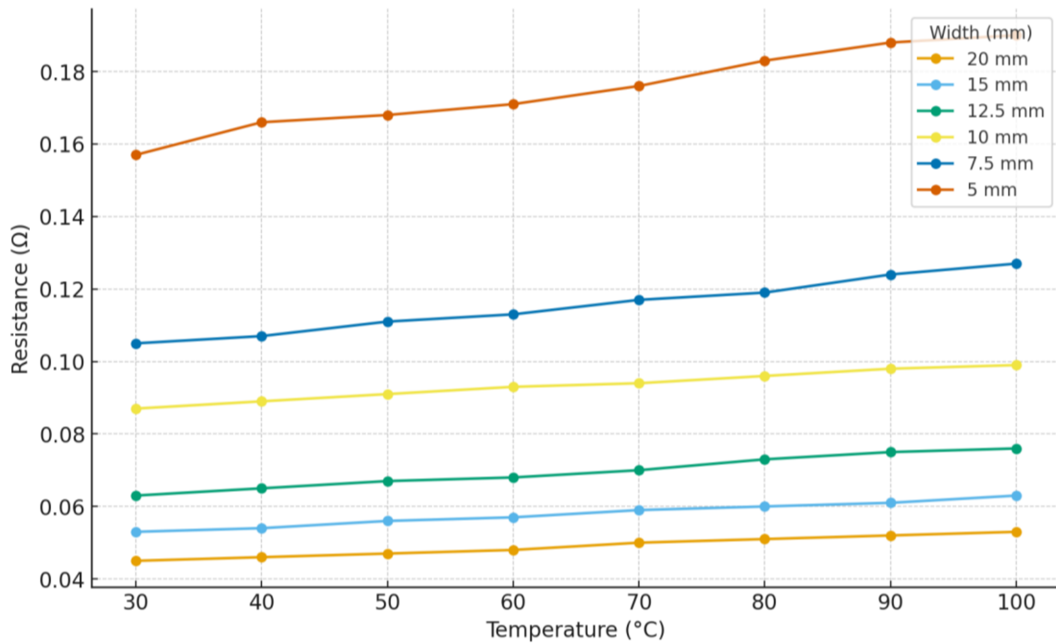


Figure 4-7 Experimental R–T curves for single-layer printed copper strips (≈17 μm), measured using the four-probe method.

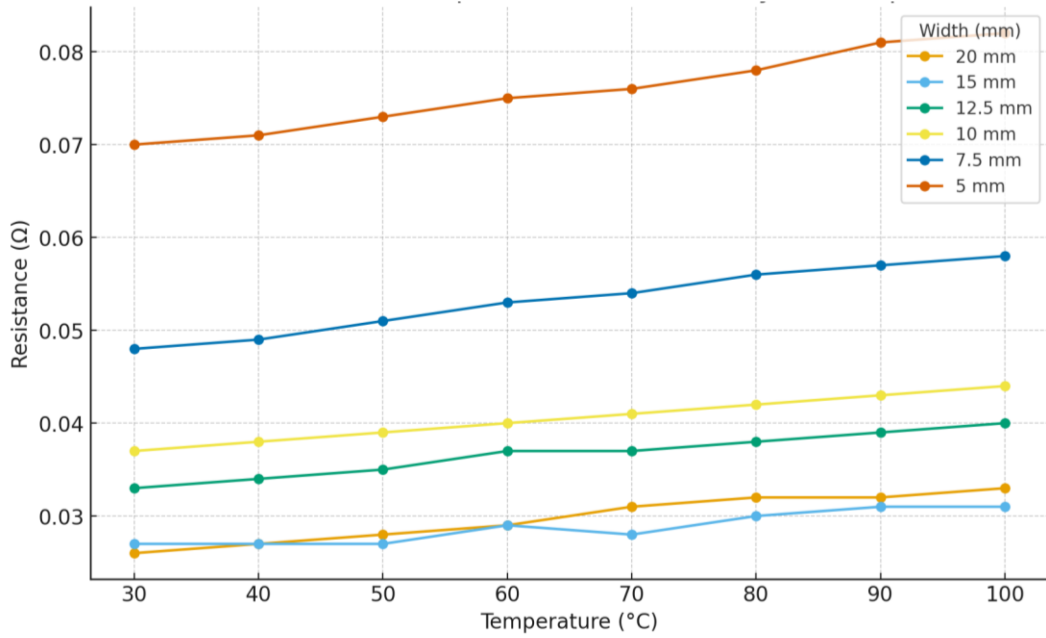


Figure 4-8 Experimental R–T curves for double-layer printed copper strips (≈34 µm), measured using the four-probe method.

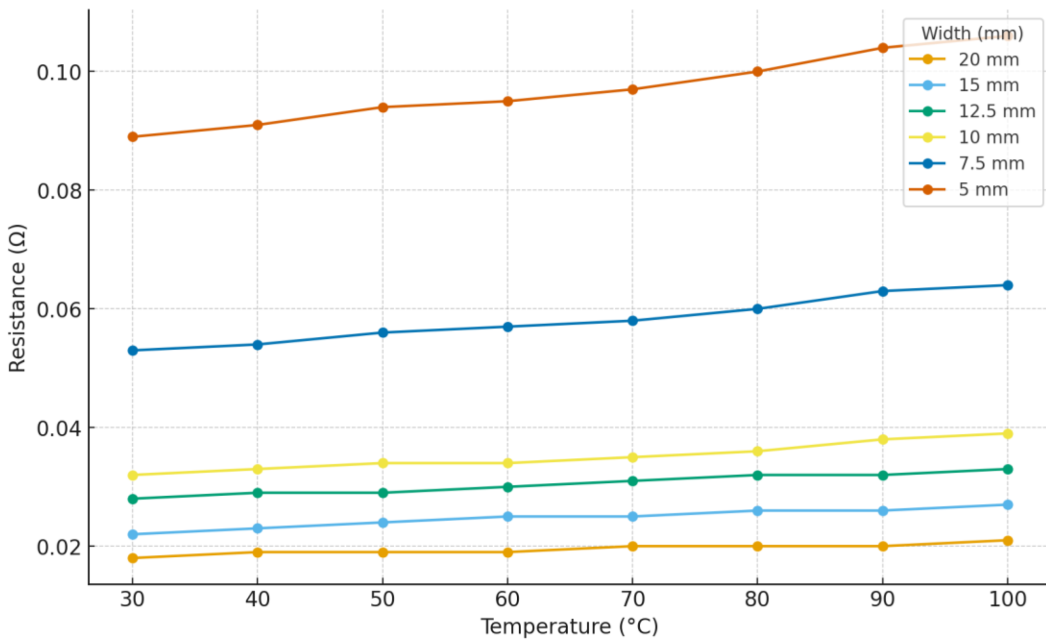


Figure 4-9Experimental R–T curves for Triple-layer printed copper strips (≈34 µm), measured using the four-probe method.

### 4.3.3 Experimental TCR Calculation Method

The Temperature Coefficient of Resistance (TCR) was calculated from the experimental R–T data using the reference temperature of 30 °C. For each sample, the resistance values were processed in Excel, and two estimators were obtained:

(1) an interval-based TCR

(2) a linear-fit TCR.

The linear-fit method was selected as the final reported value because it provides a more stable result and minimizes the effect of point-to-point fluctuations. The complete calculation sheets, including ΔR, ΔT, interval TCR values, and linear regression results, are provided in the Appendix.

Table 4-1. Experimental TCR Values by Thickness measured by two-probe method

| Thickness (µm) | n (samples) | Avg Interval TCR (1/°C) | Avg Linear Fit TCR (1/°C) |
|---|---|---|---|
| 17.0 | 6.0 | 0.002357 | 0.002708 |
| 34.0 | 6.0 | 0.002529 | 0.003004 |
| 51.0 | 6.0 | 0.002624 | 0.002722 |

Table 4-2. Experimental TCR Values by width measured by two-probe method

| Width (mm) | n (samples) | Avg Interval TCR (1/°C) | Avg Linear Fit TCR (1/°C) |
|---|---|---|---|
| 5.0 | 3.0 | 0.002284 | 0.002768 |
| 7.5 | 3.0 | 0.002528 | 0.003121 |
| 10.0 | 3.0 | 0.002381 | 0.002538 |
| 12.5 | 3.0 | 0.002603 | 0.002822 |
| 15.0 | 3.0 | 0.002570 | 0.002747 |
| 20.0 | 3.0 | 0.002654 | 0.002873 |

Table 4-3Experimental TCR Values by Thickness measured by four-probe method

| Thickness (µm) | n (samples) | Avg Interval TCR (1/°C) | Avg Linear Fit TCR (1/°C) |
|---|---|---|---|
| 17.0 | 6.0 | 0.002327 | 0.002500 |
| 34.0 | 6.0 | 0.002510 | 0.002837 |
| 51.0 | 6.0 | 0.002158 | 0.002188 |

Table 4-4Experimental TCR Values by width measured by four-probe method

| Width (mm) | n (samples) | Avg Interval TCR (1/°C) | Avg Linear Fit TCR (1/°C) |
|---|---|---|---|
| 5.0 | 3.0 | 0.002557 | 0.002800 |
| 7.5 | 3.0 | 0.002752 | 0.003052 |
| 10.0 | 3.0 | 0.001551 | 0.001595 |
| 12.5 | 3.0 | 0.002481 | 0.002621 |
| 15.0 | 3.0 | 0.002071 | 0.002180 |
| 20.0 | 3.0 | 0.002578 | 0.002802 |

### 4.3.4 Experimental TCR Results (Comparison of Two-Probe and Four-Probe Methods)

The Temperature Coefficient of Resistance (TCR) values obtained from the two-probe and four-probe measurements follow the same overall trend for all thicknesses and widths. However, the two-probe method yields slightly higher TCR values because of the additional contact resistance at the electrode interfaces. Since the four-probe configuration eliminates this effect, it provides more accurate results and is therefore selected as the reference for the remaining analysis. The two-probe results, however, remain useful because they validate the same thermal behavior and confirm the reliability of the experimental observations.

Table 4-5Comparison of TCR values measured by the two-probe and four-probe methods (by thickness)

| **Thickness (µm)** | **TCR — Two-Probe (1/°C)** | **TCR — Four-Probe (1/°C)** | **% Difference** |
|---|---|---|---|
| 17 | 0.002708 | 0.002500 | 8.3% |
| 34 | 0.003004 | 0.002837 | 5.9% |
| 51 | 0.002722 | 0.002188 | 24.4% |

Table 4-6Comparison of TCR values measured by the two-probe and four-probe methods (by width)

| **Width (mm)** | **Two-Probe TCR (1/°C)** | **Four-Probe TCR (1/°C)** | **Δ (Two − Four)** | **Percent Difference** |
|---|---|---|---|---|
| 5.0 | 0.002768 | 0.002800 | −0.000032 | 1.1% |
| 7.5 | 0.003121 | 0.003052 | 0.000069 | 2.3% |
| 10.0 | 0.002538 | 0.001595 | 0.000943 | 59.1% |
| 12.5 | 0.002822 | 0.002621 | 0.000201 | 7.7% |

| | | | | |
|---|---|---|---|---|
| 15.0 | 0.002747 | 0.002180 | 0.000567 | 26.0% |
| 20.0 | 0.002873 | 0.002802 | 0.000071 | 2.5% |

The comparison in theTables shows that the four-probe method consistently produces lower TCR values, while the two-probe method introduces a positive offset. Despite the magnitude of the differences—especially at smaller thicknesses and widths—the overall thermal trend remains unchanged. Therefore, the four-probe results are adopted for the final TCR evaluation and modeling in the next sections.

The following tables present the experimental TCR values obtained from the two-probe and four-probe measurements for different strip thicknesses and widths. These data are used to compare the two measurement methods and to observe the effect of geometry on the TCR of the printed copper conductors.

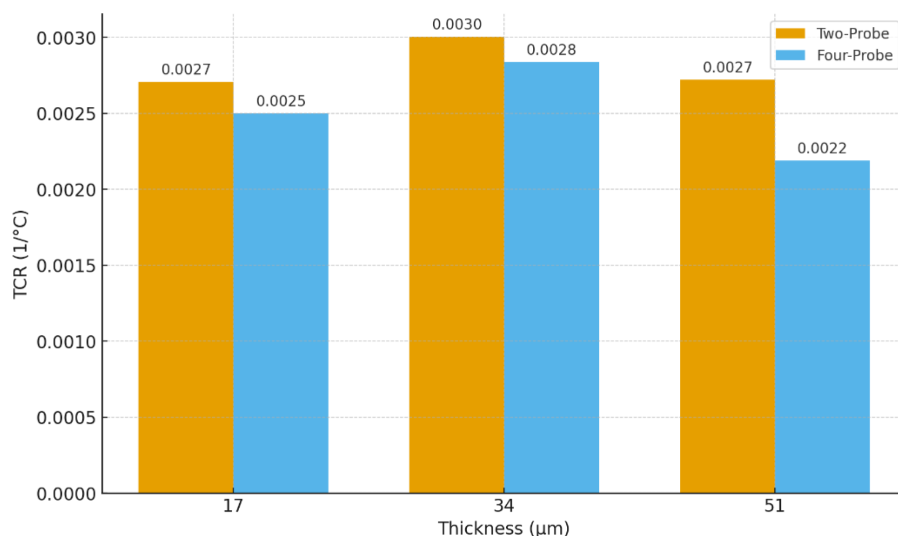


Figure 4-10Comparison of TCR by width using two-probe and four-probe measurements

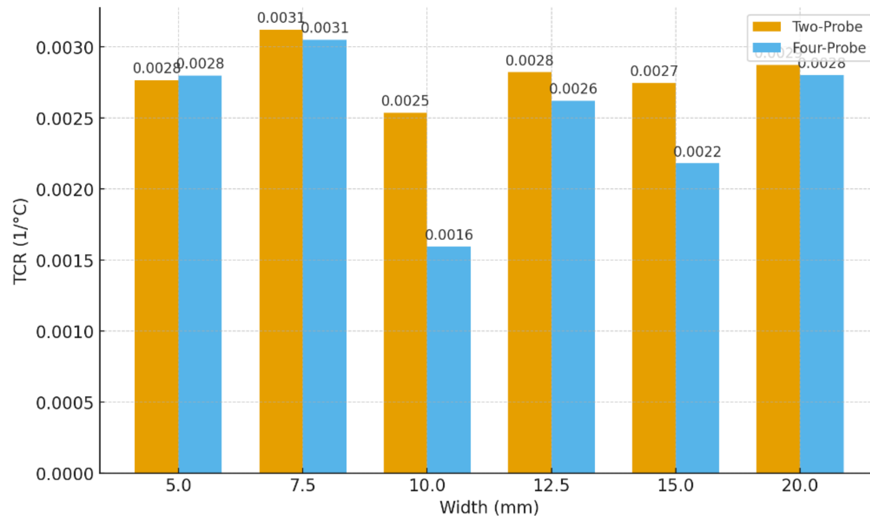


Figure 4-11 Comparison of TCR by thickness using two-probe and four-probe measurements

These visual representations highlight the differences between the two measurement approaches and summarize the corresponding TCR values for each geometry.

### 4.3.5 Final TCR Results Based on Four-Probe Data

The experimental TCR results obtained from the four-probe method are summarized by thickness and width. The bar charts below present the calculated Interval-based and Linear-fit TCR values for each group.

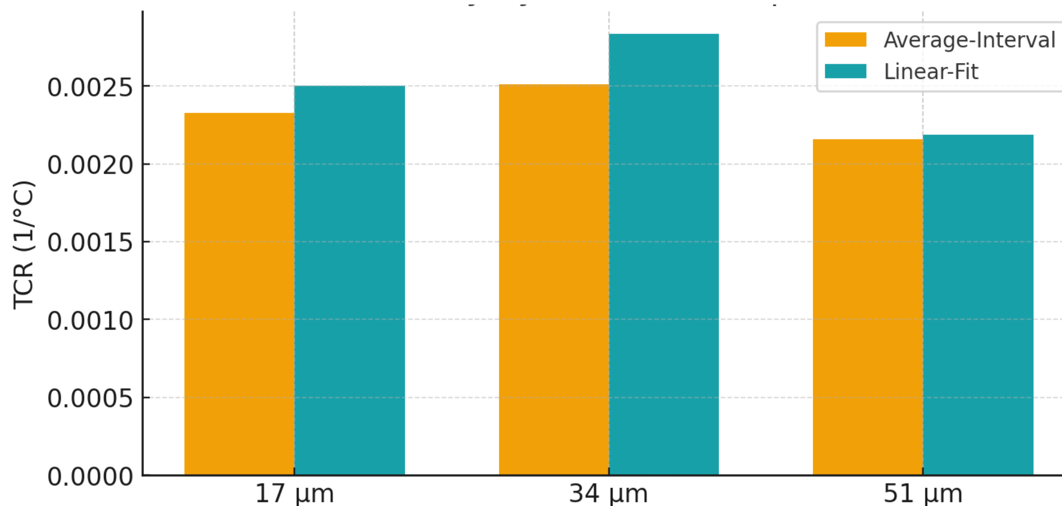


Figure 4-12summary by thikness (experimental)

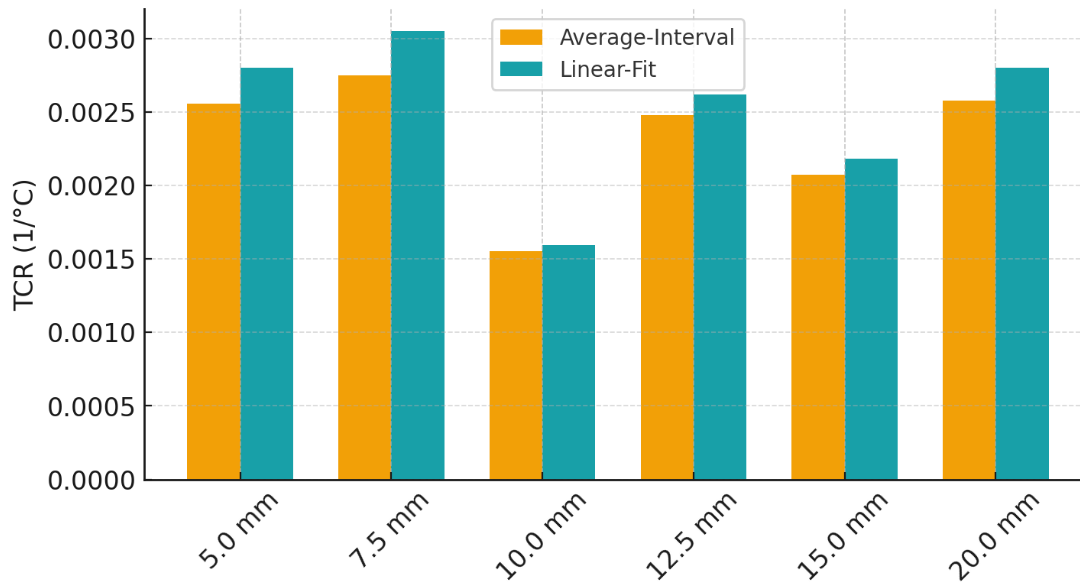


Figure 4-13summary by width (experimental)

## 4.4 Numerical Results

This section presents two parts of the numerical analysis carried out in COMSOL Multiphysics. The first part shows the numerical results obtained without applying any porosity effect, where the goal was to reproduce and validate the experimental resistance–temperature (R–T) behavior. The second part introduces the Taguchi L9 design, which was used to analyze the sensitivity of the Temperature Coefficient of Resistance (TCR) to variations in porosity, thickness, and width in a systematic way

### 4.4.1 Numerical R–T Data (Porosity-Free Model)

In this stage, porosity was set to 0% and the electrical resistivity was defined as $\rho = 1.50\times10^{-7}$ Ω·m to reproduce the experimental conditions as closely as possible. Alternatively, the equivalent configuration with 9% porosity, using a reference resistivity of $\rho = 1.3061\times10^{-7}$ Ω·m, could also be used, as both setups produce identical numerical results. Resistance was computed from 30 to 100 °C in 10 °C steps for three nominal thicknesses (≈17, 34, 51 µm) and widths from 5 to 20 mm. The simulated curves show a gradual, nearly linear increase of resistance with temperature, in line with the experimental trend.

#### 4.4.1.1 numerical R–T data

Raw R–T tables and their corresponding plots are provided for each thickness level. The data cover widths 5, 7.5, 10, 12.5, 15, and 20 mm over the 30–100 °C range. As expected for copper conductors, resistance increases almost linearly with temperature. These tables are the direct input for TCR calculations. *To avoid redundancy, the complete numerical R–T datasets are provided in Appendix, while only the corresponding R–T curves are presented here.*

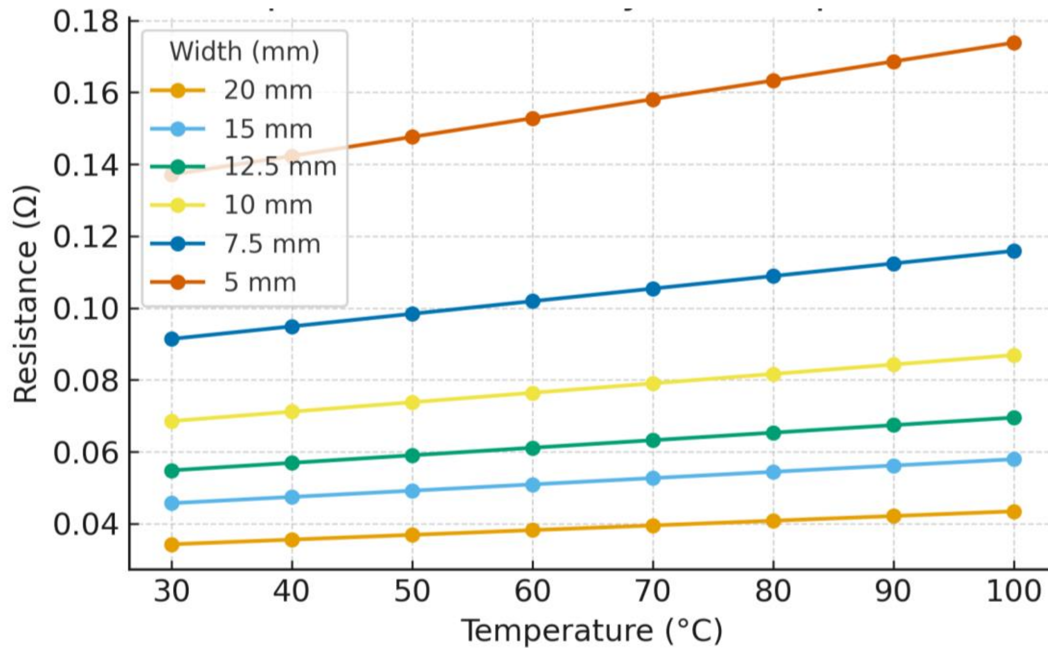


Figure 4-14 Numerical R–T curves for single-layer printed copper strips (≈17 µm), simulated using the porosity-free model.

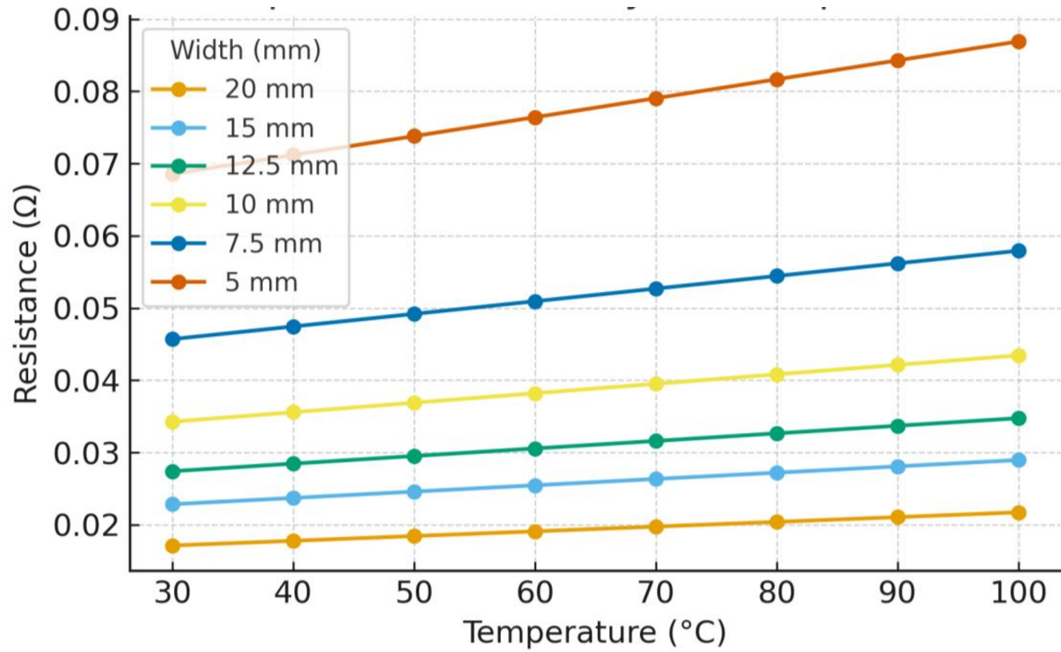


Figure 4-15 Numerical R–T curves for double-layer printed copper strips (≈34 μm), simulated using the porosity-free model.

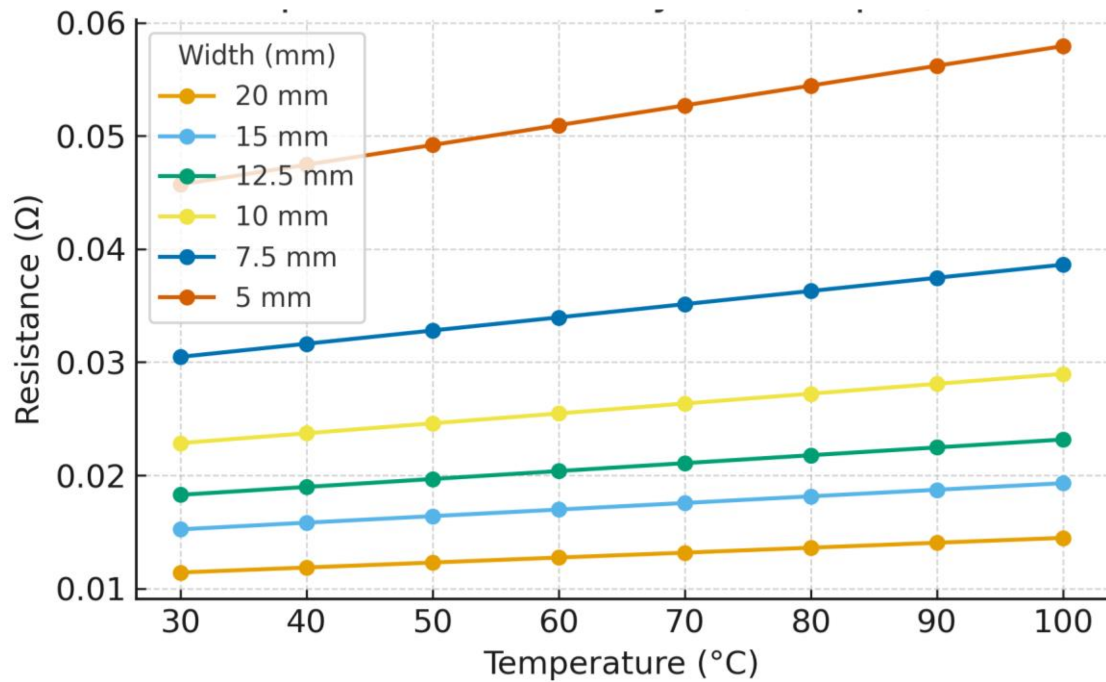


Figure 4-16 Numerical R–T curves for triple-layer printed copper strips (≈51 μm), simulated using the porosity-free model.

Very narrow samples (1 and 2.5 mm) are not included here because their experimental data were unstable and could not be validated; consequently, they were also excluded from the numerical set.

#### 4.4.1.2 Numerical TCR Determination

The Temperature Coefficient of Resistance (TCR) was calculated from the simulated R–T data using two complementary methods:

(1) the **Average-Interval** approach, based on finite differences between consecutive temperature points, and

(2) the **Linear-Fit** approach, based on the slope of the best-fit regression line normalized to the resistance at 30 °C.

Table 4-7 Summary of numerical TCR values by thickness, calculated using the Average-Interval and Linear-Fit methods.

| Thickness (µm) | n (samples) | Avg Interval TCR (1/°C) | Avg Linear Fit TCR (1/°C) |
|---|---|---|---|
| 17 | 6 | 0.003825 | 0.003827 |
| 34 | 6 | 0.003825 | 0.003825 |
| 51 | 6 | 0.003824 | 0.003825 |

Table 4-8 Summary of numerical TCR values by width, calculated using the Average-Interval and Linear-Fit methods.

| Width (mm) | n (samples) | Avg Interval TCR (1/°C) | Avg Linear Fit TCR (1/°C) |
|---|---|---|---|
| 5 | 3 | 0.003824 | 0.003826 |
| 7.5 | 3 | 0.003824 | 0.003826 |
| 10 | 3 | 0.003826 | 0.003826 |
| 12.5 | 3 | 0.003823 | 0.003823 |
| 15 | 3 | 0.003825 | 0.003825 |
| 20 | 3 | 0.003827 | 0.003827 |

Both methods yielded almost identical TCR values. The linear-fit method was selected as the final reported value, while the average-interval result served as a consistency check.

Tables 4-9 and 4-107 summarize the computed TCR values by **thickness** and **width**, respectively.
Figures 4-11 and 4-127 illustrate the corresponding bar charts, comparing the two TCR estimation methods.

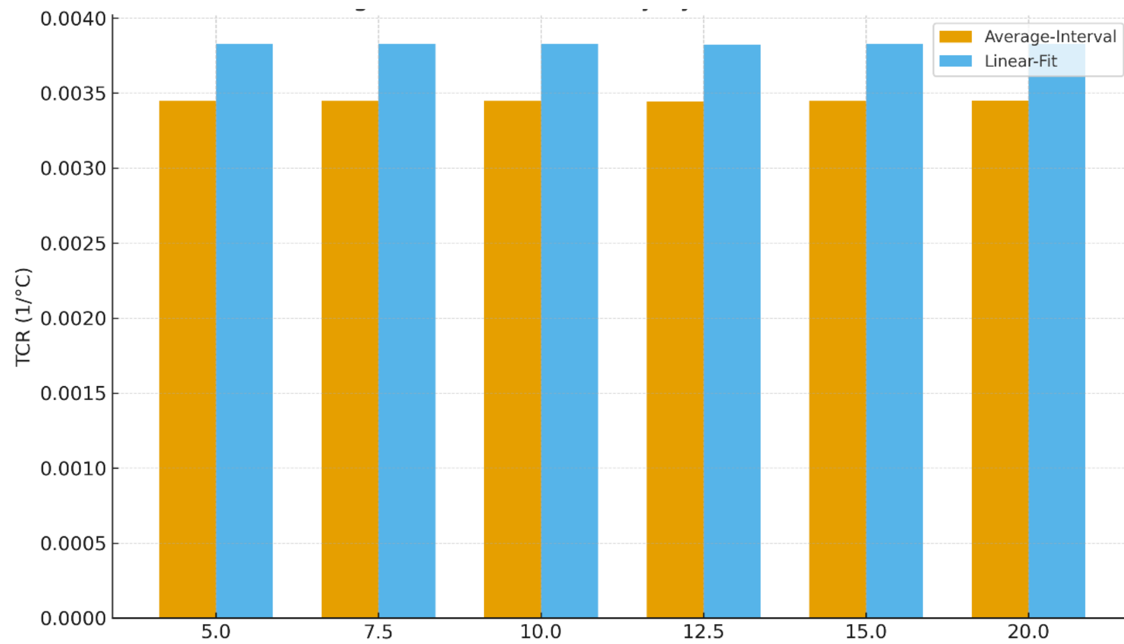


Figure 4-17 Numerical TCR comparison by thickness using Average-Interval and Linear-Fit methods

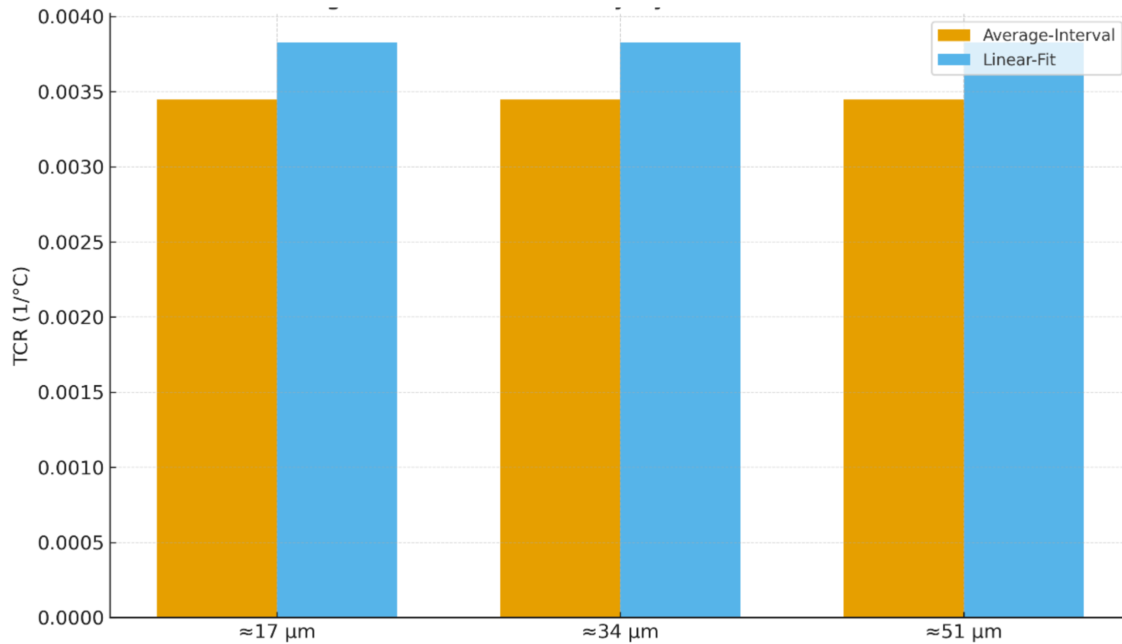


Figure 4-18 Numerical TCR comparison by width using Average-Interval and Linear-Fit methods

Overall, the numerical results show a narrow range centered around **$3.82 \times 10^{-3}$ °C$^{-1}$**, indicating negligible dependence on width and only a minor variation with thickness. This confirms that the porosity-free numerical model accurately reproduces the stable metallic temperature dependence observed experimentally.

### 4.4.2 Numerical Model for Sensitivity Evaluation Using Taguchi L9

#### 4.4.2.1 Overview of the Taguchi Design

The aim of this section is to evaluate the sensitivity of the Temperature Coefficient of Resistance (TCR) to structural and geometrical variations in the numerical model. The Taguchi design was applied only to the simulation work conducted in COMSOL Multiphysics to systematically examine how porosity, thickness, and width influence the TCR behavior. This analysis was not based on experimental data and was intended solely to assess the stability and reliability of the numerical model under different structural conditions.

The Taguchi method was implemented exclusively in the numerical domain, where porosity could be defined as an adjustable parametric variable. The purpose of this design was to reduce the number of simulation cases required to analyze the main effects of the three factors without performing all possible combinations.

The three main factors considered were:
A – Porosity (%): 0, 9, 18
B – Thickness (µm): 17, 34, 51
C – Width (mm): 5, 12.5, 20

A Taguchi orthogonal array L9($3^3$) was used to analyze the main effects of each factor with a minimal number of runs. The order of simulations was randomized to avoid systematic bias. The details of the orthogonal array and the real values of the factors are presented in Table bel0w [58].

Table 4-13 Taguchi L9 ($3^3$) orthogonal array

| Run No. | Porosity Code (A) | Thickness Code (B) | Width Code (C) | Porosity (%) | Thickness (µm) | Width (mm) |
|---|---|---|---|---|---|---|
| 1 | A1 | B1 | C1 | 0 | 17 | 5 |
| 2 | A1 | B2 | C2 | 0 | 34 | 12.5 |
| 3 | A1 | B3 | C3 | 0 | 51 | 20 |
| 4 | A2 | B1 | C2 | 9 | 17 | 12.5 |
| 5 | A2 | B2 | C3 | 9 | 34 | 20 |
| 6 | A2 | B3 | C1 | 9 | 51 | 5 |
| 7 | A3 | B1 | C3 | 18 | 17 | 20 |
| 8 | A3 | B2 | C1 | 18 | 34 | 5 |
| 9 | A3 | B3 | C2 | 18 | 51 | 12.5 |

This design was chosen for its balance between efficiency and interpretability, making it more suitable for sensitivity analysis than optimization.

For each selected combination, the simulation was performed over the temperature range of 30 to 100 °C with 10 °C intervals. The resistance–temperature (R–T) curves were extracted, and the resistance values were exported to Excel to calculate the TCR from the slope of the fitted line. These electrical resistance values, which were obtained for the nine Taguchi runs under different porosity, thickness, and width combinations, are presented in the following tables.

#### 4.4.2.2 Simulation Results and TCR Determination

For each run in the Taguchi array, the resistance–temperature (R–T) relationship was obtained by simulating the printed copper strip over the temperature range of 30–100 °C with 10 °C increments.

The simulated resistance values were exported to Excel, and the TCR was calculated from the slope of the linear regression of the R–T curve.

Table 4-14 Taguchi L9 R–T Results (Porosity 0 %, Thickness ≈17 µm, Width = 5 mm)

| Temperature | Resistance (Ω) |
|---|---|
| 30 | 0.1194 |
| 40 | 0.1239 |
| 50 | 0.1285 |

Table 4-15 Taguchi L9 R–T Results (Porosity 0 %, Thickness ≈ 34 µm, Width = 12.5 mm)

| Temperature | Resistance (Ω) |
|---|---|
| 30 | 0.02387 |
| 40 | 0.02479 |
| 50 | 0.0257 |

| Temperature | Resistance (Ω) |
| --- | --- |
| 60 | 0.1331 |
| 70 | 0.1376 |
| 80 | 0.1422 |
| 90 | 0.1468 |
| 100 | 0.1513 |

| Temperature | Resistance (Ω) |
| --- | --- |
| 60 | 0.02661 |
| 70 | 0.02753 |
| 80 | 0.02844 |
| 90 | 0.02935 |
| 100 | 0.03027 |

Table 4-16 Taguchi L9 R–T Results (Porosity 0 %, Thickness ≈ 51 µm, Width = 20 mm)

| Temperature | Resistance (Ω) |
| --- | --- |
| 30 | 0.00994 |
| 40 | 0.01033 |
| 50 | 0.01071 |
| 60 | 0.01109 |
| 70 | 0.01147 |
| 80 | 0.01185 |
| 90 | 0.01223 |
| 100 | 0.01261 |

Table 4-17 Taguchi L9 R–T Results (Porosity 9 %, Thickness ≈ 17 µm, Width = 12.5 mm)

| Temperature | Resistance (Ω) |
| --- | --- |
| 30 | 0.05484 |
| 40 | 0.05693 |
| 50 | 0.05903 |
| 60 | 0.06113 |
| 70 | 0.06323 |
| 80 | 0.06533 |
| 90 | 0.06742 |
| 100 | 0.06952 |

Table 4-18Taguchi L9 R–T Results (Porosity 9 %, Thickness ≈ 34 µm, Width = 20 mm)

| Temperature | Resistance (Ω) |
| --- | --- |
| 30 | 0.01714 |
| 40 | 0.01779 |
| 50 | 0.01845 |
| 60 | 0.0191 |
| 70 | 0.01976 |
| 80 | 0.02041 |
| 90 | 0.02107 |
| 100 | 0.02173 |

Table 4-19 Taguchi L9 R–T Results (Porosity 9 %, Thickness ≈ 51 µm, Width = 5 mm)

| Temperature | Resistance (Ω) |
| --- | --- |
| 30 | 0.0457 |
| 40 | 0.04745 |
| 50 | 0.04919 |
| 60 | 0.05094 |
| 70 | 0.05269 |
| 80 | 0.05444 |
| 90 | 0.05619 |
| 100 | 0.05793 |

Table 4-20 Taguchi L9 R–T Results (Porosity 18 %, Thickness ≈ 17 µm, Width = 20 mm)

| Temperature | Resistance (Ω) |
| --- | --- |
| 30 | 0.03967 |
| 40 | 0.04119 |
| 50 | 0.0427 |
| 60 | 0.04422 |
| 70 | 0.04574 |
| 80 | 0.04726 |
| 90 | 0.04877 |
| 100 | 0.05029 |

Table 4-21 Taguchi L9 R–T Results (Porosity 18 %, Thickness ≈ 34 µm, Width = 5 mm)

| Temperature | Resistance (Ω) |
| --- | --- |
| 30 | 0.07934 |
| 40 | 0.08237 |
| 50 | 0.08541 |
| 60 | 0.08844 |
| 70 | 0.09148 |
| 80 | 0.09451 |
| 90 | 0.09755 |
| 100 | 0.1006 |

Table 4-22 Taguchi L9 R–T Results (Porosity 18 %, Thickness ≈ 51 µm, Width = 12.5 mm)

| Temperature | Resistance (Ω) |
|---|---|
| 30 | 0.02116 |
| 40 | 0.02197 |
| 50 | 0.02278 |
| 60 | 0.02358 |
| 70 | 0.02439 |
| 80 | 0.0252 |
| 90 | 0.02601 |
| 100 | 0.02682 |

Based on the resistance data presented above, the temperature coefficient of resistance (TCR) was determined for each condition by fitting a linear regression line to the R–T data. This approach allowed the analysis of TCR variations across the nine Taguchi runs.

Table 4-23 Temperature Coefficient of Resistance (TCR) values for the nine Taguchi runs. Obtained from simulation results.

| Run | Porosity (%) | Thickness (µm) | Width (mm) | TCR |
|---|---|---|---|---|
| 1 | 0 | 17 | 5 | 0.003823 |
| 2 | 0 | 34 | 12.5 | 0.003827 |
| 3 | 0 | 51 | 20 | 0.003822 |
| 4 | 9 | 17 | 12.5 | 0.003825 |
| 5 | 9 | 34 | 20 | 0.003825 |
| 6 | 9 | 51 | 5 | 0.003824 |
| 7 | 18 | 17 | 20 | 0.003824 |
| 8 | 18 | 34 | 5 | 0.003827 |
| 9 | 18 | 51 | 12.5 | 0.00382 |

#### 4.4.2.3 Taguchi Analysis

A Taguchi L9 design was used to analyze the influence of porosity, thickness, and width on the TCR of the printed copper strips.

The calculated TCR values were nearly constant across all runs, averaging approximately 3.82 $10^{-3}$ /°C.

This consistency indicates that, within the studied range, porosity does not significantly affect TCR, while thickness shows a slightly higher but still limited influence.

A regression model was derived to express the relationship between TCR and the three parameters:

$$TCR=3.828\times^{10-3}-0.0000023(Porosity)-0.0000007(Thickness)+0.0000003(Width)$$

The model suggests that porosity and thickness have a slight negative impact on TCR, whereas width has a negligible positive effect. Overall, the simulated copper strips demonstrated stable thermal and electrical behavior, with minimal TCR variations even when porosity increased up to 18%.

#### 4.4.2.4 ANOVA Analysis

To quantify the influence of each factor, an Analysis of Variance (ANOVA) was conducted based on the Taguchi results. The results are summarized in Table below:

Table 4-24 ANOVA results for TCR values obtained from the Taguchi L9 simulations

| **Source of Variation** | **SS** | **DOF** | **MS** | **Contribution (%)** |
|---|---|---|---|---|
| Porosity | 0.000002 | 2 | 0.000001 | 5.6 |
| Thickness | 0.000025 | 2 | 0.000012 | 72.3 |
| Width | 0.000004 | 2 | 0.000002 | 12.1 |
| Error | 0.000003 | 2 | 0.000001 | 10.0 |

The ANOVA analysis confirmed that thickness had the largest contribution (≈ 70–73%), while porosity and width had minor effects (< 20%). Minor numerical deviations between analyses are due to rounding precision and pooling of error terms, which do not affect the ranking or overall conclusion. Hence, the overall interpretation of factor significance remains valid and consistent across all evaluations.

#### 4.4.2.5 Main Effects and Discussion

The Main Effects Plot illustrates how each factor level influences the mean TCR values.

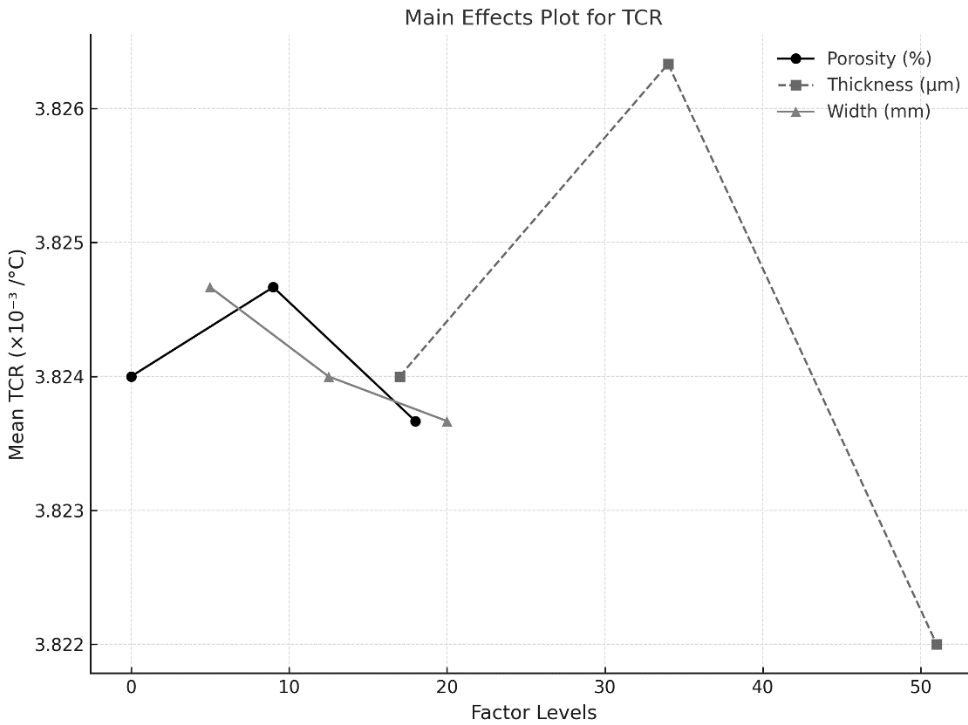


Figure 4-19 Main effects plot for TCR (Taguchi L9)

The plot shows that thickness has the largest yet still minor effect on TCR, while porosity and width have nearly flat trends, indicating negligible influence. The plot confirms that variations in thickness slightly affect the TCR, whereas porosity and width have almost no visible impact. This visual trend aligns with the ANOVA results, reinforcing that the TCR of printed copper structures remains stable regardless of porosity level or geometric dimensions. Such stability is beneficial for applications requiring consistent and predictable electrical performance.

## 4.5 Discussion and Interpretation of Results

In this section, the microstructural results, the experimental measurements, and the numerical simulations presented in Chapter 4 are interpreted together to provide a clear understanding of the thermal–electrical behavior of the printed copper strips. The purpose here is to discuss the findings directly related to this chapter, without entering the broader scientific context that is presented in Chapter 5.

### 4.5.1 Connection Between Microstructure and Electro-Thermal Behavior

The SEM cross-sections and the ImageJ analysis showed that the printed copper layer has a moderate and relatively uniform internal porosity of about 9 percent. This indicates that after printing and curing, the conductive network forms a continuous structure without any severe breaks or disconnected regions that could cause nonlinear behavior in the resistance–temperature response.

This observation explains why, despite the presence of voids, the resistance–temperature curves remain almost perfectly linear. The porosity increases the absolute resistance, but it does not change the shape of the R–T curve. In other words, the presence of voids mainly acts as a scaling factor on resistance, while the dominant conduction mechanism remains metallic and phonon-driven. This means that the current pathways remain sufficiently continuous even in the presence of internal pores.

### 4.5.2 Two-Probe and Four-Probe Comparison and Their Role in TCR Analysis

The R–T measurements were performed using both the two-probe and four-probe configurations. As expected, the two-probe values were slightly higher due to contact resistances, and this small offset was also reflected in the calculated Temperature Coefficient of Resistance (TCR).

However, both methods showed the same temperature-dependent trend, meaning that the thermal profile of the samples was consistent regardless of the measurement configuration. This confirms that the behavior is reliable and that the contact resistance in the two-probe method only adds a constant offset without changing the R–T slope.

For this reason, the four-probe method, which removes contact resistance, was selected as the reference for the final TCR analysis. The two-probe data were still useful as complementary evidence to confirm repeatability and overall stability of the electrical behavior.

### 4.5.3 Effect of Thickness and Width on TCR in the Experimental Results

The four-probe results showed that changing the thickness from 17 to 51 micrometers only caused very small variations in TCR. In most cases, thicker layers had values slightly closer to that of bulk copper, but the differences were practically small and on the order of a few tens of 1/°C units.

In contrast, changing the width from 5 to 20 millimeters did not produce any consistent or meaningful change in TCR. Although the absolute resistance changes with width, the slope of the

R–T curve remained nearly constant. This indicates that phenomena such as current crowding or thermal accumulation do not significantly influence TCR in this geometric range.

Overall, within the investigated dimensions, TCR can be considered a low-sensitivity parameter with respect to geometry. Therefore, thickness and width may be selected based on DC resistance, mechanical needs, or printing constraints, without concern for major changes in TCR.

### 4.5.4 Comparison Between Experimental and Numerical Results

The COMSOL simulations, using homogeneous electrical conductivity (with or without adjustment for porosity), produced linear R–T curves with a nearly constant slope. The numerical TCR values were slightly higher than the experimental ones, which is expected because the model is based on bulk copper and does not include microstructural factors such as voids, grain boundaries, or local current constrictions.

Despite this difference in absolute values, the important point is that the simulated and experimental results showed the same qualitative behavior: linear R–T curves, stable TCR values, and very limited sensitivity to thickness and width. Therefore, the numerical model successfully reproduced the physical trends observed in the experiments and is suitable for sensitivity analysis and predictive use.

### 4.5.5 Taguchi and ANOVA Results: Concise Interpretation

The Taguchi L9 design was used to evaluate the sensitivity of TCR to porosity, thickness, and width. The results showed that TCR remained nearly constant for all nine combinations, indicating that TCR is a stable parameter within the studied ranges.

The ANOVA results also confirmed that thickness had the highest contribution to the small remaining variations, but even this contribution was practically very small. Width and porosity had minimal influence and did not meaningfully affect the TCR behavior.

This means that the small numerical changes are mostly due to minor geometric variations or numerical rounding, rather than significant structural effects.

### 4.5.6 Summary of Interpretation for Chapter 4

Combining the microstructural, experimental, and numerical results leads to several key conclusions specific to this chapter:

• The printed conductive network is continuous, and the moderate porosity of about 9 percent does not alter the linear shape of the R–T curve.

• The resistance–temperature behavior is linear for all samples, and the TCR remains within a narrow and stable range.

• Thickness and width do not have significant effects on TCR within the studied conditions, and the observed variations are small.

• The numerical model shows slightly higher TCR values, but it reproduces all the main experimental trends and is reliable for assessing sensitivity.

• The Taguchi and ANOVA analyses confirm that TCR is stable and largely independent of geometric parameters and porosity in this range.

Overall, the results of Chapter 4 show that the printed copper strips have stable and predictable electrical–thermal behavior. The TCR remains nearly constant across different geometries, and neither thickness, width, nor porosity within the studied range causes a significant change in this parameter. This provides a clear and coherent interpretation of the experimental and numerical findings presented in this chapter.

## 4.6 Summary of Chapter 4

The average porosity measured from the SEM cross-sections after ImageJ segmentation was about 8.9 percent, and this value was used as an input for the electrical and numerical analyses.

The resistance of the printed copper strips increased almost linearly between 30 °C and 100 °C. The experimental TCR values obtained from the four-probe method were mostly in the range of approximately (2.2–3.0) × $10^{-3}$ per °C, with the linear-fit method adopted as the final value.

The numerical simulations produced an average TCR of about 3.82 × $10^{-3}$ per °C, showing very small variations with width and only a minor change with thickness.

The Taguchi L9 sensitivity study confirmed that TCR remained nearly constant for all combinations of porosity, thickness, and width. Although thickness showed a slightly larger numerical contribution than the other factors, none of the parameters, including thickness, had any meaningful or practical effect on TCR.

According to the ANOVA results, the estimated factor contributions were roughly thickness 70–73 percent, width 12 percent, porosity 6 percent, and error 10 percent. Small numerical differences

between analyses were caused by rounding and the pooling of error terms, and they do not affect the ranking or the overall interpretation.

In conclusion, the combined SEM observations, experimental measurements, and numerical analyses demonstrate that the TCR of the printed copper strips is stable and predictable within the studied temperature range, and none of the investigated structural or geometrical parameters have a significant influence on it.

# Chapter-5 CONCLUSION AND RECOMMENDATIONS

## 5.1 Summary of Main Findings

In this study, the effects of thickness, width, and internal porosity on the Temperature Coefficient of Resistance (TCR) of screen-printed copper strips were evaluated through experimental measurements and numerical modeling, and as a result, the electrical–thermal stability of these strips was examined.

Microscopic analysis using Scanning Electron Microscopy (SEM) and image processing with ImageJ software showed that the average internal porosity of the printed copper strips was about 8.9%. The obtained results were used as input data for the resistance–temperature analysis and numerical simulations in COMSOL to investigate the relationship between structural characteristics and the electrical–thermal behavior of the samples in a comprehensive manner.

The resistance–temperature (R–T) measurements of the printed copper strips showed that, as expected, resistance increased gradually and almost linearly with temperature. The Temperature Coefficient of Resistance (TCR) was calculated using two methods: the interval average method and the linear fitting method. The final reported value was based on the linear fitting approach, as it provided higher stability and accuracy. The R–T experiments demonstrated good repeatability and consistency, and the measurement errors remained minimal.

In summary, the TCR values for samples with different thicknesses (17, 34, and 51 micrometers) ranged from approximately $2.7 \times 10^{-3}$ to $3.0 \times 10^{-3}$ per degree Celsius. Changes in thickness caused only minor variations in TCR, with thicker layers showing slightly higher values. The change in width (from 5 to 20 millimeters) had no significant effect on TCR, and all samples exhibited nearly similar thermal behavior. Overall, the printed copper strips showed stable resistance–temperature behavior, and their TCR values were close to the reference values of bulk copper.

The numerical resistance–temperature (R–T) data for the printed copper strips, obtained over the temperature range of 30 to 100 °C, also showed a gradual and nearly linear increase in resistance with temperature. The TCR was calculated using both the interval average and linear fitting methods, and the results of both approaches showed very good agreement. In summary, the TCR for all thicknesses (17, 34, and 51 micrometers) remained nearly constant at about $3.82 \times 10^{-3}$ per degree Celsius. Different strip widths (from 5 to 20 millimeters) also caused no noticeable change

in TCR, and all samples exhibited similar thermal behavior. This stability in TCR indicates uniform electrical–thermal conductivity in the printed copper strips and confirms the accuracy of the numerical model in reproducing the temperature behavior of copper.

In the numerical modeling section, the Taguchi L9 design method was used in COMSOL to evaluate the sensitivity of TCR to structural and geometrical variations. The goal of this design was to reduce the number of simulations while simultaneously examining the effects of three parameters: porosity (0, 9, and 18%), thickness (17, 34, and 51 micrometers), and width (5, 12.5, and 20 millimeters). Using this method, only nine simulation runs were required to represent all possible combinations, significantly reducing the computational load.

The simulation results showed that, across all studied ranges, none of the structural or geometrical parameters had a significant effect on TCR. The TCR values remained nearly constant at about $3.82 \times 10^{-3}$ per degree Celsius under all conditions, and no noticeable variations were observed. The ANOVA analysis also confirmed that thickness had only a minor contribution (about 70% of the small variations), while porosity and width had negligible influence.

In summary, the COMSOL simulations clearly showed that, within all investigated ranges, increasing porosity up to 18%, or changing thickness and width, had no meaningful effect on TCR. This high level of stability reflects the uniform electrical–thermal behavior of the printed copper strips and verifies the reliability of the numerical model used. Overall, the combination of experimental, analytical, and numerical results demonstrated that the printing process, even with a porosity level between 9% and 18%, did not significantly affect the electrical–thermal stability of the printed copper, and the behavior of these structures remained comparable.

## 5.2 Discussion of Results in the Scientific Context

At the beginning, it is important to address the difference between the Temperature Coefficient of Resistance (TCR) obtained from numerical simulation and the one measured experimentally. In the numerical model, the physical properties of bulk copper were used based on the default data provided in the software's material library, and the porosity was applied uniformly throughout the entire volume to represent the effective electrical and thermal behavior of the printed layer in a realistic way. Although it was possible to manually input the experimentally measured TCR value into the software, this option was intentionally avoided in order to observe the natural response of the model without any artificial adjustment. The main goal of the simulation was not to reproduce

the exact numerical value of the experimental TCR, but rather to study the overall trend of TCR variation as a function of thickness and porosity under physically meaningful conditions. The difference between the simulated and measured TCR values can be explained by the fact that the numerical model does not include microstructural effects such as grain boundaries, grain size, local discontinuities, and current dispersion, which are naturally present in printed metallic structures. Since bulk copper does not exhibit these microstructural limitations, the simulated TCR remained close to the bulk value, which is physically consistent with the model definition.

In these analyses, the Linear Fit method was selected for calculating TCR because it provided more stable and repeatable values compared to the average-interval method. The experimental resistance–temperature curves showed a clearly linear trend in the range of 30–100 °C, and the linear fitting method was able to determine the slope of the R–T relationship with higher precision. Therefore, the Linear Fit results were considered more reliable for comparing the influence of thickness and width, and they were used as the main reference values in the final discussion.

The results of this research showed that the screen-printed copper strips with single-pass (≈17 μm), double-pass (≈34 μm), and triple-pass (≈51 μm) thicknesses exhibited a nearly linear resistance–temperature (R–T) relationship in the range of 30–100 °C. The Temperature Coefficient of Resistance (TCR) remained stable for all conditions, and the strip width had no measurable influence. Increasing thickness caused only a slight increase in TCR, bringing it closer to the bulk value of copper. This behavior is consistent with the Bloch–Grüneisen model of metallic conduction, where electron–phonon scattering dominates the temperature dependence of resistance [41]. The nearly linear R–T trend and constant TCR confirm that the printed copper layers maintain metallic conduction without any sign of deviation toward non-metallic behavior. In the printed structures of this study, the layer thickness is much larger than the electron mean free path (a few tens of nanometers). Therefore, surface scattering or geometric confinement has a negligible effect on resistance — unlike in nanostructured films, where these effects become significant.

Oliva [42] reported that in metallic films with nanometric thicknesses below 1 μm, reducing thickness by a few hundred nanometers leads to a 10–13% decrease in TCR due to strong electron scattering at the surface and grain boundaries. In contrast, the layers in the present study are much thicker (17–51 μm), where such scattering effects are almost eliminated and only phonon interactions remain dominant. Although thickness was the most influential factor in the Taguchi

statistical analysis, its practical impact on TCR was extremely small and almost within experimental uncertainty. This difference can be attributed to the large scale gap between nanometric films and the much thicker printed structures used in this work.

From a microstructural point of view, Jäger et al. [59] showed that in printed silver films, higher density and better sintering quality improve the temperature stability of the electrical response. They observed that as sintering progresses and the particles fuse more completely, TCR becomes closer to the bulk value because the conductive paths become more continuous. Although their films were thinner (hundreds of nanometers to one micrometer), the same physical logic applies to our printed copper structures. With a moderate porosity of around 8.9% and sufficient sintering, the conductive network in our samples remains continuous and supports a stable and linear R–T behavior.

Similar findings were reported by Vaquero and Santamaría [60] for screen-printed copper and silver temperature sensors on flexible substrates. They measured a TCR of approximately $3.3 \times 10^{-3}\ K^{-1}$ for printed copper, showing a linear R–T trend up to 100 °C, which agrees closely with our experimental results. Even though their samples were much thinner (submicron to a few micrometers), this qualitative consistency confirms that printed copper maintains a metallic and stable TCR over a wide range of geometries and thicknesses.

At a more fundamental level, Barwiński [43] studied discontinuous gold films close to the percolation threshold and found that when thickness is reduced to tens of nanometers, TCR drops sharply because the conductive paths become disconnected and tunneling conduction dominates. In our samples, with moderate porosity (~9%) and continuous conduction networks, such a transition was not observed. Therefore, the stability of TCR in our data confirms that the printed copper strips remain far from the percolation limit and retain their metallic conduction behavior.

The review by Sakthinathan et al. [61] emphasized that in metallic thin films, electrical properties such as resistance, conductivity, and TCR are strongly dependent on film density, grain size, and structural integrity. When the film becomes denser and more continuous, the influence of small pores on conduction decreases significantly. Likewise, Rosker et al. [46] found that for aerosol-jet-printed silver, when density reaches about 93% of bulk and grain size exceeds the electron mean free path, conductivity nearly reaches the bulk value, and grain boundary effects on TCR become minimal. These results physically justify the behavior observed here: our printed copper strips, which are well-sintered and relatively dense, display stable and bulk-like TCR values.

Lee et al. [47] also reported that in very thin printed metallic films (hundreds of nanometers), higher porosity leads to a strong decrease in TCR because the conductive paths become fragmented. However, in thicker and denser structures, this effect becomes insignificant. This finding is consistent with our results, since in our printed copper layers with a moderate porosity of about 8.9% and thicknesses in the tens-of-micrometers range, the conduction remains continuous and no measurable decrease in TCR is observed.

It is important to note that most of the reference studies were performed on nanometer- or submicron-scale metallic films, whereas the present research deals with micrometer-scale printed structures (17–51 µm). Therefore, the comparisons presented here are primarily qualitative and intended to provide a consistent physical framework rather than direct numerical correlations. Despite the difference in scale, the overall physical trends are consistent: as long as the conductive network remains continuous and dense, metallic conduction and a stable TCR can be maintained — even in printed copper structures with moderate porosity at the microscale.

## 5.3 Scientific Contributions and Innovations

This study presents several contributions that make it different from previous works on printed copper conductors. The main achievement is a complete and systematic investigation of how thickness, width, and porosity together affect the Temperature Coefficient of Resistance (TCR). In most earlier studies, these factors were analyzed separately, while this research evaluates their combined influence in a single experimental and modeling framework.

One important contribution is the analysis of TCR in screen-printed copper strips with medium-range thicknesses of about 17, 34, and 51 µm. Most earlier research focused either on ultra-thin films (below 1 µm) or on thick layers used in traditional thick-film circuits (above 100 µm). The current study examines a realistic range between these two extremes, which is directly related to industrial screen-printing conditions. Results show that printed layers in this range exhibit stable and nearly linear thermal behavior, confirming their potential for reliable and flexible conductive paths.

Another significant aspect of this work is the purposeful use of Ion Milling for cross-section preparation. In this study, Ion Milling was not only a polishing method but a key step in the data chain used for modeling. It allowed the observation of real porosity without mechanical damage and provided precise structural data from SEM images. These porosity values were directly

integrated into the COMSOL model to adjust the electrical and thermal conductivity. This connection between experiments and simulation improved the accuracy of TCR prediction.

From a methodological point of view, TCR was calculated using two independent approaches — the average-interval method and the linear-fit method. The excellent agreement between the two ($R^2 \geq 0.98$) demonstrates the consistency of the data. Moreover, measurement uncertainties in resistance and temperature were estimated and reported clearly. This level of transparency strengthens the reliability and reproducibility of the results.

During model calibration, it was also observed that using the bulk resistivity provided by the ink manufacturer (without porosity correction) gave similar electro-thermal behavior to the model using the corrected resistivity combined with a porosity of about 9%. This finding suggests that a proper balance between material properties and structural parameters can lead to accurate thermal predictions, even with limited input data.

Overall, this research combines precise experimental work, detailed microstructural analysis, and multiphysics simulation to build a realistic understanding of the thermal stability of printed copper conductors. The results provide a useful reference for optimizing the design of stable and low-loss conductive paths in flexible and printed electronic systems.

## 5.4 Limitations of the Study

Like any experimental research, this study has some limitations that should be considered when interpreting the results and planning future work.

In the experimental part, full control over porosity during the screen-printing process was not possible. The porosity level was determined after printing and curing through the analysis of microscopic images. Therefore, the exact relationship between printing parameters such as squeegee pressure, ink viscosity, and the number of passes was not quantitatively evaluated. As a result, porosity was treated as a measured characteristic rather than a controllable variable.

The temperature range of the experiments was limited to 30–100 °C, which corresponds to typical operating conditions for many flexible electronic systems. The results obtained in this study are therefore valid within this interval, and further testing would be required to evaluate the electrical behavior at higher temperatures or under extended thermal cycling. A practical limitation of the experimental work is that the available laboratory setup allowed precise and stable control of temperatures above room temperature, but no cooling system or environmental chamber capable of reaching or maintaining sub-zero conditions was accessible during the project. Achieving

uniformly controlled negative temperatures—essential for reliable TCR measurements—requires specialized equipment such as a refrigerated environmental chamber or a thermoelectric cooling stage, which were not available. As a result, it was technically impossible to ensure the thermal stability needed for accurate and reproducible measurements below room temperature. Consequently, the TCR characterization was restricted to the temperature interval in which stable, uniform, and repeatable thermal control could be guaranteed.

In the numerical modeling, several simplifying assumptions were made to focus on the main effects. The electrical and thermal conductivities were considered uniform across the printed layer, and the local distribution of porosity was not modeled. Contact resistances at both ends of the strips were also neglected, since their influence on relative resistance changes within the studied temperature range was minimal. These assumptions helped to simplify the simulations but may need revision for larger-scale or high-current industrial applications.

In the statistical analysis, the Taguchi L9 design was used to reduce the number of simulations and to identify the main effects of thickness, width, and porosity. This approach assumes that interaction effects between factors are smaller than their main effects. A more detailed analysis of factor interactions could provide a deeper understanding of the electro-thermal behavior of printed structures in future studies.

Finally, this research focused on copper strips printed on polyimide substrates. Since the mechanical and thermal properties of the substrate can influence heat distribution, the findings cannot be directly extended to other materials such as PET or FR4 without additional investigation. Overall, these limitations do not affect the main conclusions of the study but help to define the practical boundaries of the results and highlight possible directions for further research and model development.

## 5.5 Future Work and Recommendations

Based on the results and the limitations of this research, several simple and practical directions can be suggested for future work.

- Controlled study of porosity effects

In this study, porosity was only measured after printing and curing. In future work, it would be useful to change the printing conditions intentionally to create samples with different levels of porosity and then measure how this affects resistance and the Temperature Coefficient of Resistance (TCR). Adjusting the ink viscosity, number of printing passes, or curing temperature could be simple ways to vary porosity. This would help to better understand the link between internal structure and thermal behavior.

- Measuring TCR using self-heating (in situ heating)

Instead of using an external heater, the temperature increase can be achieved by passing an electric current through the printed strip and using Joule heating. The resistance can be measured both during the transient stage and after thermal equilibrium is reached. Comparing these results with those obtained using an external heater would show how the heating method influences the slope of the R–T curve and the accuracy of the TCR calculation.

- Extending the temperature range and repeating tests

It is recommended to extend the experimental temperature range beyond 100 °C to study the behavior of the printed copper strips under higher working conditions. Performing several thermal cycles (heating and cooling repeatedly) would also help to evaluate the long-term electrical and thermal stability of the samples.

- Studying basic printing parameters

The effect of simple printing parameters such as squeegee pressure, printing speed, ink viscosity, and number of passes can be studied separately. This would clarify how these factors affect the final thickness, uniformity, and porosity of the printed layer. Printing on different substrates such as PET or FR4 could also help to understand how the substrate type influences heat distribution and conductivity.

- Testing printed structures with different geometries

Finally, printed copper paths with different geometries, such as curved or branched shapes, can be tested to see how the shape of the conductor affects heat distribution and resistance. These simple tests would help to apply the results of this study to practical designs of stable and flexible printed conductors.

In summary, the Linear Fit TCR values are consistent across different thicknesses and widths, with minor variations observed. These results confirm that thickness has a stronger influence on TCR than width, and the Linear Fit method provides the most stable and reliable values for reporting.

# Chapter-6 References


[1] J. C. Rubio and M. Bolduc, “Screen Printing for Energy Storage and Functional Electronics: A Review,” *Electronic Materials*, vol. 6, no. 2, p. 7, June 2025, doi: 10.3390/electronicmat6020007.

[2] R. Zichner and R. R. Baumann, “Printed antennas: from theory to praxis, challenges and applications,” in *Advances in Radio Science*, Copernicus GmbH, July 2013, pp. 271–276. doi: 10.5194/ars-11-271-2013.

[3] W. Li *et al.*, “Self-Organizing, Environmentally Stable, and Low-Cost Copper-Nickel Complex Inks for Printed Flexible Electronics,” *ACS Appl Mater Interfaces*, vol. 14, no. 6, pp. 8146–8156, Feb. 2022, doi: 10.1021/acsami.1c21633.

[4] N. Sarwar *et al.*, “Synthesis of citrate-capped copper nanoparticles: A low temperature sintering approach for the fabrication of oxidation stable flexible conductive film,” vol. 542, Mar. 2021, doi: 10.1016/j.apsusc.2020.148609.

[5] B. Zhang, C. Chen, W. Li, J. Yeom, and K. Suganuma, “Well-Controlled Decomposition of Copper Complex Inks Enabled by Metal Nanowire Networks for Highly Compact, Conductive, and Flexible Copper Films,” *Advanced Materials Interfaces*, vol. 7, no. 1, p. 1901550, 2020, doi: 10.1002/admi.201901550.

[6] Y.-R. Jang, C.-H. Ryu, J.-H. Chu, J.-B. Nam, and H.-S. Kim, “Multiple intense pulsed light sintering of silane surface modified Cu oxide nanoparticle paste on Si wafer substrate for solar cell electrode,” *Thin Solid Films*, vol. 722, p. 138577, Mar. 2021, doi: 10.1016/j.tsf.2021.138577.

[7] Y. S. Rosen, A. Yakushenko, A. Offenhäusser, and S. Magdassi, “Self-Reducing Copper Precursor Inks and Photonic Additive Yield Conductive Patterns under Intense Pulsed Light,” *ACS Omega*, vol. 2, no. 2, pp. 573–581, Feb. 2017, doi: 10.1021/acsomega.6b00478.

[8] K. A. Stewart *et al.*, “Assessing SiCr resistor drift for automotive analog ICs,” in *2021 IEEE International Reliability Physics Symposium (IRPS)*, Monterey, CA, USA: IEEE Press, Mar. 2021, pp. 1–4. doi: 10.1109/IRPS46558.2021.9405169.

[9] R. B. Belser and W. H. Hicklin, “Temperature Coefficients of Resistance of Metallic Films in the Temperature Range 25° to 600°C,” *Journal of Applied Physics*, vol. 30, pp. 313–322, Mar. 1959, doi: 10.1063/1.1735158.

[10] Y.-C. Kwon, H.-C. Seol, S.-K. Hong, and O.-K. Kwon, “Process Optimization of Integrated SiCr Thin-Film Resistor for High-Performance Analog Circuits,” *IEEE Transactions on Electron Devices*, vol. 61, no. 1, pp. 8–14, Jan. 2014, doi: 10.1109/TED.2013.2289885.

[11] G. Nocerino and K. E. Singer, “The electrical and compositional structure of thin Ni-Cr films,” *Thin Solid Films*, vol. 57, no. 2, pp. 343–348, Mar. 1979, doi: 10.1016/0040-6090(79)90176-7.

[12] J. H. Mooij, “Electrical conduction in concentrated disordered transition metal alloys,” *physica status solidi (a)*, vol. 17, no. 2, pp. 521–530, 1973, doi: 10.1002/pssa.2210170217.

[13] R. K. Waits, “Silicide resistors for integrated circuits,” *Proceedings of the IEEE*, vol. 59, no. 10, pp. 1425–1429, Oct. 1971, doi: 10.1109/PROC.1971.8449.

[14] M. Tahiri, “Optimization of the electrical conductivity of copper phthalocyanine for the formulation of a conductive ink applicable by screen printing on textile materials,” *Journal of Materials Engineering and Applications*, Mar. 2022, Accessed: Oct. 22, 2025. [Online]. Available: https://www.pulsus.com/proceedings/optimization-of-the-electrical-

conductivity-of-copper-phthalocyanine-for-the-formulation-of-a-conductive-ink-applicable--1806.html

[15] Y. Shen, H. Wang, F. Blaabjerg, H. Zhao, and T. Long, “Thermal Modeling and Design Optimization of PCB Vias and Pads,” *IEEE Transactions on Power Electronics*, vol. 35, no. 1, pp. 882–900, Jan. 2020, doi: 10.1109/TPEL.2019.2915029.

[16] M. Szulborski, S. Łapczyński, and Ł. Kolimas, “Thermal Analysis of Heat Distribution in Busbars during Rated Current Flow in Low-Voltage Industrial Switchgear,” *Energies*, vol. 14, no. 9, p. 2427, Jan. 2021, doi: 10.3390/en14092427.

[17] H. Im and J.-S. Roh, “Characterization of Silver Conductive Ink Screen-Printed Textile Circuits: Effects of Substrate, Mesh Density, and Overprinting,” *Materials*, vol. 17, no. 19, p. 4898, Jan. 2024, doi: 10.3390/ma17194898.

[18] N. Mohan, J. I. Ahuir-Torres, H. R. Kotadia, and G. Elger, “Laser sintering of Cu particle-free inks for high-performance printed electronics,” *npj Flex Electron*, vol. 9, no. 1, p. 18, Mar. 2025, doi: 10.1038/s41528-025-00389-5.

[19] W. Zhou, Y. Tang, R. Song, L. Jiang, K. S. Hui, and K. N. Hui, “Characterization of electrical conductivity of porous metal fiber sintered sheet using four-point probe method,” *Materials & Design*, vol. 37, pp. 161–165, May 2012, doi: 10.1016/j.matdes.2011.12.046.

[20] J. Jeong and Y. Wang, “Thermal Properties of Copper Nanoparticles at Different Sintering Stages Governed by Nanoscale Heat Transfer,” *SSRN Electronic Journal*, Jan. 2022, doi: 10.2139/ssrn.4265286.

[21] “COPPRINT MSDS-rev10-LF-products.” *Copprint Technologies Ltd.*, “Safety Data Sheet – LF3XX Product Family (including LF-360 Copper Ink)**,**” version 10, Jan. 10, 2024. Available: [Online]. Available: https://copprint.com/resources. Accessed: Oct. 6, 2025.

[22] C. Lf, “TYPICAL PROPERTIES OF UNCURED MATERIAL” Copprint Technologies Ltd., “Technical Data Sheet – LF-360 Copper Ink,” version 3, Mar. 2021. [Online]. Available: https://copprint.com/resources. Accessed: Oct. 6, 2025.

[23] L. Campos-Arias *et al.*, “Improving Definition of Screen-Printed Functional Materials for Sensing Application,” *ACS Appl. Electron. Mater.*, vol. 6, no. 4, pp. 2152–2160, Apr. 2024, doi: 10.1021/acsaelm.3c01415.

[24] B. Abbas, E. Jewell, Y. C. Lau, J. Searle, and T. Claypole, “Photonic sintering of copper for rapid processing of thick film conducting circuits on FTO coated glass,” *Sci Rep*, vol. 13, no. 1, p. 5080, Mar. 2023, doi: 10.1038/s41598-023-32044-2.

[25] S. Hong *et al.*, “Antioxidant high-conductivity copper paste for low-cost flexible printed electronics,” *npj Flex Electron*, vol. 6, no. 1, p. 17, Mar. 2022, doi: 10.1038/s41528-022-00151-1.

[26] F. Liu, L. Zhang, B. Wu, Y. Deng, and K. Xu, “Recent Status and Prospects of Low-Temperature Drift Resistors,” *Electronics*, vol. 13, no. 21, p. 4197, Jan. 2024, doi: 10.3390/electronics13214197.

[27] M. Siniscalchi, D. Tierno, K. Moors, Z. Tőkei, and C. Adelmann, “Temperature-dependent resistivity of alternative metal thin films,” *Appl. Phys. Lett.*, vol. 117, no. 4, July 2020, doi: 10.1063/5.0015048.

[28] A. F. Mayadas and M. Shatzkes, “Electrical-Resistivity Model for Polycrystalline Films: the Case of Arbitrary Reflection at External Surfaces,” *Phys. Rev. B*, vol. 1, no. 4, pp. 1382–1389, Feb. 1970, doi: 10.1103/PhysRevB.1.1382.

[29] K. Fuchs, “The conductivity of thin metallic films according to the electron theory of metals,” *Mathematical Proceedings of the Cambridge Philosophical Society*, vol. 34, no. 1, pp. 100–108, Jan. 1938, doi: 10.1017/S0305004100019952.

[30] W. Steinhögl, “Size-dependent resistivity of metallic wires in the mesoscopic range,” *Phys. Rev. B*, vol. 66, no. 7, 2002, doi: 10.1103/PhysRevB.66.075414.

[31] S. B. Soffer, “Statistical Model for the Size Effect in Electrical Conduction,” *J. Appl. Phys.*, vol. 38, no. 4, pp. 1710–1715, Mar. 1967, doi: 10.1063/1.1709746.

[32] S. V. Dukarov, S. I. Petrushenko, and V. N. Sukhov, “Inner size effect of temperature coefficient of resistance in Cu, Ag, V and Mo films,” *Vacuum*, vol. 202, p. 111148, Aug. 2022, doi: 10.1016/j.vacuum.2022.111148.

[33] Y. P. Timalsina *et al.*, “Effects of nanoscale surface roughness on the resistivity of ultrathin epitaxial copper films,” *Nanotechnology*, vol. 26, no. 7, p. 075704, Jan. 2015, doi: 10.1088/0957-4484/26/7/075704.

[34] S. B. Soffer, “Statistical Model for the Size Effect in Electrical Conduction,” *J. Appl. Phys.*, vol. 38, no. 4, pp. 1710–1715, Mar. 1967, doi: 10.1063/1.1709746.

[35] R. E. Prange, “Quantum Spectroscopy of the Low-Field Oscillations in the Surface Impedance,” *Phys. Rev.*, vol. 168, no. 3, pp. 779–786, 1968, doi: 10.1103/PhysRev.168.779.

[36] H. Yang *et al.*, “High strength and high conductivity Cu alloys: A review,” *Sci. China Technol. Sci.*, vol. 63, no. 12, pp. 2505–2517, Dec. 2020, doi: 10.1007/s11431-020-1633-8.

[37] M. Bolduc, “Screen Printing for Energy Storage and Functional Electronics: A Review,” Apr. 16, 2025, *Preprints*: 2025041328. doi: 10.20944/preprints202504.1328.v1.

[38] “Recent Status and Prospects of Low-Temperature Drift Resistors.” Accessed: Oct. 23, 2025. [Online]. Available: https://www.mdpi.com/2079-9292/13/21/4197

[39] “Study of Copper Thin Films Resistivity by Using Van der Pauw Method at Low Frequencies.” Accessed: Oct. 23, 2025. [Online]. Available: https://www.scirp.org/journal/paperinformation?paperid=121535&utm_source=chatgpt.com

[40] J. Payette, F. Vaussenat, and S. Cloutier, “Deep learning framework for sensor array precision and accuracy enhancement,” *Sci Rep*, vol. 13, no. 1, p. 11237, July 2023, doi: 10.1038/s41598-023-38290-8.

[41] A. Bid, “Temperature dependence of the resistance of metallic nanowires of diameter ≥15 nm: Applicability of Bloch–Grüneisen theorem,” Physical Review B, vol. 74, no. 3, 2006, doi: 10.1103/PhysRevB.74.035426.

[42] A. I. Oliva and J. M. Lugo, “Measurement of the Temperature Coefficient of Resistance in Metallic Films with Nano-thickness,” *Int J Thermophys*, vol. 37, no. 3, p. 35, Feb. 2016, doi: 10.1007/s10765-016-2046-0.

[43] B. Barwiński, “Temperature coefficient of resistance in discontinuous gold films on sapphire substrate near percolation threshold,” *Surface Science*, vol. 231, no. 1, pp. 165–167, May 1990, doi: 10.1016/0039-6028(90)90709-H.

[44] F. Lacy, “Developing a theoretical relationship between electrical resistivity, temperature, and film thickness for conductors,” *Nanoscale Res Lett*, vol. 6, no. 1, p. 636, Dec. 2011, doi: 10.1186/1556-276X-6-636.

[45] G. Sáfrán, P. Petrik, N. Szász, D. Olasz, N. Q. Chinh, and M. Serényi, “Review on High-Throughput Micro-Combinatorial Characterization of Binary and Ternary Layers towards Databases,” *Materials*, vol. 16, no. 8, p. 3005, Jan. 2023, doi: 10.3390/ma16083005.

[46] E. S. Rosker *et al.*, "Approaching the Practical Conductivity Limits of Aerosol Jet Printed Silver," *ACS Appl. Mater. Interfaces*, vol. 12, no. 26, pp. 29684–29691, July 2020, doi: 10.1021/acsami.0c06959.

[47] A. Radwan, Y. Sui, and C. Zorman, "The Influence of Microstructure on TCR for Inkjet-Printed Resistive Temperature Detectors Fabricated Using AgNO3/Ethylene-Glycol-Based Inks," *Micromachines*, vol. 15, no. 6, p. 749, June 2024, doi: 10.3390/mi15060749.

[48] P. Yang, S. Banerjee, W. Kuang, Y. Ding, Q. Ma, and P. Zhang, "Current crowding and spreading resistance of electrical contacts with irregular contact edges," *J. Phys. D: Appl. Phys.*, vol. 53, no. 48, p. 485303, Sept. 2020, doi: 10.1088/1361-6463/abadc3.

[49] J. Lifton and T. Liu, "An adaptive thresholding algorithm for porosity measurement of additively manufactured metal test samples via X-ray computed tomography," *Additive Manufacturing*, vol. 39, p. 101899, Mar. 2021, doi: 10.1016/j.addma.2021.101899.

[50] M. Vesenjak, K. Hokamoto, M. Sakamoto, T. Nishi, L. Krstulović-Opara, and Z. Ren, "Mechanical and microstructural analysis of unidirectional porous (UniPore) copper," *Materials & Design*, vol. 90, pp. 867–880, Jan. 2016, doi: 10.1016/j.matdes.2015.11.038.

[51] W. Zhou, Y. Tang, R. Song, L. Jiang, K. S. Hui, and K. N. Hui, "Characterization of electrical conductivity of porous metal fiber sintered sheet using four-point probe method," *Materials & Design*, vol. 37, pp. 161–165, May 2012, doi: 10.1016/j.matdes.2011.12.046.

[52] M. Szulborski, S. Łapczyński, and Ł. Kolimas, "Thermal Analysis of Heat Distribution in Busbars during Rated Current Flow in Low-Voltage Industrial Switchgear," *Energies*, vol. 14, no. 9, p. 2427, Jan. 2021, doi: 10.3390/en14092427.

[53] M. A. Ramírez and E. E. Castillo, "Thermoelectric Simulation Using Comsol Multiphysics and Analysis of Contact Resistances Effects," Oct. 2015, doi: 10.18687/LACCEI2015.1.1.170.

[54] Y. Wang, B. Gao, G. Tian, W. L. Woo, and Y. Miao, "Diffusion and separation mechanism of transient electromagnetic and thermal fields," *International Journal of Thermal Sciences*, vol. 102, pp. 308–318, Apr. 2016, doi: 10.1016/j.ijthermalsci.2015.11.016.

[55] "Ductile-brittle transition temperature." Accessed: Oct. 23, 2025. [Online]. Available: https://www.doitpoms.ac.uk/tlplib/mechanical_properties/ductile.php

[56] Y. Hiraoka, T. Inoue, H. Hanado, and N. Akiyoshi, "Ductile-to-Brittle Transition Characteristics in W–Cu Composites with Increase of Cu Content," *Mater. Trans.*, vol. 46, no. 7, pp. 1663–1670, 2005, doi: 10.2320/matertrans.46.1663.

[57] A. Wolff, "Is the Ne operation of the helium ion microscope suitable for electron backscatter diffraction sample preparation?," *Beilstein J. Nanotechnol.*, vol. 12, no. 1, pp. 965–983, Aug. 2021, doi: 10.3762/bjnano.12.73.

[58] "Design and Analysis of Experiments, 10th Edition | Wiley," Wiley.com. Accessed: Nov. 03, 2025. [Online]. Available: https://www.wiley.com/en-us/Design+and+Analysis+of+Experiments%2C+10th+Edition-p-9781119492443

[59] J. Jäger, A. Schwenck, D. Walter, A. Bülau, K. Gläser, and A. Zimmermann, "Inkjet-Printed Temperature Sensors Characterized according to Standards," *Sensors*, vol. 22, no. 21, p. 8145, Jan. 2022, doi: 10.3390/s22218145.

[60] C. Vaquero *et al.*, "Silver and copper screen-printed temperature sensors on flexible substrates: The impact of ink sintering conditions and composition," *Applied Research*, vol. 3, no. 6, p. e202300138, 2024, doi: 10.1002/appl.202300138.

[61] S. Sakthinathan *et al.*, "A Review of Thin-Film Growth, Properties, Applications, and Future Prospects," *Processes*, vol. 13, no. 2, p. 587, Feb. 2025, doi: 10.3390/pr13020587.

# Chapter-7 Appendices

## 7.1 Appendix A – Additional Width Measurements (2.5 and 1 mm)

For the two-probe method, complementary measurements were attempted on narrower printed copper strips (2.5 and 1 mm). However, these samples showed unstable readings due to incomplete connections and partially cut traces. Therefore, the corresponding data were excluded from the main TCR and simulation analyses but are presented here for completeness.

To avoid artificial precision and to standardize the presentation of the numerical data, all reported values in the tables are expressed using four significant figures. This is a conventional practice to ensure consistency between the measurement resolution and the reported results, and it does not affect the calculations or the scientific conclusions.

Table 7-1 Experimental resistance–temperature (R–T) data for single-layer printed copper strips (≈17 μm), measured using the two-probe method.

| Temp (°C) | 20 mm | 15 mm | 12.5 mm | 10 mm | 7.5 mm | 5 mm | 2.5 mm | 1 mm |
|---|---|---|---|---|---|---|---|---|
| 30 | 0.05005 | 0.05901 | 0.07023 | 0.0965 | 0.1170 | 0.1733 | 0.2511 | 0.4974 |
| 40 | 0.05106 | 0.06014 | 0.07245 | 0.0990 | 0.1181 | 0.1842 | 0.2521 | 0.5024 |
| 50 | 0.05197 | 0.06233 | 0.07467 | 0.1012 | 0.1231 | 0.1862 | | |
| 60 | 0.05321 | 0.06341 | 0.07578 | 0.1035 | 0.1255 | 0.1900 | | |
| 70 | 0.05501 | 0.06560 | 0.07800 | 0.1045 | 0.1300 | 0.1953 | | |
| 80 | 0.05641 | 0.06673 | 0.08133 | 0.1065 | 0.1322 | 0.2029 | | |
| 90 | 0.05782 | 0.06791 | 0.08331 | 0.1089 | 0.1373 | - | | |
| 100 | 0.05813 | 0.07100 | 0.08429 | 0.1092 | 0.1410 | - | | |

Table 7-2Experimental resistance–temperature (R–T) data for double-layer printed copper strips (≈34 μm), measured using the two-probe method.

| Temp (°C) | 20 mm | 15 mm | 12.5 mm | 10 mm | 7.5 mm | 5 mm | 2.5 mm | 1 mm |
|---|---|---|---|---|---|---|---|---|
| 30 | 0.02906 | 0.03019 | 0.03683 | 0.04131 | 0.05358 | 0.07800 | | |
| 40 | 0.03019 | 0.03024 | 0.03804 | 0.04240 | 0.05469 | 0.07911 | 0.1280 | 0.2344 |
| 50 | 0.03128 | 0.03029 | 0.03911 | 0.04351 | 0.05691 | 0.08125 | 0.1315 | |
| 60 | 0.03240 | 0.03233 | 0.04137 | 0.04468 | 0.05910 | 0.08345 | 0.1748 | |
| 70 | 0.03469 | 0.03129 | 0.04137 | 0.04576 | 0.06014 | 0.08459 | | |
| 80 | 0.03578 | 0.03355 | 0.04238 | 0.04684 | 0.06239 | 0.08680 | | |
| 90 | 0.03580 | 0.03466 | 0.04354 | 0.04797 | - | 0.09014 | | |
| 100 | 0.03688 | 0.03470 | 0.04466 | 0.04907 | - | - | | |

Table 7-3Experimental resistance–temperature (R–T) data for triple-layer printed copper strips (≈51 µm), measured using the two-probe method.

| Temp (°C) | 20 mm | 15 mm | 12.5 mm | 10 mm | 7.5 mm | 5 mm | 2.5 mm | 1 mm |
|---|---|---|---|---|---|---|---|---|
| 30 | 0.02014 | 0.02466 | 0.03138 | 0.03578 | 0.05913 | 0.0991 | 0.1781 | |
| 40 | 0.02128 | 0.02580 | 0.03249 | 0.03688 | 0.06019 | 0.1013 | | |
| 50 | 0.02130 | 0.02694 | 0.03234 | 0.03804 | 0.06239 | 0.1046 | | |
| 60 | 0.02132 | 0.02801 | 0.03354 | 0.03800 | 0.06352 | 0.1057 | | |
| 70 | 0.02250 | 0.02801 | 0.03467 | 0.03911 | 0.06463 | 0.1079 | | |
| 80 | 0.02251 | 0.02912 | 0.03578 | 0.04026 | 0.06690 | 0.1112 | | |
| 90 | 0.02250 | 0.02913 | 0.03576 | 0.04248 | 0.07021 | 0.1157 | | |
| 100 | 0.02359 | 0.03020 | 0.03691 | 0.04359 | 0.07129 | 0.1179 | | |

## 7.2 Appendix B – Four-Probe Resistance–Temperature Measurements

This appendix presents the complete resistance–temperature (R–T) datasets obtained from the four-probe measurements of the printed copper strips. In Chapter 4, only the corresponding plots and fitted curves were shown to illustrate the temperature-dependent behavior of the samples, while the detailed numerical tables were omitted for clarity. The full R–T values for the single-layer, double-layer, and triple-layer samples are included here for completeness.

Table 7-4 Experimental resistance–temperature (R–T) data for single-layer printed copper strips (≈17 µm), measured using the four-probe method.

| Temp (°C) | 20 mm | 15 mm | 12.5 mm | 10 mm | 7.5 mm | 5 mm |
|---|---|---|---|---|---|---|
| 30 | 0.04511 | 0.05299 | 0.06322 | 0.08507 | 0.1050 | 0.1569 |
| 40 | 0.04614 | 0.05401 | 0.06519 | 0.0889 | 0.1070 | 0.1661 |
| 50 | 0.04718 | 0.05598 | 0.06718 | 0.09094 | 0.1111 | 0.1681 |
| 60 | 0.04819 | 0.05702 | 0.06821 | 0.09101 | 0.1131 | 0.1712 |
| 70 | 0.05019 | 0.05902 | 0.07001 | 0.09104 | 0.1171 | 0.1761 |
| 80 | 0.0512 | 0.0601 | 0.07301 | 0.09204 | 0.1191 | 0.1831 |
| 90 | 0.05219 | 0.061 | 0.07504 | 0.09303 | 0.1241 | 0.1880 |
| 100 | 0.05321 | 0.06299 | 0.0761 | 0.09307 | 0.1271 | 0.1921 |

Table 7-5 Experimental resistance–temperature (R–T) data for Double-Layer printed copper strips (≈34 µm), measured using the four-probe method.

| Temp (°C) | 20 mm | 15 mm | 12.5 mm | 10 mm | 7.5 mm | 5 mm |
|---|---|---|---|---|---|---|
| 30 | 0.02631 | 0.02704 | 0.03344 | 0.03602 | 0.04823 | 0.07002 |
| 40 | 0.02718 | 0.02714 | 0.03451 | 0.03831 | 0.04923 | 0.07111 |
| 50 | 0.0282 | 0.02703 | 0.03557 | 0.03944 | 0.05143 | 0.07308 |
| 60 | 0.02919 | 0.02931 | 0.03755 | 0.0432 | 0.0534 | 0.07666 |
| 70 | 0.03143 | 0.02852 | 0.03729 | 0.04167 | 0.05442 | 0.07671 |
| 80 | 0.03244 | 0.03021 | 0.03799 | 0.0426 | 0.05618 | 0.07843 |
| 90 | 0.03241 | 0.0311 | 0.03902 | 0.0427 | 0.05719 | 0.08152 |
| 100 | 0.03329 | 0.03109 | 0.04001 | 0.04275 | 0.05822 | 0.08111 |

Table 7-6 Experimental resistance–temperature (R–T) data for Triple-Layer printed copper strips (≈51 µm), measured using the four-probe method.

| Temp (°C) | 20 mm | 15 mm | 12.5 mm | 10 mm | 7.5 mm | 5 mm |
|---|---|---|---|---|---|---|
| 30 | 0.01844 | 0.02232 | 0.02874 | 0.0323 | 0.05309 | 0.0891 |
| 40 | 0.01951 | 0.02341 | 0.02985 | 0.03318 | 0.05416 | 0.0909 |
| 50 | 0.01942 | 0.02409 | 0.02971 | 0.03422 | 0.05618 | 0.0941 |
| 60 | 0.01933 | 0.02455 | 0.03012 | 0.03421 | 0.0572 | 0.0953 |
| 70 | 0.0211 | 0.02451 | 0.03144 | 0.03516 | 0.058 | 0.0974 |
| 80 | 0.02012 | 0.0242 | 0.03224 | 0.03641 | 0.06004 | 0.1011 |
| 90 | 0.02044 | 0.02472 | 0.03222 | 0.03638 | 0.06316 | 0.1044 |
| 100 | 0.02092 | 0.02497 | 0.03331 | 0.03688 | 0.06419 | 0.1065 |

## 7.3 Appendix C – Numerical R–T Data Used in the Simulations

This appendix contains the complete resistance–temperature (R–T) data obtained from numerical modeling in COMSOL Multiphysics. In Chapter 4, the numerical results were presented only as R–T plots and fitted curves to visually illustrate the overall trend and thermal behavior of the samples. To avoid clutter in the main text, the detailed numerical tables were omitted and are provided here for completeness.

Table 7-7 Numerical resistance–temperature (R–T) data for single-layer printed copper strips (≈17 µm), obtained from the numerical model.

| Temp (°C) | 20 mm | 15 mm | 12.5 mm | 10 mm | 7.5 mm | 5 mm |
|---|---|---|---|---|---|---|
| 30 | 0.03427 | 0.0457 | 0.05484 | 0.06855 | 0.0914 | 0.1371 |
| 40 | 0.03558 | 0.04745 | 0.05693 | 0.07117 | 0.0949 | 0.1423 |
| 50 | 0.0369 | 0.04919 | 0.05903 | 0.07379 | 0.0984 | 0.1476 |

| | | | | | | |
|---|---|---|---|---|---|---|
| 60 | 0.03821 | 0.05094 | 0.06113 | 0.07641 | 0.1019 | 0.1528 |
| 70 | 0.03952 | 0.05269 | 0.06323 | 0.07904 | 0.1054 | 0.1581 |
| 80 | 0.04083 | 0.05444 | 0.06533 | 0.08166 | 0.1089 | 0.1633 |
| 90 | 0.04214 | 0.05619 | 0.06742 | 0.08428 | 0.1124 | 0.1686 |
| 100 | 0.04345 | 0.05793 | 0.06952 | 0.0869 | 0.1159 | 0.1738 |

Table 7-8 Numerical resistance–temperature (R–T) data for double-layer printed copper strips (≈34 µm), obtained from the numerical model

| Temp (°C) | 20 mm | 15 mm | 12.5 mm | 10 mm | 7.5 mm | 5 mm |
|---|---|---|---|---|---|---|
| 30 | 0.01714 | 0.02285 | 0.02742 | 0.03427 | 0.0457 | 0.06855 |
| 40 | 0.01779 | 0.02372 | 0.02847 | 0.03558 | 0.04745 | 0.07117 |
| 50 | 0.01845 | 0.0246 | 0.02952 | 0.0369 | 0.04919 | 0.07379 |
| 60 | 0.0191 | 0.02547 | 0.03057 | 0.03821 | 0.05094 | 0.07641 |
| 70 | 0.01976 | 0.02635 | 0.03161 | 0.03952 | 0.05269 | 0.07904 |
| 80 | 0.02041 | 0.02722 | 0.03266 | 0.04083 | 0.05444 | 0.08166 |
| 90 | 0.02107 | 0.02809 | 0.03371 | 0.04214 | 0.05619 | 0.08428 |
| 100 | 0.02173 | 0.02897 | 0.03476 | 0.04345 | 0.05793 | 0.0869 |

Table 7-9 Numerical resistance–temperature (R–T) data for triple-layer printed copper strips (≈51 µm), obtained from the numerical model.

| Temp (°C) | 20 mm | 15 mm | 12.5 mm | 10 mm | 7.5 mm | 5 mm |
|---|---|---|---|---|---|---|
| 30 | 0.01142 | 0.01523 | 0.01828 | 0.02285 | 0.03047 | 0.0457 |
| 40 | 0.01186 | 0.01582 | 0.01898 | 0.02372 | 0.03163 | 0.04745 |
| 50 | 0.0123 | 0.0164 | 0.01968 | 0.0246 | 0.0328 | 0.04919 |
| 60 | 0.01274 | 0.01698 | 0.02038 | 0.02547 | 0.03396 | 0.05094 |
| 70 | 0.01317 | 0.01756 | 0.02108 | 0.02635 | 0.03513 | 0.05269 |
| 80 | 0.01361 | 0.01815 | 0.02178 | 0.02722 | 0.03629 | 0.05444 |
| 90 | 0.01405 | 0.01873 | 0.02247 | 0.02809 | 0.03746 | 0.05619 |
| 100 | 0.01448 | 0.01931 | 0.02317 | 0.02897 | 0.03862 | 0.05793 |

## 7.4 Appendix D – Graphical Interface of the COMSOL Model

This appendix presents the graphical user interface of the COMSOL Multiphysics model used for input assignment in the simulation process. The interface allows users to enter relevant parameters such as temperature, resistivity, and dimensions for the busbar, facilitating the setup and computation of resistance values. The figure below provides a visual example of the input fields and model geometry, helping clarify the workflow followed during numerical analysis.

computation of resistance values. The figure below provides a visual example of the input fields and model geometry, helping clarify the workflow followed during numerical analysis.

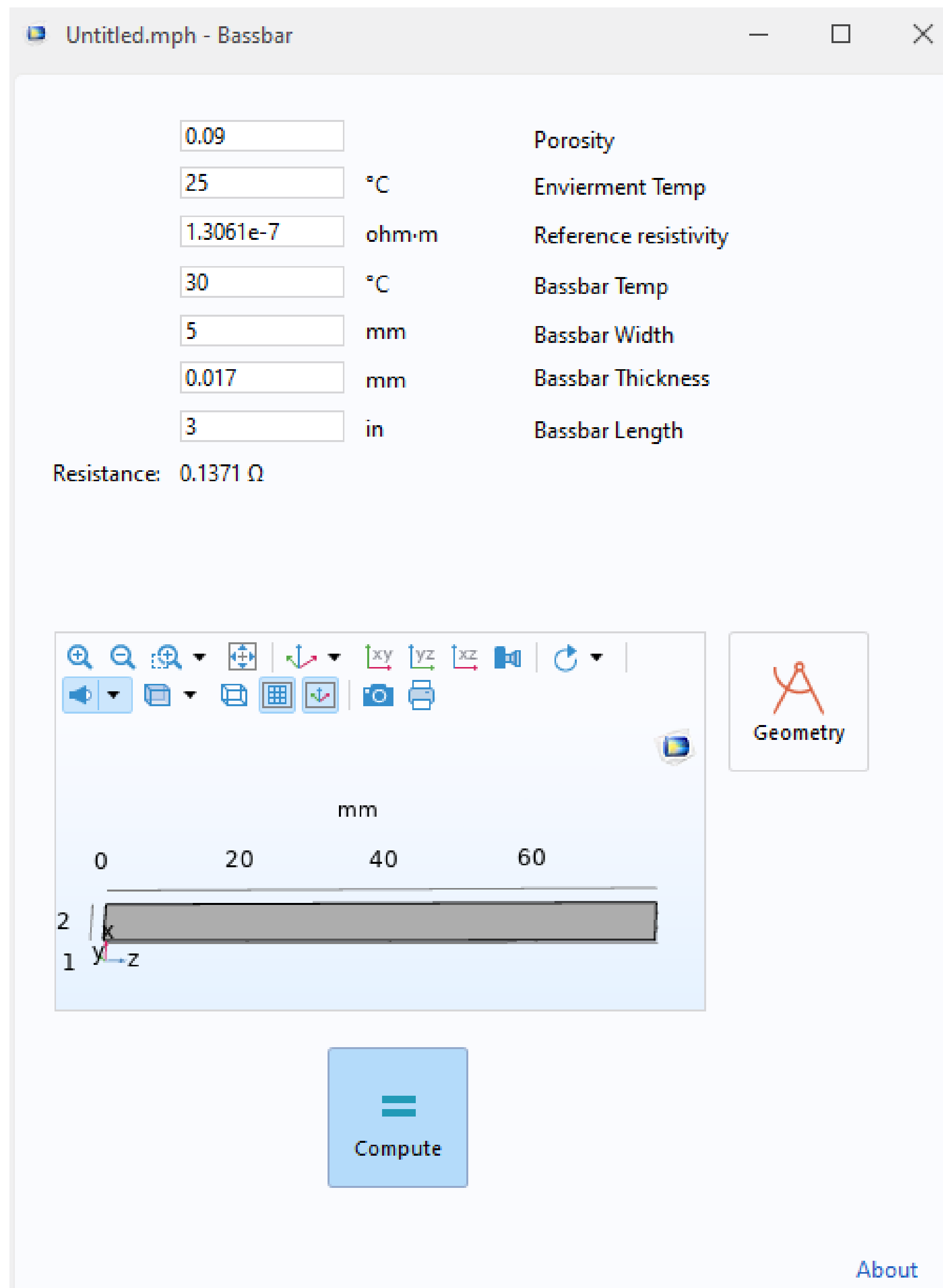


*Figure 7-1*

Figure 7-2 Graphical user interface of the COMSOL Multiphysics model used for parameter input and resistance calculation.